

# Department of Electrical Engineering

Master's Thesis

## Online Identification of Running Resistance and Available Adhesion of Trains

Master's Thesis in Vehicular Systems  
by

**Jesper Ahlberg**  
**Esbjörn Blomquist**

LITH-ISY-EX--11/4317--SE  
Linköping 2011



**Linköping University**  
**INSTITUTE OF TECHNOLOGY**



# Online Identification of Running Resistance and Available Adhesion of Trains

by

**Jesper Ahlberg**  
**Esbjörn Blomquist**

LITH-ISY-EX--11/4317--SE

Supervisors: **Henrik Salomonsson**  
ISY, Linköping university  
**Dr. Piotr Lukaszewicz**  
**Senior Consultant**  
Transrail Sweden AB  
**Mario Lagos**  
**Senior Consultant**  
Transrail Sweden AB

Examiner: **Dr. Erik Frisk**  
**Associate Professor**  
ISY, Linköping university

Linköping, September 16th, 2011



<b>Presentationsdatum</b>   Date of presentation 2011-08-23  <b>Publiceringsdatum (elektronisk version)</b> Date of publication 2011-09-16	<b>Institution och avdelning</b>  <b>Institutionen för systemteknik</b> <b>Department of Electrical Engineering</b>	  <b>Linköping University</b> INSTITUTE OF TECHNOLOGY
---	--	---

<b>Språk</b>   Language  <input type="checkbox"/> Svenska <input checked="" type="checkbox"/> Annat (ange nedan)  <u>Engelska/English</u>  <b>Antal sidor</b>   Pages 123	<b>Typ av publikation</b> Report category <input type="checkbox"/> Licentiatavhandling <input checked="" type="checkbox"/> Examensarbete <input type="checkbox"/> C-uppsats <input type="checkbox"/> D-uppsats <input type="checkbox"/> Rapport <input type="checkbox"/> Annat (ange nedan)	<b>ISBN</b> –  <b>ISRN</b> LiTH-ISY-EX--11/4317--SE  <b>Serietitel (licentiatavhandling)</b>   Title of series –  <b>Serienummer/ISSN (licentiatavhandling)</b> Serial number –
---	--	--

<b>URL för elektronisk version</b> <a href="http://www.ep.liu.se">http://www.ep.liu.se</a>
---

<b>Publikationens titel</b>   Title Online Identification of Running Resistance and Available Adhesion of Trains Online identifiering av tågs gångmotstånd och tillgänglig adhesion  <b>Författare</b>   Author Jesper Ahlberg & Esbjörn Blomquist
---

<b>Sammanfattning</b>   Abstract  <p>Two important physical aspects that determine the performance of a running train are the total <i>running resistance</i> that acts on the whole train moving forward, and the available <i>adhesion</i> (utilizable wheel-rail-friction) for propulsion and breaking. Using the measured and available signals, <i>online identification</i> of the current running resistance and available adhesion and also <i>prediction</i> of future values for a distance ahead of the train, is desired. With the aim to enhance the precision of those calculations, this thesis investigates the potential of online identification and prediction utilizing the <i>Extended Kalman Filter</i>.</p> <p>The conclusions are that problems with <i>observability</i> and <i>sensitivity</i> arise, which result in a need for sophisticated methods to <i>numerically derive</i> the acceleration from the velocity signal. The <i>smoothing spline approximation</i> is shown to provide the best results for this numerical differentiation. Sensitivity and its need for high accuracy, especially in the acceleration signal, results in a demand of higher sample frequency. A desire for other profound ways of collecting further information, or to enhance the models, arises with possibilities of future work in the field.</p>
---

<b>Nyckelord</b>   Keywords running resistance, extended kalman filter, parameter estimation, acceleration estimation, adaptive models, adhesion, freight trains, numerical differentiation
--



*For freedom of thought...*



# Abstract

Two important physical aspects that determine the performance of a running train are the total *running resistance* that acts on the whole train moving forward, and the available *adhesion* (utilizable wheel-rail-friction) for propulsion and braking. Using the measured and available signals, *online identification* of the current running resistance and available adhesion and also *prediction* of future values for a distance ahead of the train, is desired. With the aim to enhance the precision of those calculations, this thesis investigates the potential of online identification and prediction utilizing the *Extended Kalman Filter*.

The conclusions are that problems with *observability* and *sensitivity* arise, which result in a need for sophisticated methods to *numerically derive* the acceleration from the velocity signal. The *smoothing spline approximation* is shown to provide the best results for this numerical differentiation. Sensitivity and its need for high accuracy, especially in the acceleration signal, results in a demand of higher sample frequency. A desire for other profound ways of collecting further information, or to enhance the models, arises with possibilities of future work in the field.

# Sammanfattning

Två viktiga fysikaliska aspekter som bestämmer prestandan för ett tåg i drift är det totala *gångmotståndet* som verkar på hela tåget, samt den tillgängliga *adhesionen* (användbara hjul-räl-friktionen) för framdrivning och bromsning. Från de tillgängliga signalerna önskas identifiering, samt prediktering, av dessa två storheter, under drift. Med målet att förbättra precisionen av dessa skattningar undersöker detta examensarbete potentialen av skattning och prediktering av gångmotstånd och adhesion med hjälp av *Extended Kalman Filtering*.

Slutsatsen är att problem med *observerbarhet* och *känslighet* uppstår, vilket resulterar i ett behov av sofistikerade metoder att *numeriskt beräkna* acceleration från en hastighetssignal. Metoden *smoothing spline approximation* visar sig ge de bästa resultaten för denna numeriska derivering. Känsligheten och dess medförda krav på hög precision, speciellt på accelerationssignalen, resulterar i ett behov av högre samplingsfrekvens. Ett behov av andra adekvata metoder att tillföra ytterligare information, eller att förbättra modellerna, ger upphov till möjliga framtida utredningar inom området.

# Acknowledgments

We would like to thank Mario Lagos, Transrail Sweden AB, and the company at large, for creating the opportunity for us to make this master's thesis. Mario has also been a valuable asset in meetings and discussions. We would especially like to thank Piotr Lukaszewicz, Transrail Sweden AB, for all the help and for being such an endless source of information when it comes to theory, train physics and not least the shaping of a high quality thesis, both at meetings in Sundbyberg and with continuous mail correspondence. Without his help this thesis would not be what it is. We would also like to thank everyone at Transrail for making us feel very welcome at the office in Sundbyberg when we spent time there and for the help whenever we needed something.

Many thanks also to our supervisor Henrik Salomonsson at Vehicular Systems at the Department of Electrical Engineering, Linköping University, for the time, meetings and discussions when we were stuck. Also not least for all the great feedback on the thesis, which helped to improve it significantly. We would also like to thank Erik Frisk at Vehicular Systems at the Department of Electrical Engineering, Linköping University, for all his sharp expertise in the field of parameter estimation. Things just always seemed so much more clear after each meeting with him. Many thanks also for all the help with this master's thesis in general. Thanks also to Torkel Glad at Automatic Control at the Department of Electrical Engineering, Linköping University for happily answering technical questions.

We would like to thank Philipp Gerber at HaslerRail AG, Bern, Switzerland, for answering questions and providing information on Teloc velocity measurement, and David Gubler for letting us use his wonderful pictures of the IORE locomotive and train configuration.

We also want to give our love and thanks to our family, friends, and also our girlfriends for putting up with all the late night (early morning) work with the report, and all the jokes of low adhesion.

Last but not least, we want to thank each other for the great cooperation during this master's thesis.



# Table of Content

<b>Abstract</b> .....	<b>1</b>
<b>Acknowledgments</b> .....	<b>3</b>
<b>List of Symbols</b> .....	<b>9</b>
<b>Definitions &amp; Abbreviations</b> .....	<b>13</b>
<b>1 Introduction</b> .....	<b>15</b>
1.1 Thesis Background.....	15
1.1.1 Related Research.....	16
1.2 Problem Formulation.....	17
1.3 Objectives.....	18
1.4 Thesis Contribution.....	18
1.5 Methods.....	19
1.5.1 Kalman Filtering.....	19
1.5.1.1 The Extended Kalman Filter.....	19
1.5.2 Numerical Derivation.....	20
1.5.3 Observability.....	20
1.5.3.1 Covariance Analysis.....	21
1.5.3.2 Rank & Nullspace.....	22
1.5.4 Sensitivity.....	24
1.6 Method Criticism.....	25
1.6.1 The Extended Kalman Filter.....	25
1.6.2 Numerical Derivation.....	25
1.6.3 Observability.....	25
1.7 Organization.....	26
1.8 Software.....	26
1.9 Limitations.....	26
1.10 Report Outline.....	27
<b>2 Theoretical Background</b> .....	<b>31</b>
2.1 Running Resistance.....	31
2.2 Acceleration.....	34
2.3 Tractive Force.....	35
2.4 Adhesion.....	35
<b>3 Signals</b> .....	<b>39</b>
3.1 Available Data.....	39
3.1.1 Teloc.....	39
3.1.2 BIS.....	41
3.1.3 GPS.....	41

3.2	Test Signals for Simulation.....	42
3.2.1	Speed & Acceleration.....	42
3.2.2	Tractive Force.....	43
3.2.3	Gradient & Curve Radius.....	43
3.2.4	Train Configuration.....	44
<b>4</b>	<b>Running Resistance.....</b>	<b>47</b>
4.1	The Running Resistance Model.....	47
4.2	Deducing a System Model.....	49
4.3	Initial Parameter Values.....	51
4.4	Online Identification .....	51
4.4.1	A First Approach: EKF with 7 States.....	52
4.4.1.1	Results.....	54
4.4.1.2	Observability.....	55
4.4.1.3	Possible Solution.....	55
4.4.2	Removing States $x_a$ & $x_v$ .....	56
4.4.2.1	Results.....	58
4.4.2.2	Observability.....	58
4.4.2.3	Possible Solution.....	59
4.4.3	Removing State E.....	59
4.4.3.1	Results.....	60
4.4.3.2	Observability.....	62
4.4.3.3	Sensitivity.....	64
4.5	Conclusions.....	68
<b>5</b>	<b>Acceleration.....</b>	<b>71</b>
5.1	Two-point Differentiation.....	71
5.2	Kalman Filtering.....	72
5.3	Smoothing Spline Approximation.....	73
5.4	Evaluation.....	73
5.4.1	Noise.....	74
5.4.2	Time Delay.....	77
5.4.3	Scale Error.....	79
5.4.4	Conclusions.....	80
<b>6</b>	<b>Running Resistance with Acceleration Estimation.....</b>	<b>81</b>
6.1	Recorded Data.....	81
6.1.1	The Data.....	81
6.1.2	Online Identification of Running Resistance .....	82
6.1.2.1	Results.....	82
6.1.2.2	Discussion.....	86
6.2	Simulation.....	87
6.2.1	Sample Time: 1 s.....	87
6.2.2	Sample Time: 20 ms.....	88
6.3	Conclusions.....	88
<b>7</b>	<b>Adhesion.....</b>	<b>91</b>
7.1	Deducing a System Model.....	91
7.2	Initial Parameter Values.....	92
7.3	Online Identification.....	93
7.3.1	A First Approach: EKF with 3 States.....	93

7.3.1.1	Results.....	95
7.3.1.2	Problems.....	95
7.3.1.3	Possible Solution.....	96
7.3.2	Removing Parameter Y.....	97
7.3.2.1	Results.....	98
7.3.2.2	Observability.....	98
7.3.2.3	Sensitivity.....	99
7.4	Conclusions.....	100
<b>8</b>	<b>Conclusions &amp; Future Work.....</b>	<b>101</b>
8.1	Conclusions.....	101
8.2	Future Work.....	102
<b>9</b>	<b>References.....</b>	<b>105</b>
<b>A</b>	<b>Description of CATO.....</b>	<b>109</b>
<b>B</b>	<b>Teloc Velocity Measurement.....</b>	<b>111</b>



# List of Symbols

## Forces

$F_{RT}$	Total running resistance. [N]
$F_R$	Running resistance. [N]
$F_M$	Mechanical rolling resistance. [N]
$F_{MA}$	Constant part of the mechanical rolling resistance. [N]
$F_{MB}$	Part of the mechanical rolling resistance dependent on the first power of the speed. [N]
$F_D$	Running resistance from air drag. [N]
$F_{DB}$	Part of the aerodynamic resistance dependent on the first power of the speed. [N]
$F_{DC}$	Part of the aerodynamic resistance dependent on the second power of the speed. [N]
$F_G$	Running resistance due to gradients. [N]
$F_C$	Running resistance due to curves. [N]
$F_I$	Running resistance due to inertia. [N]
$F_t$	Measured tractive (propelling) force. [N]
$F_{ta}$	Adhesive force. [N]
$F_{tJ}$	Tractive (propelling) force at the wheel rims. [N]
$F_w$	Final propelling force at the wheel rims. [N]
$F_b$	Breaking force at the wheel rims. [N]
$F_{reg}$	Resistance force from the motors due to regeneration (regenerative breaking). [N]
$F_v$	Speed dependent part of the running resistance. [N]

$F_a$  Acceleration dependent part of the tractive force. [N]

## Constants

$I$  Identity matrix. [-]

$g$  Acceleration due to gravity. [m/s<sup>2</sup>]

$L_T$  Total length of the train. [m]

$M$  Mass. [kg]

$M_J$  Mass including effects of rotary inertia. [kg]

$M_T$  Total mass of the train. [kg]

$K_D$  Empirical constant in air drag equation. [kg/m<sup>2</sup>]

$K_J$  Mass accounting for effects of rotary inertia of a locomotive. [kg]

$n_{ax}$  Number of axles. [-]

$n_{loco}$  Number of locomotives. [-]

$n_{wag}$  Total number of wagons. [-]

$n_{trac}$  1 during traction, 0 if coasting. [-]

$n_d$  Number of driven axles. [-]

$r_w$  Wheel radius. [m]

$Q$  Axle-load. [N]

$\alpha_{max}$  Maximum adhesion coefficient. [-]

$\mu_{max}$  Maximum friction of the rail, depending on the texture and condition of the contact area that varies with roughness, weather and contamination. [-]

$\kappa$  Coefficient dependent on the locomotive's slip control and its ability to stay close to the maximum friction. [-]

$\gamma$  Coefficient for the part in the running resistance system model that depends on the acceleration. [kg]

## Parameters

$A$  Parameter for the constant part of the running resistance. [N]

$B$	Parameter for the speed dependent part of the running resistance. [kg/s]
$C$	Parameter for the part of the running resistance depending on the speed in square. [kg/m]
$D$	First parameter of the curve resistance. [m]
$E$	Second parameter of the curve resistance. [m]
$X$	Parameter for the constant part of the available adhesion. [-]
$Y$	First parameter of the speed dependent part of the available adhesion. [-]
$Z$	Second parameter of the speed dependent part of the available adhesion. [-]

## Signals

$a$	Acceleration of the train. [m/s <sup>2</sup> ]
$F_t$	Tractive effort. [N]
$G$	Gradient. [‰]
$r$	Curve radius. [m]
$v$	Speed of the train in its forward direction along the track. [m/s]
$\zeta$	The slippage ratio. [-]
$\upsilon$	The slippage ratio for braking. [-]
$\omega$	Angular speed of the wheel. [rad/s]
$v_w$	Wind speed. [m/s]
$\beta$	The angle between the track and the horizontal plane.

## Filter

$x$	State vector.
$u$	Input signal vector.
$y$	Vector containing the measured reference signal(s).
$h$	Vector containing the model function(s).

$f$	Vector containing the state update function(s).
$P$	Covariance matrix of the EKF, containing the estimations of the state covariances.
$K$	State gain vector.
$H$	The model function, $h$ , differentiated with respect to the state vector, $x$ .
$F$	The state update function, $f$ , differentiated with respect to the state vector, $x$ .
$R$	The covariance matrix of the measured reference signals, which is used as a design parameter in the EKF.
$Q$	The covariance matrix of the states, which is used as a design parameter in the EKF.

## Observability & Sensitivity

$O$	The observability matrix
$H_w$	The model function, $h$ , differentiated with respect to the input signal vector, $u$ .

# Definitions & Abbreviations

Adhesion	The part of the friction that can be used for actual propulsion.
Adhesive mass	The total mass resting on the driven axles.
BIS	Track Information System.
CATO	Computer Aided Train Operation. A system developed by Transrail Sweden AB.
Coasting	Neither tractive nor braking forces affects the train; "pure rolling".
Creep	A difference in speed between the periphery of a driven wheel and the actual vehicle speed.
EKF	Extended Kalman Filter.
GPS	Global Positioning System.
IORE	Electric locomotive built for ore transport.
Kalman filtering	A mathematical method for estimations from measurements.
Kernel	See Nullspace.
Nullspace	The nullspace of a matrix $A$ is the set of every vector $x$ for which $Ax = 0$ .
Running resistance	All forces acting against a train's direction.
Slip	See Creep.
Smoothing Spline Approximation	Derivation method where an analytical function is fitted to a window of samples of the signal, and that analytical function is differentiated.
SVD	Singular Value Decomposition.

Teloc	Microprocessor-controlled event recorder mounted in many Swedish freight locomotives. Developed by HaslerRail AG.
Traction	Propulsion.
Transrail	Transrail Sweden AB.
Two-point differentiation	Simple derivation method using 2 subsequent points.
Uad	A type of ore wagon.
UKF	Unscented Kalman Filter.

---

# 1

## Introduction

---

This introductory chapter will describe the background of this thesis and what earlier work has been made in this area of expertise. The problem will be formulated followed by the objectives of the thesis work. With this defined, the different methods used will be presented and evaluated. In the end of the chapter the structure of the project such as organization, limitations and the outline of the rest of the report will be described.

### 1.1 Thesis Background

Two important physical aspects that determine the performance of a running train is the total resistance that acts on the whole train moving forward, and the available adhesion for traction and braking. The total resistance, called running resistance, consists mainly of mechanical rolling resistance, air drag and resistance due to curves and grades. Adhesion is a term for the grip between a wheel and the rail, or in this context the part of the wheel-rail-friction in the longitudinal direction that can be used for actual propulsion or deceleration. Both the running resistance and the adhesion is affecting the performance of a train; acceleration, driving times and also energy consumption, and they both vary in time and space.

Transrail Sweden AB (henceforth called only Transrail) is a Swedish company working with methods for optimal operations of trains, including reduction of energy consumption (Eco-driving). The company have developed a system named CATO (Computer Aided Train Operation) that

provides instructions on how to optimally drive the train, to the driver. See Appendix A for a short description of CATO. The quality of these instructions are, among other things, dependent on the calculation of the running resistance and adhesion, and the parameters on which they depend.

### 1.1.1 Related Research

It appears more work in the area has been done for road-driven vehicles than for railroad vehicles. However, some of the theory can indirectly or directly be applied to rail-road vehicles as well, both for running resistance and adhesion. Parts of the running resistance can theoretically be calculated in more or less the same way in both cases, however other parts differ and special conditions and phenomenon for railroad vehicles have to be taken into account.

Research aimed more specifically at this area of investigation can be found, for example [1], a doctoral thesis by P. Lukaszewicz, which provide extensive knowledge on running resistance and also presents empirical models for both running resistance and adhesion. Behind the thesis lies experimental data from thorough testing of both passenger and freight trains. A deeper study of the aerodynamic resistance is provided by R.S. Raghunathan et. al. in [26]. A compilation of a total running resistance model, similar to the one composed in this thesis, for train simulation is made in [17] by F. Gauffin.

More investigations seem to be found in the area of adhesion than on the subject of running resistance, for railroad vehicles. Experimental results about the relation between adhesion and slip for different wheel-rail conditions is provided by O. Polach in [19], by M. Spiriyagin et. al. in [23] and by H. Chen et. al. in [22]. Studies of adhesion more with aim on traction and slip control is provided by M. Spiriyagin et. al. in [21] and D. Frylmark and S. Johnsson in [3].

Also attempting to estimate running resistance parameters using Kalman filtering are P. Howlett et. al. in [7]. They evaluate the attempt in simulation with a satisfactory result. However, they make a number of simplifications, not made in this thesis:

- Resistance due to curves is not taken into account.
- Tractive effort removed, making the model valid only in coasting.
- Grade resistance is not included in simulations.

- No compensation for rotary inertia in the train model.
- Running resistance model is normalized by setting the train mass to 1.
- Not realistic parameter values for freight trains.

The paper seems to focus on demonstrating the UKF rather than making a realistic evaluation of train parameter estimation.

## 1.2 Problem Formulation

Sometimes it happens that a train gets stuck and can't move forward. This is always undesired and very expensive. The cause of this is a too low adhesion, thus limiting the available tractive effort, compared to the running resistance. For example this could happen in a back slope (rise in running resistance) in the autumn with wet leaves on the rail (causing a reduction in adhesion). Heavy damage can also be inflicted on the wheels and rail due to low adhesion with associated wheel spin and slippage.

It is of great importance that low adhesion is detected, the running resistance is well estimated, and the implications these have on the propulsion therefore can be calculated. It is not an easy task to find the actual adhesion for a running train or to control traction with respect to available adhesion. Much research have been made and many papers have been written on this subject ([3], [18], [19], [20], [21], [22], [23]), but there is still not an easy solution and more could be won in better estimation. The methods used by Transrail at present utilizes mainly static models based on empirical data which is difficult to obtain.

The need for greater accuracy puts a demand on more sophisticated approaches for calculation of adhesion and running resistance. Many of the variables in the models are complex, with random components and dependencies on train configuration, wind and weather. Modern locomotives are equipped with sensors monitoring variables such as position, propulsion, line voltage, temperature etc. Online identification of the running resistance and the available adhesion for any train in service is desired, using the measured and available signals. Also desired is prediction of future values for a distance ahead of the train to provide information that for instance can be used to optimize energy consumption and keep time schedules.

## 1.3 Objectives

To further improve the train performance algorithms by taking into account weather and other external unpredictable influences, Transrail wants to enhance the precision of the calculation of running resistance and adhesion by investigating the potential of online identification and prediction. Static empirical models for these are currently used, which are well working and will be a good basis for this thesis work, but a more dynamic and adaptive behavior of these is desired, so that the models adjust to the current train and prevailing conditions. Transrail wants to find out if the variables available online on a train are enough to get a good estimation, and are also interested in which signals that would be desirable to have access to in order to identify and predict the running resistance and available adhesion with a satisfactory result.

To know the accuracy demands of the input signals to this online calculation, a sensitivity analysis is wanted. Desired is also a synthesis of the algorithms in the programming language Python along with plots and results from simulations.

## 1.4 Thesis Contribution

This thesis is believed to provide insight in parameter estimation for self-adapting models, together with methods for evaluating observability and sensitivity for such problems. In addition, it presents how to use these methods for running resistance and adhesion for railroad vehicles, and evaluates the difficulties specifically for these fields. Up to date models and physics regarding running resistance and adhesion for trains in general are provided. Suggestions of how to improve results and possible further interesting paths for investigation are also presented.

The thesis is believed to contribute with a state of the art method for estimating the acceleration from the available velocity signal with as high precision as possible for the running resistance and adhesion identification. It can also serve as a reference for the extended kalman filter formulas.

## 1.5 Methods

### 1.5.1 Kalman Filtering

A common way of estimating parameters in a model is to make use of Kalman filtering. However, the *Kalman Filter* is formulated for linear models and thus can not handle systems with nonlinear models and behavior. [4]

Another version of the Kalman filter, the *Linearized Kalman Filter*, can be used to handle nonlinear models, however it requires the nominal trajectory to be known and calculated in advance. [4]

The *Extended Kalman Filter*, EKF, can be used when the nominal trajectory is not known, which is normally the case. The problem is solved using the information available from the estimates by the filter itself. The best estimation available, the latest estimation, is used to create a new linearization in each update. This means that the  $K$ - (gain) and  $P$ - (covariance) matrices can't be calculated beforehand. The EKF is widely used in many applications. [4]

Even though the EKF is a very popular approach, there are situations when the EKF performs poorly. This occurs particularly when the models used are highly nonlinear ([5]). Another approach is then to use the *Unscented Kalman Filter*, UKF, which uses a set of chosen points in the state space in order to capture the effect of model nonlinearities ([4]). The UKF utilizes the *unscented transform*, which is described in [4] and [5].

The work presented in this thesis has been made utilizing the *Extended Kalman Filter*.

#### 1.5.1.1 The Extended Kalman Filter

With some minor modifications, the following filter formulas for EKF are provided by [4]:

1. Initialization:

$$\hat{x}_{0|0} = x_0 \quad P_{0|0} = \Pi_0 \quad k = 0 \quad (1.1)$$

Where  $x_0$  is the initial estimation of the state-vector,  $\Pi_0$  the covariance of  $x_0$  and  $k$  is the discrete time-sample.

2. Measurement update:

$$\hat{x}_{k|k} = \hat{x}_{k|k-1} + K_k(y_k - h(\hat{x}_{k|k-1}, u_k)) \quad (1.2)$$

$$K_k = P_{k|k-1} H_k^T (H_k P_{k|k-1} H_k^T + R_k)^{-1} \quad (1.3)$$

$$P_{k|k} = (I - K_k H_k) P_{k|k-1} \quad (1.4)$$

$$H_k := \left( \nabla_x h(x, u_k) \Big|_{x=\hat{x}_{k|k-1}} \right)^T \quad (1.5)$$

3. Time update:

$$\hat{x}_{k+1|k} = f(\hat{x}_{k|k}, 0) \quad (1.6)$$

$$P_{k+1|k} = F_k P_{k|k} F_k^T + Q_k \quad (1.7)$$

$$F_k := \left( \nabla_x f(x, 0) \Big|_{x=\hat{x}_{k|k-1}} \right)^T \quad (1.8)$$

where  $f(x, w)$  denotes the state update and  $w$  the noise vector corresponding to the states.

4. Let  $k = k+1$  and repeat from 2.

## 1.5.2 Numerical Derivation

Three methods of numerical derivation have been used where the first is a simple two-point differentiation which is satisfactory for a noise-free signal. The other two, Kalman filtering and smoothing spline approximation, can attenuate noise well ([12]). These approaches are all described in detail in Chapter 5.

## 1.5.3 Observability

When dealing with parameter estimation, it is important to investigate the observability as a measurement, not only for if the parameters are observable at all, but also how observable they are to gain knowledge about which

performance the estimation can provide. When dealing with nonlinear systems this analysis is often more arduous ([6]). This section describes which methods that will be used to investigate, and measure, observability.

### 1.5.3.1 Covariance Analysis

For each update the *Extended Kalman Filter* provides an updated matrix,  $P$ , which is the covariance matrix of the estimated states. The diagonal of this matrix consists of the variance of the states and can be studied in order to get insight in how reliable the result of the estimation is.

For a parameter estimation where the one-step prediction is described as:

$$\hat{x}_{k+1|k} = f(\hat{x}_{k|k}, 0) = \hat{x}_{k|k} \quad (1.9)$$

which means:

$$F_k := \left( \nabla_x f(x, 0) \Big|_{x=\hat{x}_{k|k-1}} \right)^T = I \quad (1.10)$$

the one-step prediction for the covariance matrix is:

$$P_{k+1|k} = F_k P_{k|k} F_k^T + Q_k \quad (1.11)$$

With:

$$F_k = I \quad (1.12)$$

this yields:

$$P_{k+1|k} = P_{k|k} + Q_k \quad (1.13)$$

The updated covariance matrix  $P$  is:

$$P_{k|k} = (I - K_k H_k) P_{k|k-1} \quad (1.14)$$

When the filter can't solve the equations needed in order to couple the measured reference signal to a certain state, the state gain

$$K_k = P_{k|k-1} H_k^T (H_k P_{k|k-1} H_k^T + R_k)^{-1} \quad (1.15)$$

will be zero for that state.

Assuming the state gain for state  $\theta_1$  is:

$$K_{k, \theta_1} = 0 \quad (1.16)$$

the current covariance estimation for state  $\theta_1$  will be the same as the one-step prediction of the covariance for the last time-update as:

$$P_{k|k, \theta_1} = P_{k|k-1, \theta_1} \quad (1.17)$$

and thus the covariance for state  $\theta_1$  will increase linearly with  $Q_{k, \theta_1}$  as:

$$P_{k+1|k, \theta_1} = P_{k|k, \theta_1} + Q_{k, \theta_1} = P_{k|k-1, \theta_1} + Q_{k, \theta_1} \quad (1.18)$$

where  $Q_{k, \theta_1}$  refers to the element in  $Q$  corresponding to the variance of the state  $\theta_1$ .

This means that by investigating the diagonal elements of the covariance matrix,  $P$ , of the parameter estimation and localizing sections where the covariance increases linearly for that state, it's possible to assume lack of observability for the state in that section. [14]

### 1.5.3.2 Rank & Nullspace

Assume the observability matrix for a filter implementation in a given interval  $[k_0, k_f]$  is:

$$O_{k_0, k_f} = \begin{pmatrix} H_{k_0} \\ H_{k_0+1} F_{k_0+1, k_0} \\ \vdots \\ H_{k_f-1} F_{k_f-1, k_0} \end{pmatrix} \quad (1.19)$$

With the  $H$  and  $F$  matrices according to Section 1.5.1.1.

The estimated states would then be observable on  $[k_0, k_f]$  if and only if  $O$  has full rank. [10]

Also note that this implies restrictions of the interval length so that:

$$\text{rows}(O_{k_0, k_f}) \geq \text{columns}(O_{k_0, k_f}) \quad (1.20)$$

holds. [10]

In the case of parameter estimation with the one-step prediction according to:

$$\hat{x}_{k+1|k} = f(\hat{x}_{k|k}, 0) = \hat{x}_{k|k} \quad (1.21)$$

and therefore:

$$F_k := \left( \nabla_x f(x, 0) \Big|_{x=\hat{x}_{k|k-1}} \right)^T = I \quad (1.22)$$

the observability matrix becomes:

$$O_{k_0, k_f} = \begin{pmatrix} H_{k_0} \\ H_{k_0+1} \\ \vdots \\ \vdots \\ H_{k_f-1} \end{pmatrix} \quad (1.23)$$

This window can provide information during run-time about the performance of the filter in terms of local observability. If rank is lost, observability is also lost in the interval. This does not necessarily mean that no state is observable, but all states aren't, individually.

What this loss of rank does not answer, is which state or states the filter can't estimate in the given time interval.

To gain knowledge of this, the nullspace (or kernel) of  $O_{k_0, k_f}$  can be investigated. The nullspace consists of all the directions of the states that aren't observable. Only base-vectors orthogonal to this nullspace would represent states that are observable at the time. By projecting base-vectors corresponding to each state onto the nullspace of  $O_{k_0, k_f}$ , a measurement of how observable each state is could be derived. Fully observable states should be orthogonal to the nullspace, meaning the projection would be zero. For a significant non-zero value of this projection for a certain state, the observability of that particular state should be questioned.

## Singular Value Decomposition

In order to calculate the matrix rank and nullspace from the observation matrix in *Python*, the function *svd* in the *Scipy* package *Linalg* has been used ([27]). This function is a Python implementation of singular value decomposition (SVD). The function returns the  $U$  and  $V^H$  matrices according to:

$$O = U \Sigma V^H \quad (1.24)$$

It also returns a variable,  $\sigma$ , which is a vector with the diagonal elements of  $\Sigma$ , which consists of the singular values of  $O$ .  $V^H$  denotes the hermitean conjugate, i. e. the conjugate and transponate, of  $V$ .

The number of non-zero singular values, which here means the number of non-zero elements of  $\sigma$ , is equal to the rank of  $O$  ([11]).

To calculate the nullspace projection matrix the rows in  $V^H$  corresponding to the zero-elements of  $\sigma$  are used as columns in a matrix  $A$ . Note that these columns of  $A$  are orthonormal vectors. The projection matrix,  $P$ , is then calculated according to [11], as:

$$P = AA^T \quad (1.25)$$

which means a projection,  $P_v$ , of a vector  $v$  onto the nullspace would be calculated as:

$$P_v = AA^T v \quad (1.26)$$

The tolerance threshold for an element to be considered non-zero has been chosen to  $10^{-3}$  for the implementations and figures evaluated in this thesis, however other values have been investigated as well.

### 1.5.4 Sensitivity

In order to get some insight in how disturbances in the input signals affect the output signal, the system model can be differentiated with respect to the input signals as:

$$H_w = (\nabla_u h(x, u))^T \quad (1.27)$$

The elements of  $H_w$  gives an indication of how much the output signal will be affected by errors in the input signal corresponding to that element.

## 1.6 Method Criticism

### 1.6.1 The Extended Kalman Filter

The Extended Kalman Filter utilizes a linearization around the current point to handle the nonlinear model. This can lead to bad performance when dealing with highly nonlinear models. Also the calculation of the Jacobian for each update can be computationally costly, depending on the problem. [5]

### 1.6.2 Numerical Derivation

The two-point differentiation method performs poorly with even the slightest amount of noise present (assuming a reasonably high sample frequency), and low-pass filtering of the signal before applying it would be a good idea. Both smoothing spline approximation and the Kalman filter approach are more difficult to implement and tuning of design parameters is needed. The type and amount of noise along with the signal dynamics, the sample frequency and the acceptable time delay of the result are all aspects influencing the design parameters, and good knowledge of the signal that is differentiated really helps.

### 1.6.3 Observability

In order to determine if a system is observable, the rank and nullspace are studied. However, observability isn't binary in the sense that a system or a state is either fully observable or not observable at all. States can exchange observability and gradually lose observability. As described in Section 1.5.3.2, a tolerance is used to determine if the singular value for the observability matrix is zero or non-zero. This tolerance affects the interpretation of when the states are observable and not. Worth to mention though, is that the system itself will not be affected by this decision, and the tolerance can be chosen to match the behavior presented by the filter

calculations, for instance through the covariance matrix,  $P$ .

## 1.7 Organization

This master's thesis was made for Transrail Sweden AB (referred to as Transrail only in the rest of this thesis), wherefrom much guidance and experience has been provided. Theoretical knowledge and experience has been provided foremost from the division of Vehicular Systems but also from the division of Automatic Control, both at the Department of Electrical Engineering at Linköping University.

## 1.8 Software

The synthesis and simulations of the models and algorithms in this thesis has been done in the programming language *Python* with the scientific Python library, including primarily *Numpy*, *Scipy* and *Matplotlib*. Together with the *Eclipse IDE*, along with the plug-in module *Pydev*, this forms a substantial environment for mathematical operations similar to Matlab. All the plots, simulations and data analysis during this thesis work has been made with it. The report is written in *OpenOffice.org 3.3*.

## 1.9 Limitations

- The simulations and models provided are only valid for freight trains.
- Limitations from the locomotive manufacturers due to confidentiality:
  - Possibly already available, desired signals can not be used.
  - Information regarding accuracy of the used signals is not provided.
  - More accurate and extensive data from test runs is not available.
- Simulations are limited to make use of the available signals

presented.

- The models used in the simulations are considered to be perfect. No robustness analysis has been made.
- Some approximations and simplifications have been made:
  - Disregarding slip, introducing errors in the tractive force and adhesion models.
  - Assuming no wind.
  - The maximum friction along the track is considered constant.
  - The influence on the adhesion due to curves is not studied.
- Parameter estimation is not performed while breaking.
- Coasting is not explicitly simulated.
- The adhesion model used is only valid when the locomotive operates at the adhesion limit (which only occurs in the case of poor rail conditions).
- Limitations of the recorded data provided:
  - No suitable information in the provided data to perform a data simulation for the adhesion estimation.
  - Low sample rate of 1 Hz.

## 1.10 Report Outline

### Chapter 2: Theoretical Background

In this chapter, the term running resistance and its components in the context of train physics will be described followed by equations for the acceleration and tractive force of a train. Lastly, the concept of adhesion will be presented closer.

### Chapter 3: Signals

This chapter will describe the signals involved. This includes available signals from the train, but also investigations of other possible sources of information. Simulations of the available signals, used in the following chapters, will also be described here.

## **Chapter 4: Running Resistance**

The running resistance equation will be studied closer in this chapter, and a system model for use in an EKF deduced. Parameter estimation for the running resistance will then be thoroughly investigated and simulated, followed by a sensitivity analysis.

## **Chapter 5: Acceleration**

The acceleration of the train is a key signal in the task of parameter estimation for the running resistance. This chapter is therefore dedicated to an investigation of differentiation methods for estimating the acceleration from a velocity signal.

## **Chapter 6: Running Resistance with Acceleration Estimation**

Using data recorded on running trains, it is possible to get an indication of how usable the parameter estimation is in reality. This chapter evaluates results from such recordings with discussions about the possible problems.

## **Chapter 7: Adhesion**

In the same way as for the running resistance, parameter estimation for the available adhesion is investigated in this chapter.

## **Chapter 8: Conclusions & Future Work**

This chapter will wrap up the thesis in a concluding section followed by possible interesting matters to further investigate, called future work.

## **Appendix A: Description of CATO**

In the first appendix is given a brief description of the CATO system developed by Transrail, as described in a leaflet from 2009.

## **Appendix B: Teloc Velocity Measurement**

The second appendix is a more thorough examination of the velocity measurement as performed by the Teloc, and consists mainly of a clipping from the Teloc 1500 manual.



---

# 2

## Theoretical Background

---

In this chapter, the term *running resistance* and its components in the context of train physics will be described followed by equations for the *acceleration* and *tractive force* of a train. Lastly, the concept of *adhesion* will be presented closer.

### 2.1 Running Resistance

Running resistance is the generic term for forces acting on a train against its direction of travel. Among such forces are the resistance due to grades and the resistance caused by air drag, referred to as *grade resistance*,  $F_G$ , and *aerodynamic resistance*,  $F_D$ , respectively. A third category is *mechanical rolling resistance*,  $F_M$ , originating mainly from frictional forces between the wheel and the rail and losses in bearings. Additionally, when a train is accelerating, resistance due to inertia arises, called *inertia resistance*,  $F_I$ . The total running resistance,  $F_{RT}$ , can thus be divided into four parts ([2]):

$$F_{RT} = F_M + F_D + F_G + F_I \text{ [N]} \quad (2.1)$$

The mechanical rolling resistance increases with increasing speed, but it also has a constant part and a component that increment as the train is rounding a curve, called *curve resistance*,  $F_C$ , depending on the curve radius,  $r$ . This can be described as:

$$F_M(v, r) = F_{MA} + F_{MB}(v) + F_C(r) \text{ [N]} \quad (2.2)$$

## 2 Theoretical Background

---

Air resistance also grows with higher speed, both linearly and quadratically, which can be written:

$$F_D(v) = F_{DB}(v) + F_{DC}(v^2) \quad [\text{N}] \quad (2.3)$$

According to Lukaszewicz in [1], writing out the running resistance,  $F_R$ , a bit more in-depth results in:

$$F_R = F_{MA} + F_{MB}(v) + F_{DB}(v) + F_{DC}(v^2) + F_C(r) + F_G(G) \quad [\text{N}] \quad (2.4)$$

The inertia resistance is here omitted and will instead be compensated for in the acceleration and tractive force equations in the following sections. All these forces depend on the train configuration and vary with attributes like masses, lengths, axle loads and types of both locomotive(s) and wagons.

A well-recognized way ([1], [24], [25], [17]) of describing the mechanical resistance and the air drag together is with a second grade polynomial:

$$F_M(v) + F_D(v) = A + Bv + Cv^2 \quad [\text{N}] \quad (2.5)$$

Although, this is not entirely correct, because the curve resistance is part of the mechanical rolling resistance,  $F_M$ , and has to be taken into account. This will be done in the running resistance chapter.

The following equations, (2.6) – (2.10), are the empirically compiled expressions for the individual running resistance components of freight trains according to Lukaszewicz in [1]. The constant part of the mechanical resistance is empirically found to be:

$$F_{MA} = 2000 n_{loco} + \sum_{j=1}^{n_{wag}} (65 + 6 \cdot 10^{-4} Q_j) n_{ax,j} \quad [\text{N}] \quad (2.6)$$

where  $n_{loco}$  is the number of locomotives in the train set,  $n_{wag}$  is the number of wagons,  $Q_j$  the average axle load of each wagon, and  $n_{ax,j}$  the number of axles on wagon  $i$ . The linearly speed dependent part of the running resistance originates from both mechanical and aerodynamic resistance. It comprises what is not covered by the constant and quadratic term in the empirical model and is determined by:

$$F_{MB}(v) + F_{DB}(v) = (-22 + 0.6 L_T) v \quad [\text{N}] \quad (2.7)$$

where  $L_T$  is the total length of the train. Further, the term depending on the second power of the speed is:

$$F_{DC}(v, v_w) = (5.4 + K_D L_T) \left( v^2 + v v_w + \frac{v_w^2}{2} \right) \text{ [N]} \quad (2.8)$$

where  $v_w$  is the wind speed in the longitudinal direction and  $K_D$  depends upon train configuration and vary with how many of the freight wagons that are of uncovered open type compared to covered type. It takes a value according to different percentages of the amount of open type wagons in a train set according to Table 2.1.

Percent open type wagons	$K_D$
0.0 – 12.5	$5.2 \cdot 10^{-2}$
12.5 - 37.5 (25 ± 12.5)	$6.9 \cdot 10^{-2}$
37.5 - 62.5 (50 ± 12.5)	$8.6 \cdot 10^{-2}$
62.5 - 87.5 (75 ± 12.5)	$9.2 \cdot 10^{-2}$
87.5 - 100	$9.7 \cdot 10^{-2}$

*Table 2.1: Values of  $K_D$  for different percentages of open type wagons in a freight train, according to [1].*

The second parenthesis in  $F_{DC}$  is basically the speed relative to the air, in square, but with a modification of the squared wind speed, due to the observed ([1]) impact of measured head and tail wind. Further, the model for resistance due to gradients is:

$$F_G(G) = \sum_{j=1}^{n_{loco} + n_{wag}} g M_j \frac{G_j}{1000} \text{ [N]} \quad (2.9)$$

where  $M_j$  is the individual vehicle mass, and  $G_j$  is the gradient in meters climbed per kilometer traveled, i. e. per mille. Lastly, the curve resistance is determined empirically and approximately by:

$$F_C(r) = \sum_{j=1}^{n_{loco} + n_{wag}} g M_j \frac{0.455}{r_j - 55} \text{ [N]} \quad (2.10)$$

and is only valid for  $r_j \geq 350$  where  $r_j$  is the curve radius in meters.

## 2.2 Acceleration

The equation of motion describing the acceleration,  $a$ , of a train, can be written ([1]):

$$a = \frac{F_w - F_R}{\sum_{j=1}^{n_{loco}} M_j + \sum_{j=1}^{n_{wag}} M_{J,j}} \quad [\text{m/s}^2] \quad (2.11)$$

for a train in *propulsion* (powering), if all axles of the locomotive(s) are driven.  $F_w$  is the propelling force at the wheel rims,  $M$  stands for mass, and  $M_J$  means the mass including the effect of rotary inertia.  $n_{loco}$  is the number of locomotives and  $n_{wag}$  is the number of wagons. Next, the acceleration during *coasting* is calculated by ([1]):

$$a = \frac{-F_R}{\sum_{j=1}^{n_{loco} + n_{wag}} M_{J,j}} \quad [\text{m/s}^2] \quad (2.12)$$

where  $n$  is the total number of vehicles, both locomotives and wagons.

Further ([1]):

$$a = -\frac{F_b + F_R}{\sum_{j=1}^{n_{loco} + n_{wag}} M_{J,j}} \quad [\text{m/s}^2] \quad (2.13)$$

is describing the acceleration during *breaking* (if all axles are broken), where  $F_b$  is the breaking force at the wheel rims. But if the train is breaking regeneratively, the acceleration is determined by ([8]):

$$a = -\frac{F_{reg} + F_R}{\sum_{j=1}^{n_{loco}} M_{J,j} + \sum_{j=1}^{n_{wag}} M_j} \quad [\text{m/s}^2] \quad (2.14)$$

where  $F_{reg}$  is the resistance force from the motors due to regeneration.

## 2.3 Tractive Force

The propulsion force, called *tractive force*,  $F_t$ , is commonly calculated from measurements of motor currents on the locomotive. The real tractive force,  $F_{t,j}$ , at the wheel rims is however somewhat lower than this calculated signal delivered from the measurement equipment, due to influence of rotational inertia in wheels, axles, gear etc. ([1]):

$$F_{t,j}(a) = F_{t,j} - K_{J,j}a(1+\zeta_j) \quad [\text{N}] \quad (2.15)$$

for each driven axle  $j$ , where  $a$  is the acceleration modified with a slippage ratio  $\zeta$ , described closer in the next section, and:

$$K_J = \frac{1}{r_w^2} (u^2 J_{rot} + J_{gear} + J_w) \quad [\text{kg}] \quad (2.16)$$

where  $J_{rot}$ ,  $J_{gear}$  and  $J_w$  is the rotational inertia of rotor, gear and wheel-set, respectively,  $u$  is the gear ratio and  $r_w$  is the wheel radius. The propulsion is however sometimes limited by adhesion so that the final propelling force at the wheel rims is ([1]):

$$F_w = \min(F_{t,j}, F_{ta,max}) \quad [\text{N}] \quad (2.17)$$

where  $F_{ta,max}$ , is the maximum adhesive force described in the following section.

## 2.4 Adhesion

*Adhesion* is a term for the grip between two surfaces, described by an *adhesion coefficient* in the same way as with friction. In this context of train physics it means the part of the wheel-rail-friction in the longitudinal direction that can be used for actual propulsion or deceleration. Adhesion is stochastic to its nature and describes a mutual relationship in a dynamic tribological system, such as speed dependent interaction between wheel-rail, dampers etc. It varies with the roughness of the contact area and the weather, being significantly reduced by water and contamination. Adhesion also tends to decrease with higher train speed as the negative impact of track irregularities on wheel-rail contact increases ([3], [18]). Friction itself,

however, expresses a relationship between just two surfaces.

In order to develop *adhesive forces*, a difference in speed between the periphery of the wheel,  $r_w\omega$ , and the actual train speed,  $v$ , is needed. This speed difference is normally defined as *slip*, or *creep* (according to different researchers slip is sometimes used instead of creep when dealing with accelerating tractive forces). The slip for traction is defined by ([1], [3]):

$$\zeta = \frac{r_w\omega - v}{v} \quad [-] \quad (2.18)$$

and slip for braking by:

$$\upsilon = \frac{v - r_w\omega}{v} \quad [-] \quad (2.19)$$

where  $r_w$  is the wheel radius.

Research ([18], [19], [22], [23]) has shown that adhesion (the adhesion coefficient) is a function of creep (or slip) as shown in Figure 2.1. When the train is in traction, the creep can reach 5%, or even 10% if water or contamination is involved, indicated by Figure 2.2.

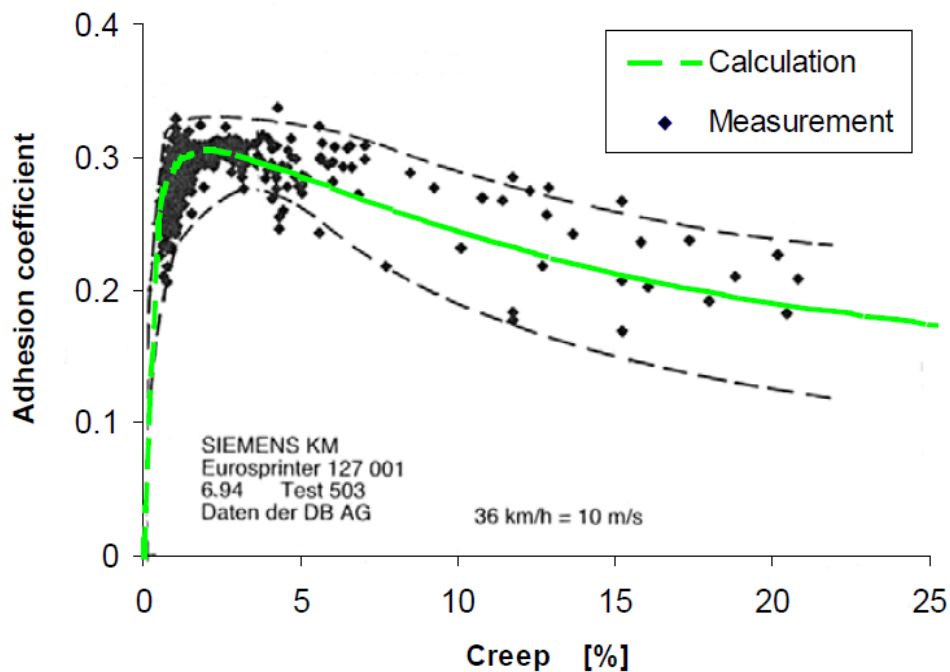


Figure 2.1: Adhesion coefficient as a function of creep. (Image from [18])

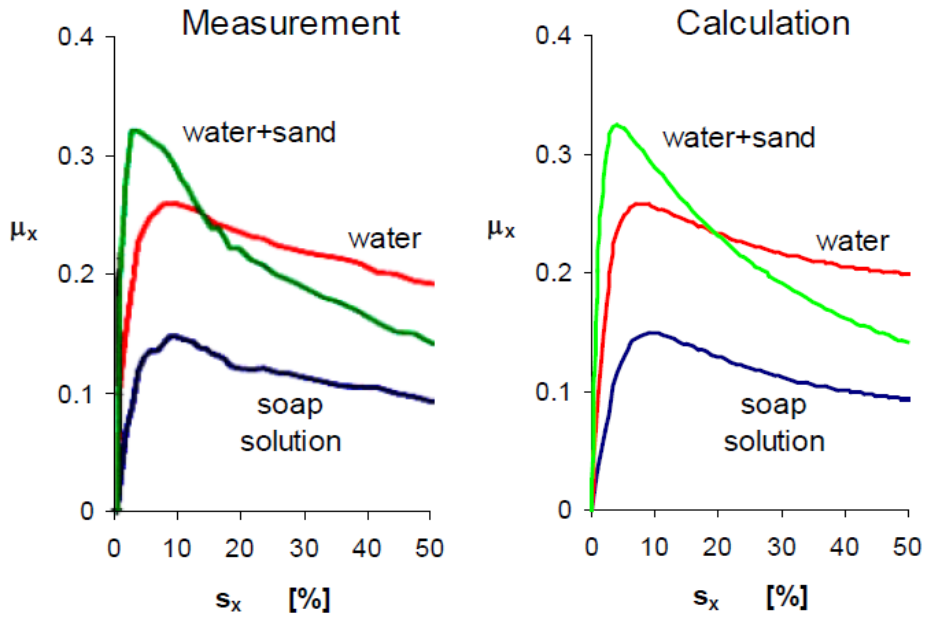


Figure 2.2: Adhesion coefficient ( $\mu_x$ ) as a function of creep ( $s_x$ ) for various adhesion conditions. (Image from [18])

As stated in the previous section, the propelling force is limited by adhesion and can never exceed the maximum adhesive force,  $F_{ta,max}$ , determined by ([1], [3]):

$$F_{t\alpha,max,j}(v, \mu_{max}) = Q_j \alpha_{max,j}(v, \mu_{max}) \quad [\text{N}] \quad (2.20)$$

for each axle  $j$ , where  $Q$  is the axle load and  $\alpha_{max}$  is the maximum adhesion. The maximum adhesion as a function of speed is determined for this work by ([8]):

$$\alpha_{max}(v, \mu_{max}) = \mu_{max} \kappa \left( X + \frac{1}{Y + Z v} \right) \quad [-] \quad (2.21)$$

where  $\mu_{max}$  describes the current maximum wheel-rail-friction, depending on the texture and condition of the contact area that varies with weather, roughness and contamination.  $\kappa$  is a vehicle specific constant dependent on the slip control and its ability to stay close to the maximum friction.  $X$ ,  $Y$  and  $Z$  are the model parameters. As indicated by this model and stated above, the maximum available adhesion will decrease with increasing speed.



---

# 3

## Signals

---

This chapter will describe the signals involved. This includes available signals from the train, but also investigations of other possible sources of information. Simulations of the available signals, used in the following chapters, will also be described here.

### 3.1 Available Data

The following signals of use are available from a computer on board the train:

$v$	Speed of the train. [m/s]
$F_t$	Tractive force. [N]
$r$	Curve radius of track from the BIS database. [m]
$G$	Gradient of track from the BIS database. [‰]

#### 3.1.1 Teloc

The *speed* and the *tractive force* is provided by the measurement equipment on board the train. Teloc 2200 and Teloc 2500, developed by HaslerRail AG in Switzerland, are measurement instruments commonly used in many freight and ore locomotives in Sweden. According to the Teloc 1500 manual,

### 3 Signals

---

[13], the speed is measured with a pulse generating sensor on one or several of the train's axles, producing an analogue signal with the minimum sample time of 20 ms. The Teloc 2500 is functionally identical to the Teloc 1500 ([28]). See Appendix B for a clipping from the Teloc 1500 manual and formulas for speed calculation.

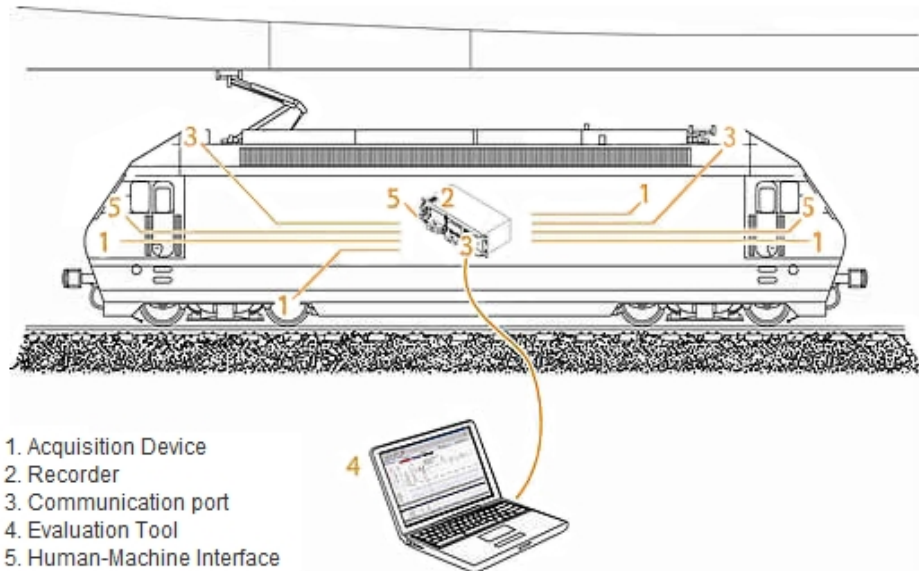


Figure 3.1: Data acquisition system. (Image from HaslerRail AG)

If the speed is measured on one or several *driven* axles, during propulsion, it may deliver an up to 10% too high value, due to creep (see Section 2.4).

According to [30], often two separate speed sensors are used, one on a driven, one on a non-driven axle. The two speed signals are then compared. For safety reasons the calculated train speed is usually the one whichever is higher. But it's also possible to configure the speed calculation taking the higher speed when decelerating or the slower of the two speeds when accelerating. "It's the customer who decides" says Philipp Gerber at HaslerRail AG, Bern, Switzerland.

This is however not the case for freight trains according to [8], where locomotives are re-coupled often with different wagon sets, and measurement of the speed is only performed on the axles of the locomotive, i. e. driven axles.

In a recording from a running train of the Teloc speed signal it was found to have a resolution of  $2.8 \cdot 10^{-3}$  m/s (0.01 km/h).

The tractive force is not a directly measured signal but calculated from the motor current and merged with the braking effort. The Teloc will also create an acceleration signal from the velocity measurement using the simple two-point differentiation method (see Appendix B for details). But, as described in this thesis, there are better ways to calculate the acceleration.

### 3.1.2 BIS

*BIS* is a database that is provided by the Swedish Transport Administration (Trafikverket) and consists of information such as track data on curves and grades for different sections of the Swedish railway. The database can be accessed on board a train to get information about the track at the current as well as future positions of the train.

### 3.1.3 GPS

With a *GPS* (Global Positioning System) device – time, position, speed and altitude can be measured independent of the measurement equipment on board the train. A couple of recordings of such GPS signals from running trains were analyzed, and the GPS used gave a resolution for the speed of  $2.8 \cdot 10^{-5}$  m/s ( $10^{-4}$  km/h). The accuracy of the particular GPS device used is not known. However, sources ([31]) indicates that GPS devices can offer speed measurement with an accuracy of at least 0.1 m/s, a number decreasing due to the fast development in the area.

If the GPS device used is able to give an altitude signal with good accuracy, this signal could be a valuable complement to the gradient data from BIS. A signal recording that was provided by Transrail containing both track data from BIS *and* GPS signals was processed for evaluation. The altitude signal was first filtered and gradient values was then created from it and compared to the BIS data, for a section of the recorded run. The result can be seen in Figure 3.2, showing good agreement between the two and indicates the potential of using both signals to increase the accuracy using sensor fusion (utilizing for example the Kalman filter).

It might be possible to calculate the curve radius in an equivalent manner, from the longitude and latitude GPS signals. Taking at least 3 subsequent position points, a radius can be computed. This is not evaluated in this thesis.

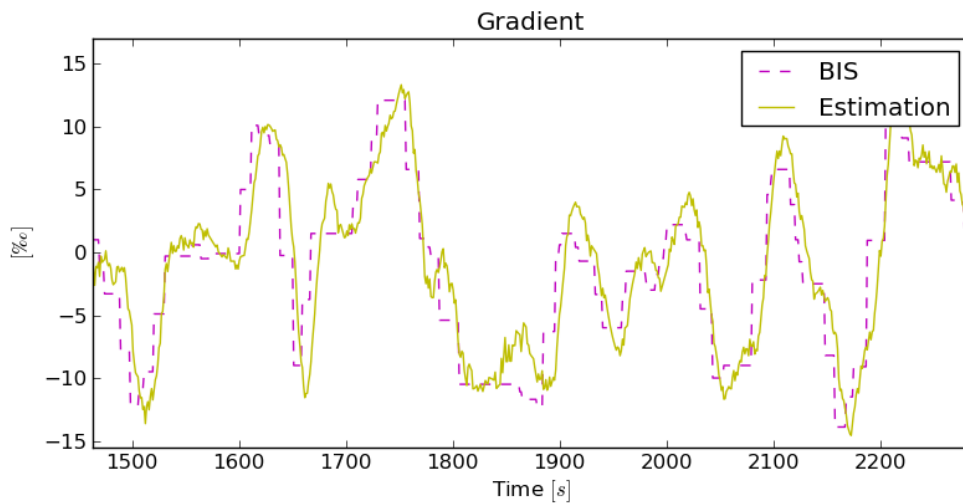


Figure 3.2: Gradient signal as provided by BIS together with grades calculated from a GPS altitude signal, called Estimation.

## 3.2 Test Signals for Simulation

### 3.2.1 Speed & Acceleration

When recorded data of running freight trains was analyzed, the maximum running speed was 15-20 m/s, depending on whether the train was loaded or empty, the acceleration peaked at about 0.15 m/s<sup>2</sup> and the sample time was approximately 1 second. For testing purposes in simulation, a simple function of the speed is created as half of a sin<sup>2</sup>(t) period with a top value of 20 over a time span of about 6 min to match the peak acceleration of 0.15:

$$v(t) = 20 \cdot \sin^2\left(\frac{\pi t}{360}\right) \text{ [m/s]} \quad (3.1)$$

However, it is desired to have a total period of simulation time of much longer than 6 min. Taking an hour would result in 10 drives as shown in Figure 3.3 where the acceleration has been scaled with a factor 10 for visual reasons.

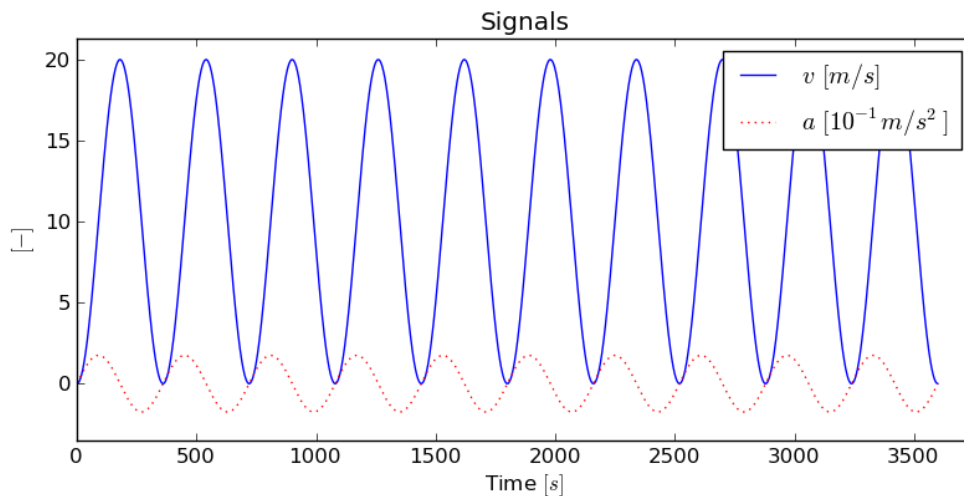


Figure 3.3: Speed and corresponding acceleration for simulation. The acceleration is scaled 10 times for visual reasons.

### 3.2.2 Tractive Force

Mathematical models are derived, in the case of the running resistance as well as the adhesion, that describe the tractive force as a function of the other signals. The tractive force signal,  $F_t$ , is therefore created online in each simulation. This results in coasting not being explicitly simulated.

### 3.2.3 Gradient & Curve Radius

The gradient and curve radius signals are, as mentioned, not measured but taken from a database. These are both step functions with sections of constant values. In the analyzing of recorded data, the gradient signal,  $G$ , varied approximately between -12 and 12 per mille (where positive values represent back slopes), and the curve radius signal,  $r$ , varied roughly between 400 and 15,000. Negative values represent curves to one side and positive to the other, although a radius can not be negative, all values are considered positive. The value zero for  $r$  represent infinite radius.

These intervals are not to be taken as a precise investigation of the signal boundaries, but are only interesting for producing realistic signals in simulation. A track database for testing purposes is produced for the 36 km distance of the simulation. This database has two curves, one to the left and one to the right, and a couple of slopes.

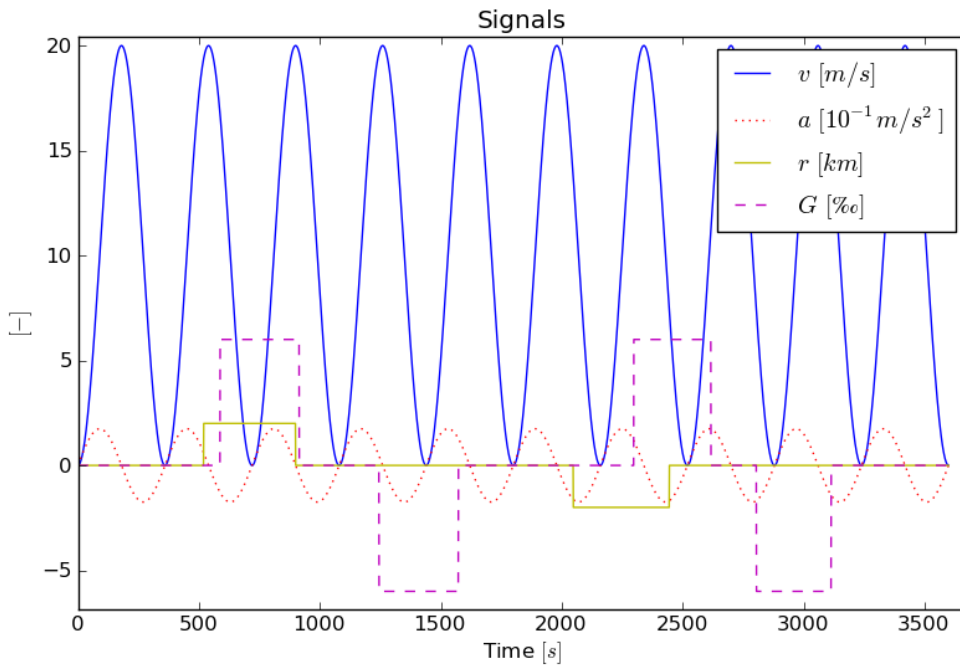


Figure 3.4: The input signals for simulation: speed, acceleration, curve radius and gradient.

Running a simulation along this track with the velocity as described above, reading the gradients and curve radii along the way, will show these signals in relation to the simulation time and the speed as in Figure 3.4, where the curve radius is shown in kilometers, and the acceleration multiplied by 10, for visual reasons.

#### 3.2.4 Train Configuration

The train used in all simulations is a 52 wagon ore train with 2 locomotives. The data of the wagons are according to a common Swedish ore car, called *Uad*, with 4 axles of 25 ton maximum axle load, 8.4 meters in length, air drag corresponding to 100% open type, and the extra mass accounting for rotary inertia is 850 kg. [8]

The two locomotives are considered being of type *IORE* which are often coupled two after each other in long freight train configurations. An *IORE* is 22.9 meter long, has 6 axles, all driven, weights 180 ton, considered being of 100% covered type, and the added mass accounting for rotary inertia is 26 ton. The value for  $K_j$ , calculated as (2.16), is approximately 4,333 kg per axle ([8]). The total length of this train is 482.6 m and the total weight is 5,560 ton.



*Figure 3.5: Standard ore train configuration in north of Sweden, with two IORE locomotives followed by 52 ore wagons. (Pictures taken by David Gubler on the route Abisko – Stordalen)*



---

# 4

## Running Resistance

---

The running resistance equation will be studied closer in this chapter, and a system model for use in an EKF deduced. Parameter estimation for the running resistance will then be thoroughly investigated, followed by a sensitivity analysis.

### 4.1 The Running Resistance Model

Instead of declaring the running resistance with respect to the physical interpretation, as described in Section 2.1, the total running resistance can be described with respect to the available signals, described in Section 3.1:

$$F_R(v, r, G) = F_v(v) + F_C(r) + F_G(G) \quad [\text{N}] \quad (4.1)$$

where  $F_v$  is speed dependent,  $F_C$  is curve radius dependent and  $F_G$  is the gradient dependent part. In Section 2.1 a way of describing the speed dependency of the running resistance is found:

$$F_v(v) = A + Bv + Cv^2 \quad [\text{N}] \quad (4.2)$$

with a constant part,  $A$ ;  $B$  for the speed dependent part; and the parameter  $C$  for the part depending on the speed in square. Together with the models for gradient resistance and curve resistance, the total running resistance model becomes:

$$F_R(v, r, G) = A + Bv + Cv^2 + \sum_{j=1}^{n_{loco}+n_{wag}} \frac{DgM_j}{r_j+E} + \sum_{j=1}^{n_{loco}+n_{wag}} gM_j \frac{G_j}{1000} \text{ [N]} \quad (4.3)$$

with parameters  $D$  and  $E$  in the curve resistance model.  $M_j$  is the individual vehicle mass,  $n_{loco}$  and  $n_{wag}$  are the number of locomotives and wagons in the train configuration respectively, and  $r_j$  and  $G_j$  are the curve radius and gradient signals, calculated individually for each vehicle.  $g$  is the gravitational acceleration in Stockholm ( $9.818 \text{ m/s}^2$ ).

Sometimes ([3], [17], [24]) gradient resistance and curve resistance is defined with the train regarded as one center of mass, with models then becoming simply:

$$F_G(G) = gM_T \frac{G}{1000} \text{ [N]} \quad (4.4)$$

$$F_C(r) = gM_T \frac{D}{r+E} \text{ [N]} \quad (4.5)$$

with  $M_T$  being the total mass of the train.

In Figure 4.1 a simple simulation of the curve resistance for these different approaches shows the size of the error that the latter models will spawn. With the error of course depending on the length of the train. A short train will not give such large error as the 52 wagon train used in this simulation. The grade resistance will have the same typical behavior (with the difference that it can be negative). The signals used in the simulation is shown in Figure 4.2.

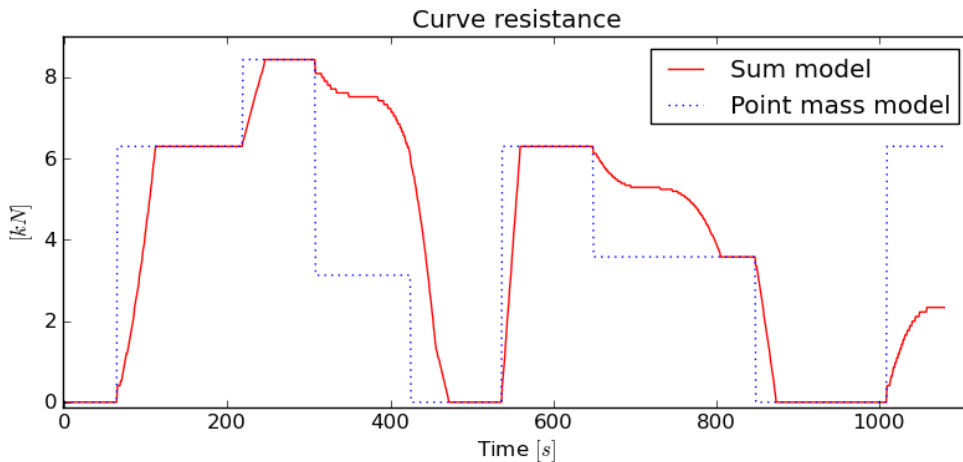


Figure 4.1: Simulation of curve resistance comparing point mass model to the more accurate sum model.

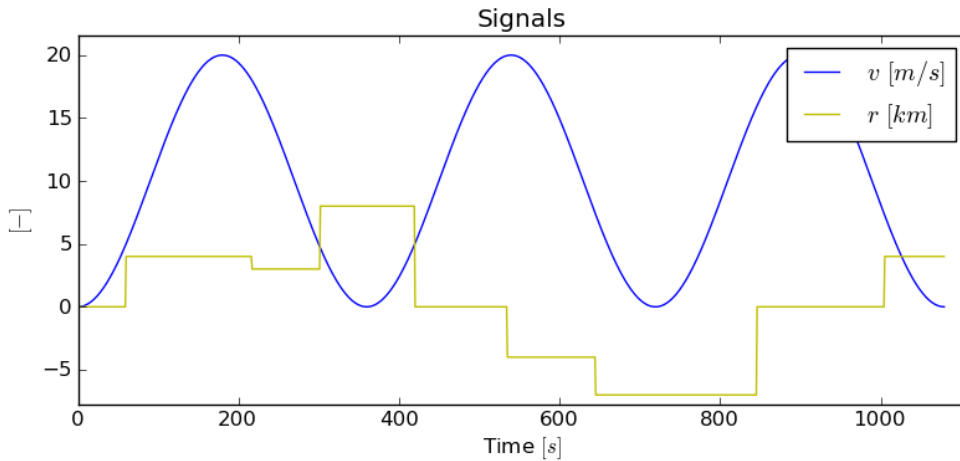


Figure 4.2: Signals for the curve resistance simulation of point mass model and sum model.

Regarding the gradient resistance model, it is also common ([3], [15]) to see it defined as:

$$F_G(\beta) = g M_T \sin(\beta) \quad [\text{N}] \quad (4.6)$$

where  $\beta$  is the angle between the track and the horizontal plane, calculated from the gradient signal as:

$$\beta(G) = \arcsin\left(\frac{G}{1000}\right) \quad (4.7)$$

This is obviously identical to (4.4), as  $G$  is describing the height climbed in meters per kilometer track traveled.

## 4.2 Deducing a System Model

The running resistance is not measured directly, instead it is observed indirectly via the tractive force signal, making a few limitations and simplifications described below.

First, if the available adhesion is high compared to the tractive effort, far from the situation where the slip control system has to intervene, the propelling force at the wheel rims will be equal to the tractive force:

$$F_w = F_{\omega} \quad (4.8)$$

#### 4 Running Resistance

---

This will of course only be valid in traction, and not when the train is in breaking mode. When coasting, this will be valid also, because both will be equal to zero. Taking Equations (2.11) and (2.12) describing the acceleration of a train during traction and coasting, and with the assumption made above, combining them with Equation (2.15) for the tractive force, a relation between the tractive force and the running resistance is acquired:

$$a = \frac{\left( F_t - \sum_{j=1}^{n_d} K_{J,j} a (1 + \zeta_j) \right) n_{trac} - F_R(v, r, G)}{n_{trac} \sum_{j=1}^{n_{loco}} M_j + \sum_{j=1}^{n_{wag}} M_{J,j} + (1 - n_{trac}) \sum_{j=1}^{n_{loco}} M_{J,j}}, \quad F_t \geq 0 \quad [\text{m/s}^2] \quad (4.9)$$

where  $n_{trac}$  indicates traction by:

$$n_{trac} = \begin{cases} 0, & F_t = 0 \quad (\text{coasting}) \\ 1, & F_t \neq 0 \quad (\text{traction}) \end{cases} \quad (4.10)$$

Second, assuming high adhesion, the simplification of removing the factor  $(1 + \zeta)$  is made. If the adhesion is very low it can be up to 10%, however in this case of very low slip, it is assumed to be only a few percent. Another reason for removing it is simply that the slip is not among the available signals (described in Section 3.1), therefore no information exists about the slippage ratio.

Finally, extracting  $F_t$  in (4.9):

$$F_t(v, a, r, G) = F_R(v, r, G) + a \gamma, \quad F_t \geq 0 \quad [\text{N}] \quad (4.11)$$

with

$$\gamma = n_{trac} \sum_{j=1}^{n_{loco}} M_j + \sum_{j=1}^{n_{wag}} M_{J,j} + (1 - n_{trac}) \sum_{j=1}^{n_{loco}} M_{J,j} + n_{trac} K_J \quad [\text{kg}] \quad (4.12)$$

$$K_J = \sum_{j=1}^{n_d} K_{J,j} \quad [\text{kg}] \quad (4.13)$$

and  $n_{trac}$  as (4.10), using  $F_R$  from (4.3) this will serve as the system model in the following sections.

### 4.3 Initial Parameter Values

It is important to have good initial values for the state variables in extended Kalman filtering ([6]), which is used in the following sections. In this case, the initial values for the parameters  $A$  to  $E$  can be found in the equations in Section 2.1:

$$A = 2000 n_{loco} + \sum_{j=1}^{n_{wag}} (65 + 6 \cdot 10^{-4} Q_j) n_{ax,j} \quad [\text{N}] \quad (4.14)$$

$$B = 0.6 L_T - 22 \quad [\text{kg/s}] \quad (4.15)$$

$$C = 5.4 + K_D L_T \quad [\text{kg/m}] \quad (4.16)$$

$$D = 0.455 \quad [\text{m}] \quad (4.17)$$

$$E = -55 \quad [\text{m}] \quad (4.18)$$

The value of  $K_D$  could be looked up in Table 2.1, but performing quadratic regression on that table a formula is acquired:

$$K_D = -0.04 x^2 + 0.0852 x + 0.0516 \quad [\text{kg/m}^2] \quad (4.19)$$

where  $x$  denotes the amount of open type wagons (0-1).

### 4.4 Online Identification

In order to get the parameters in the model for the running resistance to adapt to a running train, Extended Kalman Filtering (EKF) is used to continually get estimations for the parameters. See Section 1.5.1 for details on Kalman filtering. EKF is deemed appropriate since it is a very common approach to handle nonlinear models. UKF is also a possible approach, which here has been considered a possible solution path, should the implementations show indication of problems relating to the choice of method. However, the problems that arise in this section are not deemed to be related to this choice.

As described in Section 3.1, the available signals are speed ( $v$ ), gradient ( $G$ ), curve radius ( $r$ ) and tractive force ( $F_t$ ), with  $F_t$  being the reference signal. But

the system model, Equation (4.11), includes also the acceleration,  $a$ , which is not among the available signals, and this will turn out to be the big challenge in the task of parameter estimation for the running resistance.

The parameters are not expected to vary much in time for the simulations made in this section, the problem considered is rather that the models and parameters can vary for different train configurations. This means that the parameters are expected to lie somewhat steady once they reach their correct value for a certain train configuration. However, it is important to keep in mind that, in reality, disturbances such as for instance wind can affect the train configuration differently over time, which could result in varying parameters.

The assumption of non-varying parameters means that simulations can be done by creating a train that differs from the initial parameters (See Section 4.3), and letting the estimated parameters converge to the parameters of the differing train. In the evaluation simulations of the extended Kalman filters below, the “real” train is assumed to differ in the parameters from the initial values by 10%.

The filters are simulated with the standard simulation environment described in Section 3.2. The filters run continuously, even while breaking. In the realistic case, the used model for tractive force (4.11) is not defined for breaking, however to purely evaluate the observability and theoretical aspects of the filter performance it is easier to study these behaviors without turning the filter off for those special cases. In the following investigations the models used are assumed to be absolutely correct, even for breaking. This means no errors will be seen in the simulations as a result of this decision.

### 4.4.1 A First Approach: EKF with 7 States

A first approach would be to choose the parameters  $A$  to  $E$  as state variables in the EKF, along with a state for the speed and one for the acceleration in order for the filter to also make estimations for these. The state vector,  $x$ , signals,  $u$ , and reference signals,  $y$ , becomes:

$$x = \begin{pmatrix} A \\ B \\ C \\ D \\ E \\ x_v \\ x_a \end{pmatrix} \quad u = \begin{pmatrix} v \\ r \\ G \end{pmatrix} \quad y = \begin{pmatrix} v \\ F_t \end{pmatrix} \quad (4.20)$$

where  $x_v$  is the state for the speed and  $x_a$  the state for the acceleration. Having the speed as a state allows for the acceleration to be integrated into this state and then compared to the speed regarded as a reference signal. The time update of the states becomes:

$$f(\hat{x}_{k|k}, 0) = \begin{pmatrix} \hat{A}_{k|k} \\ \hat{B}_{k|k} \\ \hat{C}_{k|k} \\ \hat{D}_{k|k} \\ \hat{E}_{k|k} \\ \hat{x}_{v|k} + \hat{x}_{a|k} \Delta t \\ \hat{x}_{a|k} \end{pmatrix} \quad (4.21)$$

Or, described as the matrix  $F$ :

$$F = \begin{pmatrix} 1 & 0 & 0 & 0 & 0 & 0 & 0 \\ 0 & 1 & 0 & 0 & 0 & 0 & 0 \\ 0 & 0 & 1 & 0 & 0 & 0 & 0 \\ 0 & 0 & 0 & 1 & 0 & 0 & 0 \\ 0 & 0 & 0 & 0 & 1 & 0 & 0 \\ 0 & 0 & 0 & 0 & 0 & 1 & \Delta t \\ 0 & 0 & 0 & 0 & 0 & 0 & 1 \end{pmatrix} \quad (4.22)$$

where  $\Delta t$  is the time elapsed since the last update:

$$\Delta t = t_k - t_{k-1} \text{ [s]} \quad (4.23)$$

The system model function  $h$  will correspond to the measurement signals,  $y$  in (4.20), with the speed state for the speed and the system model from (4.11) for the tractive force reference signal:

$$h(\hat{x}_{k|k-1}, u_k) =$$

$$\left( \begin{array}{c} \hat{x}_v \\ \hat{A}_{k|k-1} + \hat{B}_{k|k-1} v_k + \hat{C}_{k|k-1} v_k^2 + \sum_{j=1}^{n_{\text{loco}}+n_{\text{wag}}} \frac{\hat{D}_{k|k-1} g M_j}{r_{j,k} + \hat{E}_{k|k-1}} + F_G(G_k) + \hat{x}_{a,k|k-1} \mathcal{Y} \end{array} \right) \quad (4.24)$$

Deducing  $H$  from this yields:

$$H = \left( \begin{array}{ccccccc} 0 & 0 & 0 & 0 & 0 & 1 & 0 \\ 1 & v_k & v_k^2 & \sum_{j=1}^{n_{\text{loco}}+n_{\text{wag}}} \frac{g M_j}{r_{j,k} + \hat{E}_{k|k-1}} & \sum_{j=1}^{n_{\text{loco}}+n_{\text{wag}}} \frac{-\hat{D}_{k|k-1} g M_j}{(r_{j,k} + \hat{E}_{k|k-1})^2} & 0 & \mathcal{Y} \end{array} \right) \quad (4.25)$$

The filter will be updated according to Section 1.5.1.1 and can be tuned with the design-parameters  $Q$  and  $R$ , which are here chosen as:

$$Q = \left( \begin{array}{ccccccc} 3000 & 0 & 0 & 0 & 0 & 0 & 0 \\ 0 & 100 & 0 & 0 & 0 & 0 & 0 \\ 0 & 0 & 20 & 0 & 0 & 0 & 0 \\ 0 & 0 & 0 & 0.001 & 0 & 0 & 0 \\ 0 & 0 & 0 & 0 & 0.001 & 0 & 0 \\ 0 & 0 & 0 & 0 & 0 & 0.1 & 0 \\ 0 & 0 & 0 & 0 & 0 & 0 & 0.001 \end{array} \right) \quad R = \left( \begin{array}{cc} 5 \cdot 10^4 & 0 \\ 0 & 1 \end{array} \right) \quad (4.26)$$

The original model for running resistance (4.3) together with the estimated parameters provide an estimation for the current running resistance as:

$$\begin{aligned} \hat{F}_{R,k|k}(v_k, r_k, G_k) &= \\ &= \hat{A}_{k|k} + \hat{B}_{k|k} v_k + \hat{C}_{k|k} v_k^2 + \sum_{j=1}^{n_{\text{loco}}+n_{\text{wag}}} \frac{\hat{D}_{k|k} g M_j}{r_{j,k} + \hat{E}_{k|k}} + F_G(G_k) \quad [\text{N}] \end{aligned} \quad (4.27)$$

with  $F_G(G_k)$  as (2.9).

#### 4.4.1.1 Results

The parameter values estimated by the filter does not show any real indication of converging towards their real values as can be seen in Figure

4.3. Note that the parameters are normalized.

#### 4.4.1.2 Observability

A closer look at (4.12) shows that the term  $\gamma$  actually only depends on constants and the term  $n_{trac}$ , which only changes binary between 0 (while coasting) and 1 (during traction). This means that for the majority of the runtime,  $\gamma$  is constant.

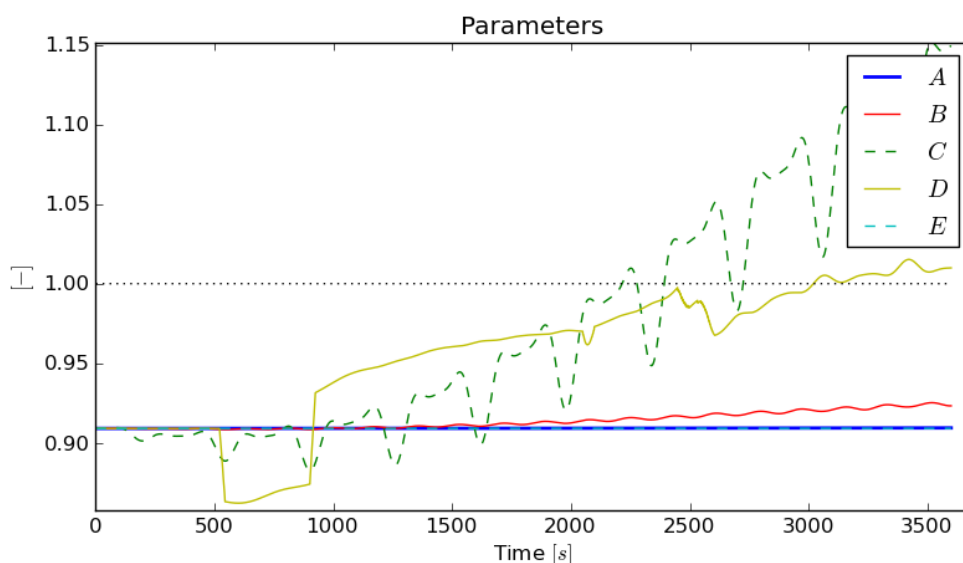


Figure 4.3: The estimated parameters for the 7 state EKF.

Further investigation of the matrix  $H$  (4.25) reveals that problems with observability will arise if  $\gamma$  is constant since the first and last columns of  $H$  will represent the same direction. This means the measured signal will not be able to separate the two states  $A$  and  $x_a$ .

It's also possible to simulate the filter and investigate the covariance matrix and observability as described in Section 1.5.3.1. The variances of the states increase more or less linearly for all states except the non-parameter states  $x_v$  and  $x_a$ , as can be seen in Figure 4.4. Note that the variances are normalized. This lack of observability indicates that the measured signals does not provide enough information to estimate the states desired.

#### 4.4.1.3 Possible Solution

One way to increase the possibility to get observability and converging

parameters is to reduce the number of states estimated by the EKF. Since  $A$  is an important parameter to estimate and can not be separated from  $x_a$ , one approach is to remove the state  $x_a$  and thereby not estimating the acceleration. This renders the state  $x_v$  useless since the only purpose for it was to provide a relation between the acceleration and the speed. The conclusion would be to remove both  $x_a$  and  $x_v$  as states.

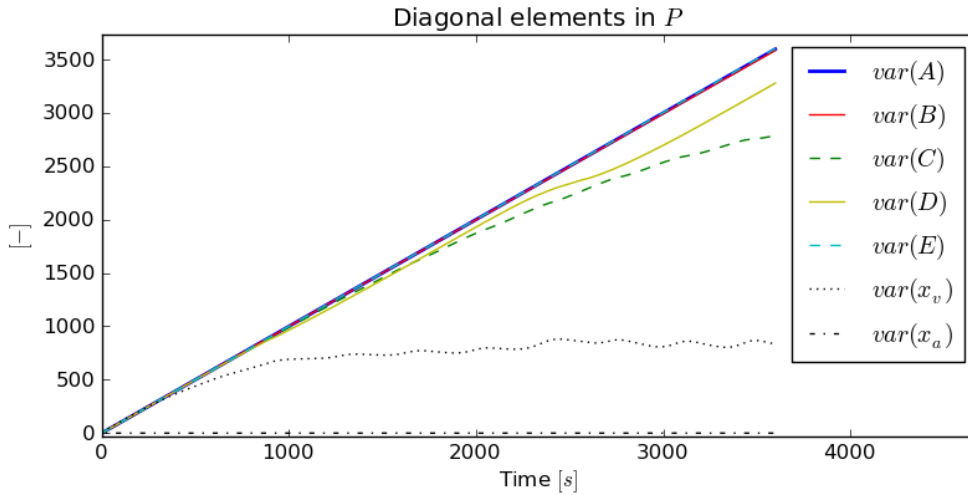


Figure 4.4: The normalized variances of the seven states in the EKF.

This decision also results in removal of the speed as reference signal since it is of no use anymore. This can be seen mathematically by examining the  $H$ -matrix in (4.25). The first row of  $H$  will consist of only zeros if the last two columns were to be removed. This means there is no longer a connection between any model and the reference signal  $v$ .

#### 4.4.2 Removing States $x_a$ & $x_v$

Instead of estimating the acceleration, it could be regarded as an input signal to the system. Since the only available signal related to the acceleration would be the speed, derivation of this signal would be needed. This will be discussed more in depth in Chapter 5.

The new filter with reduced states would have the following state-vector, input signals and reference signal:

$$x = \begin{pmatrix} A \\ B \\ C \\ D \\ E \end{pmatrix} \quad u = \begin{pmatrix} v \\ a \\ r \\ G \end{pmatrix} \quad y = F_t \quad (4.28)$$

The time update of the states becomes:

$$f(\hat{x}_{k|k}, 0) = \begin{pmatrix} \hat{A}_{k|k} \\ \hat{B}_{k|k} \\ \hat{C}_{k|k} \\ \hat{D}_{k|k} \\ \hat{E}_{k|k} \end{pmatrix} \quad (4.29)$$

Or, described as the matrix  $F$ :

$$F = \begin{pmatrix} 1 & 0 & 0 & 0 & 0 \\ 0 & 1 & 0 & 0 & 0 \\ 0 & 0 & 1 & 0 & 0 \\ 0 & 0 & 0 & 1 & 0 \\ 0 & 0 & 0 & 0 & 1 \end{pmatrix} \quad (4.30)$$

If the first reference signal, the speed, is removed, the following system model is what remains:

$$h(\hat{x}_{k|k-1}, u_k) = \hat{A}_{k|k-1} + \hat{B}_{k|k-1} v_k + \hat{C}_{k|k-1} v_k^2 + \sum_{j=1}^{n_{loco}+n_{wag}} \frac{\hat{D}_{k|k-1} g M_j}{r_{j,k} + \hat{E}_{k|k-1}} + F_G(G_k) + a \gamma \quad (4.31)$$

This means that  $H$  becomes:

$$H = \left( 1 \quad v_k \quad v_k^2 \quad \sum_{j=1}^{n_{loco}+n_{wag}} \frac{g M_j}{r_{j,k} - \hat{E}_{k|k-1}} \quad \sum_{j=1}^{n_{loco}+n_{wag}} \frac{-\hat{D}_{k|k-1} g M_j}{(r_{j,k} + \hat{E}_{k|k-1})^2} \right) \quad (4.32)$$

The filter will be updated according to Section 1.5.1.1 and can be tuned with the design-parameters  $Q$  and  $R$ , which are here chosen as:

$$Q = \begin{pmatrix} 3000 & 0 & 0 & 0 & 0 \\ 0 & 100 & 0 & 0 & 0 \\ 0 & 0 & 20 & 0 & 0 \\ 0 & 0 & 0 & 0.001 & 0 \\ 0 & 0 & 0 & 0 & 0.001 \end{pmatrix} \quad R = 5 \cdot 10^4 \quad (4.33)$$

Using the estimated parameters an estimation for the current running resistance could also here be calculated with (4.27).

#### 4.4.2.1 Results

Being simulated with the standard simulation environment described in Section 3.2, the parameter behavior can be seen in Figure 4.5. Note that the parameters are normalized. As can be seen, all parameters actually move towards their real values except for the parameter  $E$ .

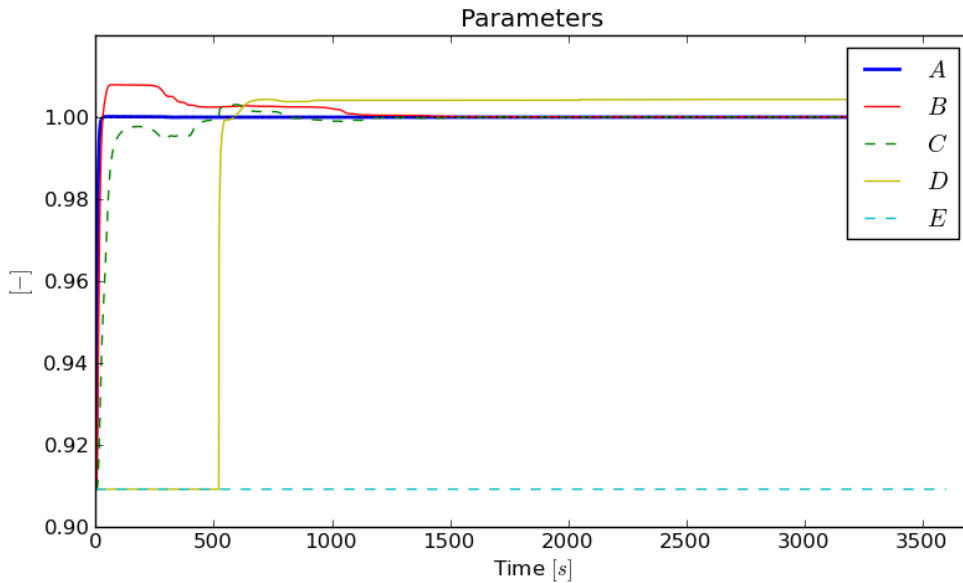


Figure 4.5: The parameter behavior for the 5 state EKF.

#### 4.4.2.2 Observability

As expected, studying the  $P$ -matrix, the variance of parameter  $E$  is increasing linearly, which indicates lack of observability (Figure 4.6).

Studying the nullspace of the observation matrix as described in Section 1.5.3.2 it is possible to see that the base-vector of state  $E$  constantly is a null-

direction (Figure 4.7).

The conclusion is that  $E$  is not observable with the presented model and reference signal for the given simulation.

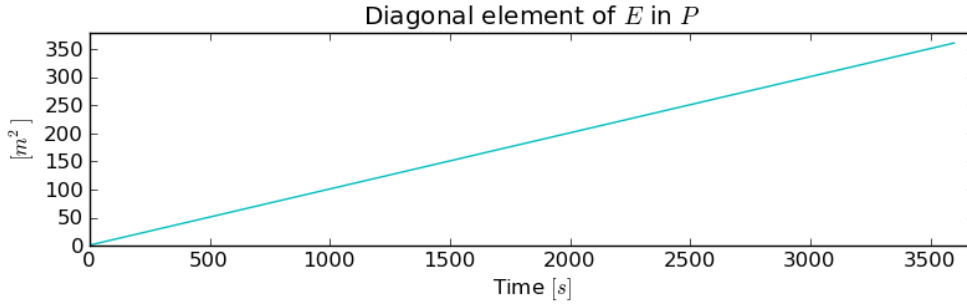


Figure 4.6: The variance of parameter  $E$ .

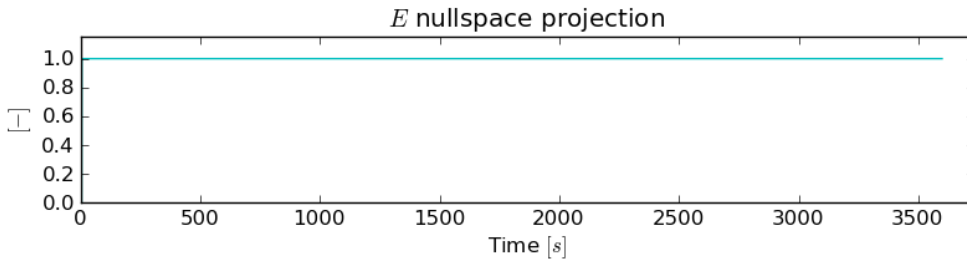


Figure 4.7: The nullspace projection of parameter  $E$ .

#### 4.4.2.3 Possible Solution

Since  $E$  is not observable and only acting as an offset for the input signal,  $r$ ; it is deemed appropriate to freeze it to its initial value according to Section 4.3 and thereby reducing the number of estimated states.

#### 4.4.3 Removing State $E$

This new approach is a filter with 4 states. The new state-vector, input-signals and reference signal are:

$$x = \begin{pmatrix} A \\ B \\ C \\ D \end{pmatrix} \quad u = \begin{pmatrix} v \\ a \\ r \\ G \end{pmatrix} \quad y = F_t \quad (4.34)$$

The time update of the states becomes:

$$f(\hat{x}_{k|k}, 0) = \begin{pmatrix} \hat{A}_{k|k} \\ \hat{B}_{k|k} \\ \hat{C}_{k|k} \\ \hat{D}_{k|k} \end{pmatrix} \quad (4.35)$$

Or, described as the matrix  $F$ :

$$F = \begin{pmatrix} 1 & 0 & 0 & 0 \\ 0 & 1 & 0 & 0 \\ 0 & 0 & 1 & 0 \\ 0 & 0 & 0 & 1 \end{pmatrix} \quad (4.36)$$

Using the system model according to (4.31) and freezing the  $E$ -parameter to its initial estimation ( $\hat{E}_0$ ) from Section 4.3 yields  $H$  as:

$$H = \begin{pmatrix} 1 & v_k & v_k^2 & \sum_{i=1}^{n_{loco}+n_{wag}} \frac{g M_j}{r_{j,k} + \hat{E}_0} \end{pmatrix} \quad (4.37)$$

The filter will be updated according to Section 1.5.1.1 and can be tuned with the design-parameters  $Q$  and  $R$ , which are here chosen as:

$$Q = \begin{pmatrix} 3000 & 0 & 0 & 0 \\ 0 & 100 & 0 & 0 \\ 0 & 0 & 20 & 0 \\ 0 & 0 & 0 & 0.001 \end{pmatrix} \quad R = 5 \cdot 10^4 \quad (4.38)$$

Using the estimated parameters an estimation for the current running resistance could also here be calculated with (4.27).

#### 4.4.3.1 Results

The filter manages to estimate the parameters  $A$ ,  $B$ ,  $C$  and  $D$  with a certain accuracy, which can be seen in Figure 4.8. After about 1,200 seconds of simulation, the parameter deviation from the real values are lower than 0.5% for all parameters as seen in Figure 4.9. One explanation for this seemingly long time is observability, as described in Section 4.4.3.2. The important result though, is that the parameters seem to converge toward their correct values with time.

The parameter  $D$  lies steady at its initial value for some time, after which it at around 500 seconds run-time quickly changes towards the correct estimation. The reason for this is that the first curve appears first at this particular time. This can be seen in Figure 3.4 which displays the input signals of the simulation.

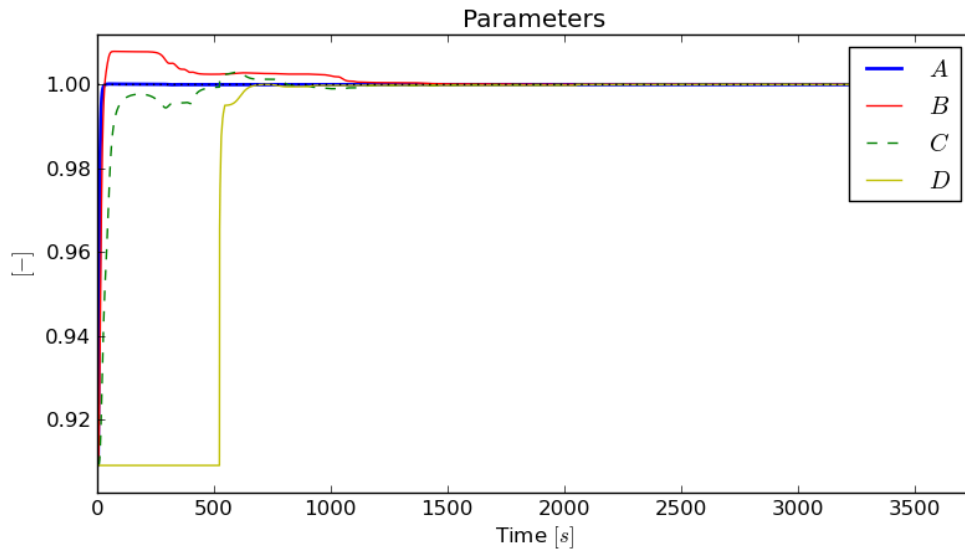


Figure 4.8: The parameter behavior for the EKF with 4 states.

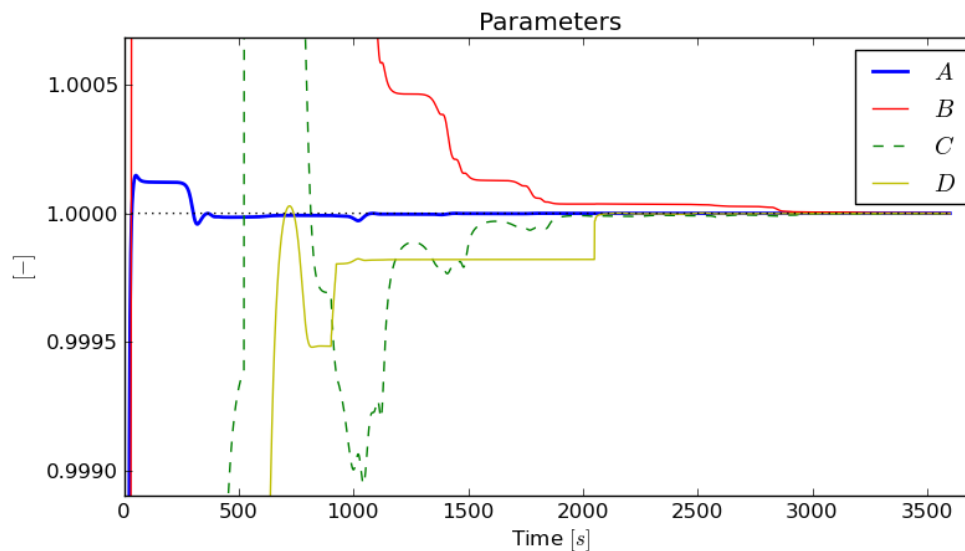


Figure 4.9: A more detailed view of the parameters around their stabilizing point. After about 1,200 seconds all parameters are well within a 0.5% deviation interval.

### 4.4.3.2 Observability

To further investigate the performance of the filter an analysis of the observability is made. The covariance can be studied for the 4 states of the filter by examining the covariance matrix,  $P$ . The diagonal elements of  $P$ , actually the variances of the states, can be seen in Figure 4.10. As explained in Section 1.5.3.1 a linearly growing variance for a parameter is usually a sign for loss of observability. This behavior can be seen for all parameters in different sections of the simulation.

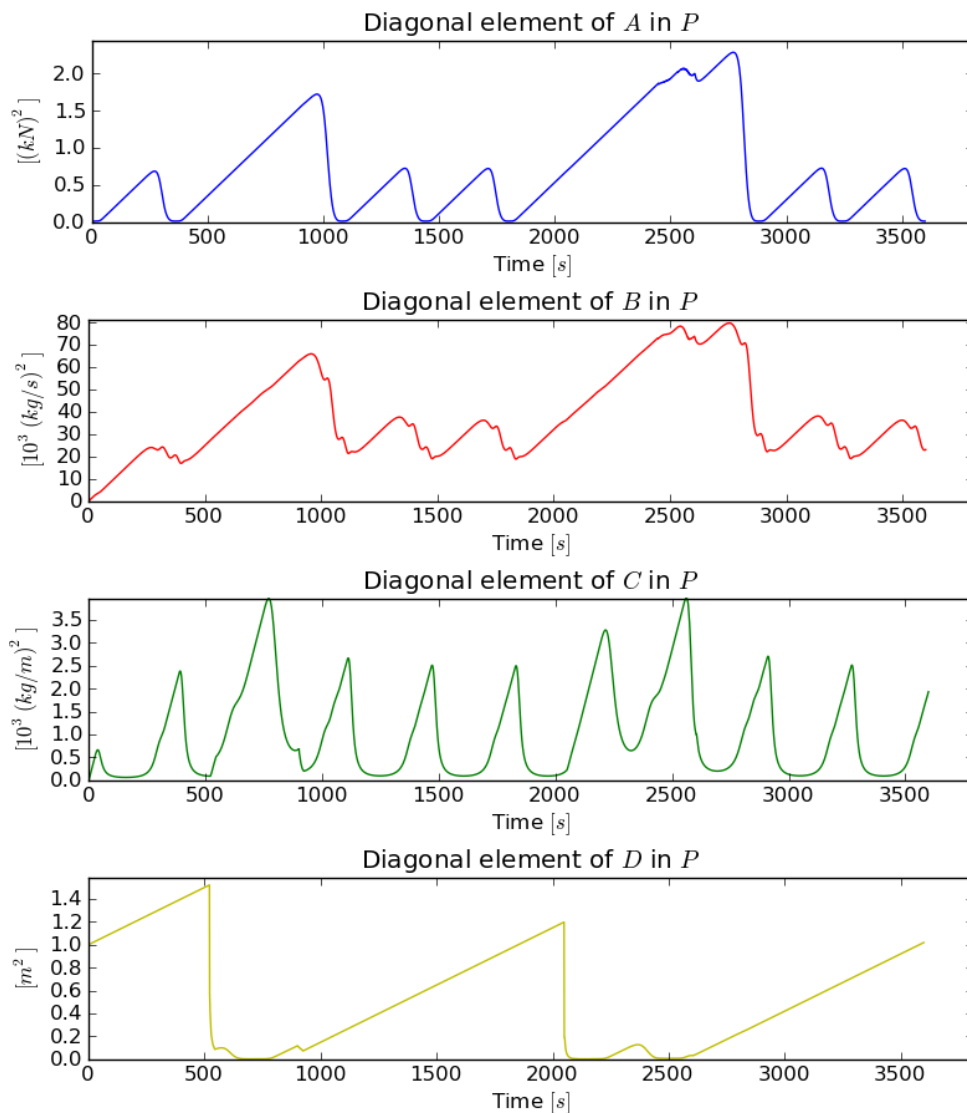


Figure 4.10: The variances of parameters in the 4 state EKF.

Relating to the signals, it's possible to notice that the small peaks of  $A$  correlates to the speed signal in the sense that a high speed seems to generate

a high variance for  $A$ . The two large peaks in  $A$  correlates to the two parts where  $r$  is non-zero, i. e. where a curve occurs. The behavior of  $B$  is very similar to  $A$ . The variance for  $C$ , seems to be low for a high value of the speed, which is the opposite of what was observed for  $A$  and  $B$ .

Since  $D$  is only observable when a curve occurs, the fact that the variance for  $D$  is low only when  $r$  becomes non-zero is expected. More interesting to note is that the variances for all the other parameters increase at those times.

The sections with lost observability, and thus linearly increasing variance, will result in the state estimation being constant for the corresponding parameter in that interval. This means the parameters will converge towards their desired values slower if the observability is poor, something that can be seen in the behavior of the parameter estimation in figures 4.8 and 4.9. As soon as parameter  $B$  has observability, it converges quickly towards the correct value, however, it contains large sections of low observability, resulting in a constant value in the corresponding intervals. The same applies for all parameters.

In order to deeper investigate this behavior, a more thorough analysis of the observability of the states can be made by studying the nullspace projections of each state according to Section 1.5.3.2. The nullspace projections of the parameters for this simulation can be seen in Figure 4.11. For a fully observable parameter its nullspace projection would be zero and for a completely non-observable parameter the projection would be 1. Comparing the nullspace projections to the variances for different states it is possible to see that as the variances increase – the projections increase.

All the parameters have non-zero nullspace projections at certain sections of the simulation. At the same time, the variances of the parameters that can be seen in the  $P$ -matrix are also often increasing linearly in different intervals. This indicates frequent lack of observability in all the parameters.

Yet, looking at the parameter behavior in figures 4.8 and 4.9 it seems that the parameters actually do reach their desired value after a certain time. This can be explained with the fact that the parameters of the real train are not expected to vary in time, as described in the beginning of Section 4.4. This assumption means that as long as there exists a time interval where a parameter is observable to a certain extent, its estimation will improve during that time interval. It also means that if the initial estimation is correct, the parameters will not change during run-time. This holds only for the simulated case with no disturbances. Noise, time delays, model flaws and

other errors will of course affect the estimations.

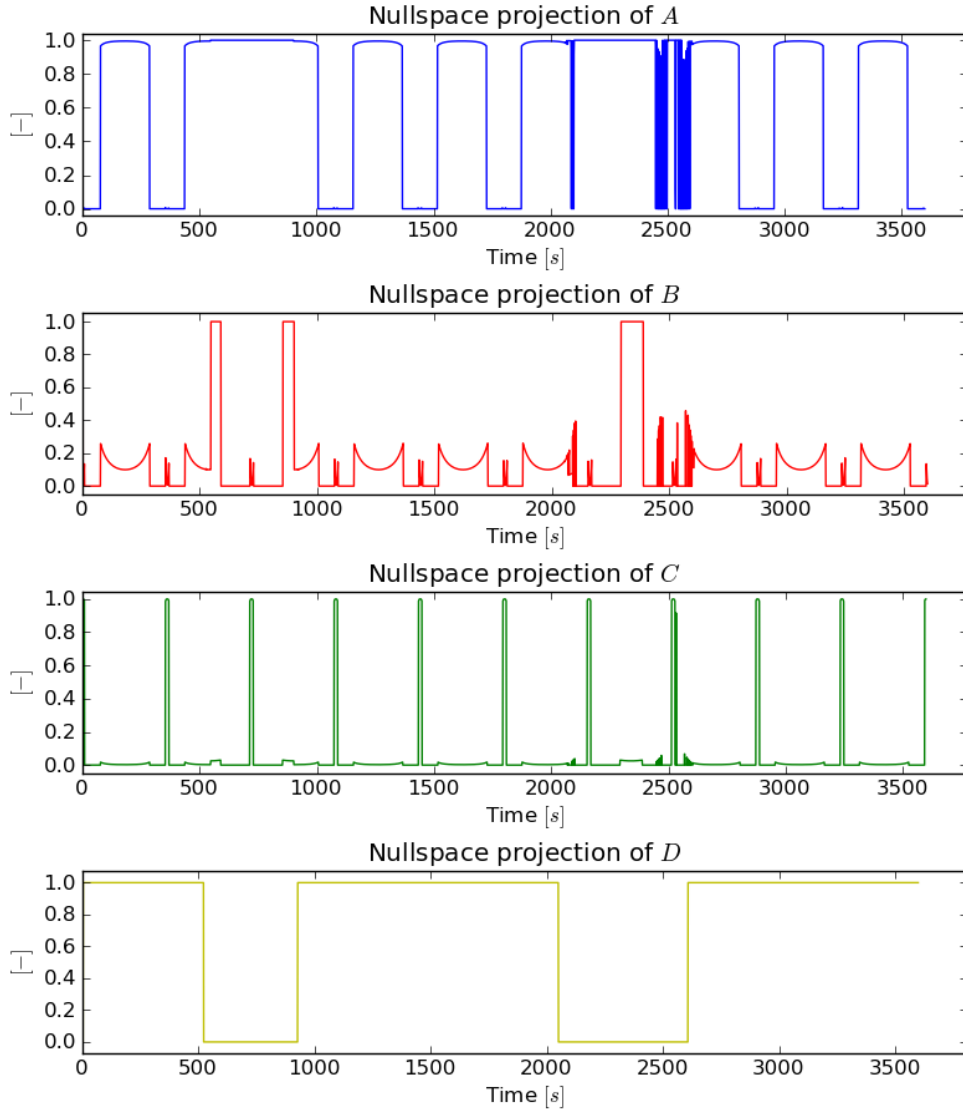


Figure 4.11: The nullspace projections of the parameters in the 4 state EKF.

### 4.4.3.3 Sensitivity

To investigate how sensitive the model is to errors in the input signals, the model function is differentiated according to Section 1.5.4.

$$\begin{aligned}
 H_w &= (\nabla_u h(x, u))^T = \\
 &= \left( \hat{B}_{k|k-1} + 2\hat{C}_{k|k-1} v_k \quad \gamma \quad - \sum_{j=1}^{n_{\text{loco}} + n_{\text{wag}}} \frac{gM_j \hat{D}_{k|k-1}}{(r_{j,k} + \hat{E}_0)^2} \quad \sum_{j=1}^{n_{\text{loco}} + n_{\text{wag}}} \frac{gM_j}{1000} \right) \quad (4.39)
 \end{aligned}$$

The elements of  $H_w$  gives an indication of how much the output signal, which in this case is the estimation of the tractive force, will be affected by errors in the input signal corresponding to that element.

For the simulation setup used, the size of those elements can be studied further to get a picture of which errors in the input signals that affect the estimation the most.

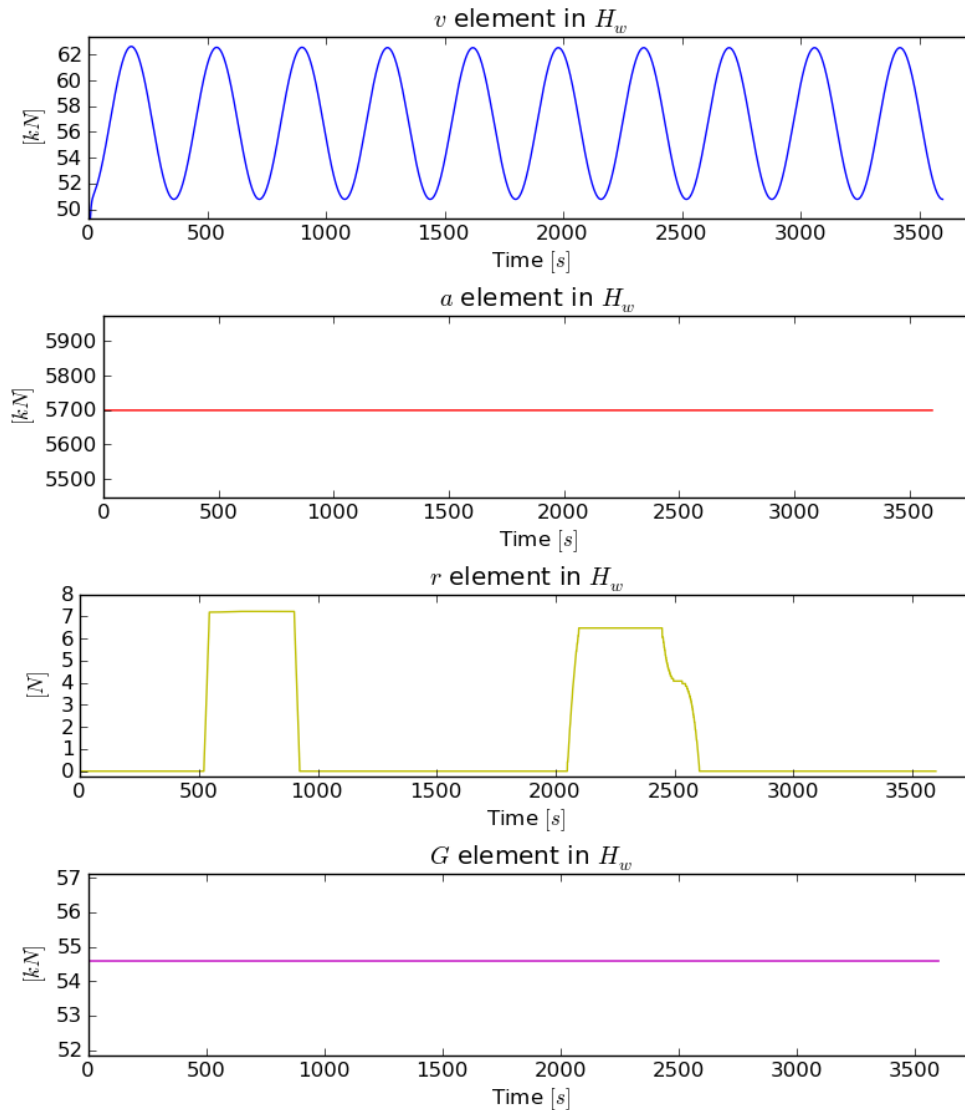


Figure 4.12: The elements of  $H_w$  showing how errors in the input signals affect the output signal, tractive force.

As can be seen in Figure 4.12, errors in the acceleration will, by far, have the greatest impact on the estimated output signal. It affects the output signal nearly 100 times more than errors in the speed of the same quantity. For example, an error of 1 m/s in the velocity signal would result in an error

## 4 Running Resistance

around 60 kN for “normal” speeds (10 – 20 m/s), while an error of 1 m/s<sup>2</sup> in the acceleration signal would result in an error of around 5,700 kN.

This observation can be clarified further by investigating the term  $\gamma$ . As (4.12) shows, the  $\gamma$ -term depends on the train mass and inertia, which, for the 52 wagon ore-train setup in the simulation, is large. Even a small change in acceleration for masses of that quantity corresponds to a large force.

To gain better understanding of the importance of the accuracy of the acceleration, the acceleration dependent part of the tractive force:

$$F_a(a) = \gamma a \quad [\text{N}] \quad (4.40)$$

from (4.11) can be compared with the running resistance,  $F_R$ , which can be seen in Figure 4.13. As expected, as soon as significant acceleration occurs,  $F_a$  will, by far, be the largest component.

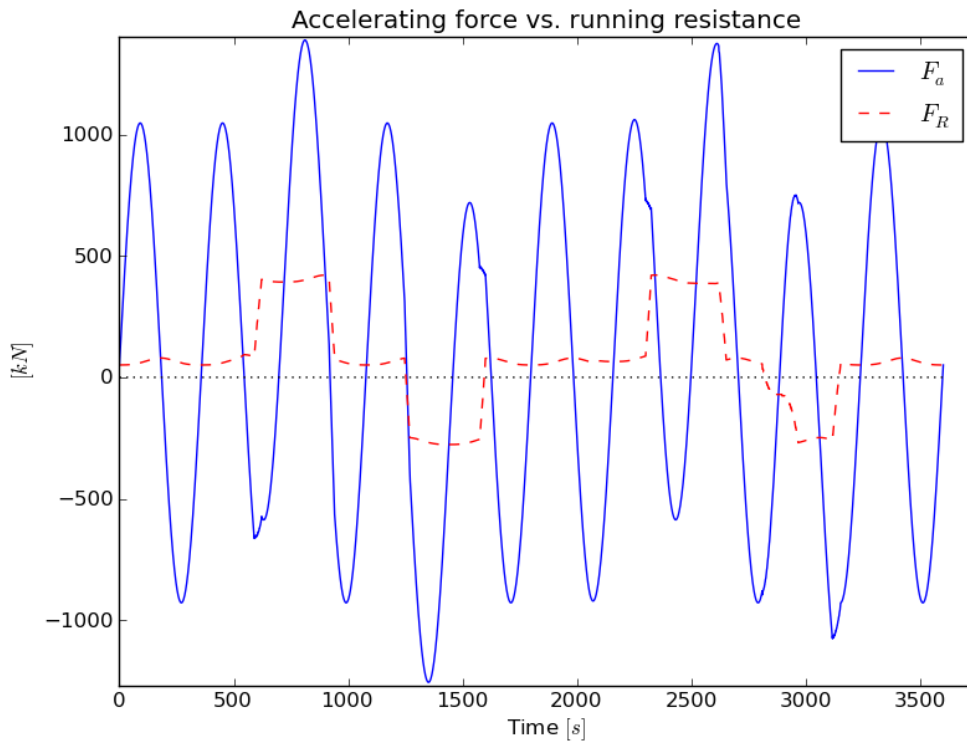


Figure 4.13: The accelerating force,  $F_a$ , and the running resistance,  $F_R$ , for the simulation.

This means that when the train is accelerating – the running resistance, which is what we want to estimate, is often a small part of the measured signal,  $F_t$ , compared to the accelerating force,  $F_a$ . With this knowledge, consider that the desired parameters to estimate, in their turn, corresponds to parts of the

running resistance. I. e. the attempted estimations are often very small portions of the measured signal.

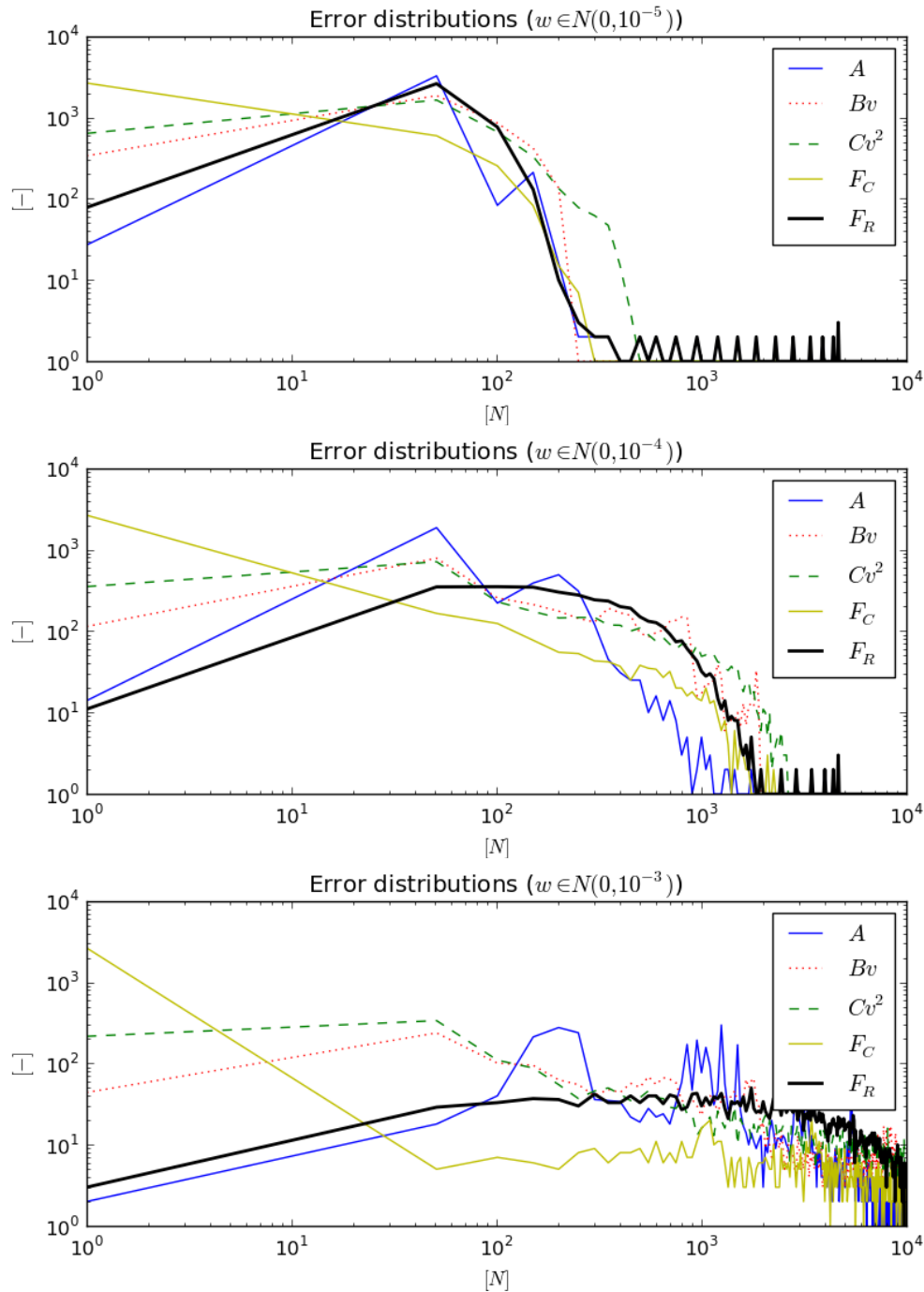


Figure 4.14: The error distributions of the running resistance and its parts caused by noise on the acceleration with different standard deviations.

For a perfect acceleration signal this difference in size would not matter,

since the accelerating force would only be subtracted from the measured signal  $F_t$  in order to derive the running resistance perfectly. This is also the result from the simulation. In reality however, this causes problems, since very small errors in  $a$  will cause errors in  $F_a$  that are very large in relation to  $F_R$ .

To investigate the requirement of the acceleration in terms of precision, noise,  $w$ , is added to it:

$$a_w = a + w, \quad w \in N(0, \sigma) \quad [\text{m/s}^2] \quad (4.41)$$

Figure 4.14 shows the error distributions corresponding to noise with standard deviations ( $\sigma$ ) of  $10^{-5}$ ,  $10^{-4}$  and  $10^{-3}$   $\text{m/s}^2$ . According to Figure 4.13 the magnitude of the running resistance is approximately 100 kN, disregarding from grades. Figure 4.14 shows errors up to 10 kN thus 10% of the running resistance (on flat track).

To have a maximum error of approximately 2 kN in the running resistance,  $F_R$ , the standard deviation of the noise in  $a$  has to be less than  $10^{-4}$ .

## 4.5 Conclusions

The two main problems that arise are observability and sensitivity. Neither of these are correlated to the choice of EKF. The analysis made is not expected to result in any different conclusions, should the same simulations be made with UKF.

The only filter that, during simulation, was able to estimate all states was the filter with 4 states:  $A$ ,  $B$ ,  $C$  and  $D$ . In this working implementation the parameter  $E$  was considered constant at its initial estimation according to Section 4.3.

The system observability is overall low, which indicates that it is hard to extract as much information as desired from the measured reference signal, tractive force, even with the reduced number of states. The impact of this is not so severe in the simulation case, since the parameters will move in the correct direction whenever there is information. In reality however, this will cause problems, since the available information is not always correct.

A curve is required in order for the parameter  $D$  to be observable. However, this reduces observability for the rest of the states. High velocity provides  $C$  with better observability. Although  $A$  requires *low* values of this signal to be observable, something that seems to apply for  $B$  as well, even though not so distinct.

The removal of the acceleration and thereby also the speed as states results in the fact that the acceleration is considered an input signal to the system. In reality, this means that it has to be numerically differentiated from the velocity, since it is the only available and related input signal. Sensitivity analysis shows that the system is very sensitive to errors in the acceleration signal. These high accuracy requirements on the acceleration demand sophisticated methods for numerical differentiation, which will be presented in the next chapter.



---

# 5

## Acceleration

---

As described in Section 4.4.3.3, the acceleration of the train is a key signal in the task of parameter estimation for the running resistance. This chapter is therefore dedicated to this issue solely. As seen in Section 3.1, the speed is among the available data, but not the acceleration. The acceleration can however be calculated from the speed in a number of different ways, some of which will be described and evaluated here.

The most straight-forward method for derivation of a sampled signal is the *two-point differentiation*. The drawback of this method is that all supposable noise will largely affect the result. A much more sophisticated approach is to use *Kalman filtering* to estimate the derivative. This method has very good noise reducing capabilities, but it is known to cause a time delay. The third method investigated here is the *smoothing spline approximation* approach. This way of finding a derivative of a signal is found not to have the drawbacks of the other two to the same extent ([12]).

### 5.1 Two-point Differentiation

This simple derivation method is used as a reference since it gives the most instantaneous value with no account taken to the past except for one sample before the current one:

$$a_k = \frac{v_k - v_{k-1}}{\Delta t} \quad [\text{m/s}^2] \quad (5.1)$$

where

$$\Delta t = t_k - t_{k-1} \text{ [s]} \quad (5.2)$$

Depending on sample-time this method is heavily affected by noise. One way of dealing with this is to pre-filter the speed signal with a low-pass filter. Without any noise at all it is however known to be a very good approximation method.

## 5.2 Kalman Filtering

Another way to determine the acceleration is to use the *Kalman filter* as an observer for the acceleration. If the states consist of the speed and acceleration, which will be estimated by the filter, while the measured signal is the speed the following filter can be defined:

$$x = \begin{pmatrix} x_v \\ x_a \end{pmatrix} \quad y = v \quad (5.3)$$

where  $x_v$  and  $x_a$  denotes the states for the speed and acceleration respectively. The time update for those states are then formulated as:

$$f(\hat{x}_{k|k}, 0) = \begin{pmatrix} \hat{x}_{v,k|k} + \hat{x}_{a,k|k} \Delta t \\ \hat{x}_{a,k|k} \end{pmatrix} \quad (5.4)$$

Or, described as the matrix F:

$$F = \begin{pmatrix} 1 & \Delta t \\ 0 & 1 \end{pmatrix} \quad (5.5)$$

where  $\Delta t$  is the time elapsed since the last update (5.2).

The system function is simply the estimation of state  $x_v$  which will be compared to the measured signal:

$$h(\hat{x}_{k|k-1}) = \hat{x}_{v,k|k-1} \quad (5.6)$$

which gives

$$H = \begin{pmatrix} 1 & 0 \end{pmatrix} \quad (5.7)$$

The filter is updated according to 1.5.1.1 and can be tuned with the design-parameters  $Q$  and  $R$ . The state  $x_a$  provides an updated estimation for the acceleration in each time step.

## 5.3 Smoothing Spline Approximation

The idea here is to approximate the measured signal, in this case the speed, with an analytical function using regression. The derivative is then computed analytically from the fitted analytical function. A window of samples is used for the approximation and the window size has to be decided.

In this project, the *Interpolate* module of the *Scipy* package for *Python* has been used for this derivation method (see Section 1.8 for details on the software used). The *splrep* function creates a cubic spline function from a set of data, with a smoothness factor,  $s$ , controlling the tradeoff between closeness and smoothness of fit. Following this with a call to *splev* will return the value of the derivative in a given point, for instance the last point in the interval,  $x[-1]$ . An example would be:

```
tck = splrep(x, y, s=15)
deriv = splev(x[-1], tck, der=1)
```

where  $x$  is the window of time samples as an array, and  $y$  contains the corresponding signal values. See [27] for a complete description of these functions.

## 5.4 Evaluation

The speed signal for simulation described in Section 3.2 with the corresponding analytical acceleration will be used for evaluating the above methods of derivation in simulation. For the Kalman filter approach, different design parameters,  $Q$  and  $R$ , have been tested, and were finally chosen, for evaluation against the other methods, as:

$$Q = \begin{pmatrix} 1 & 0 \\ 0 & 100 \end{pmatrix} \quad R = 10^4 \quad (5.8)$$

Three different window sizes of the spline approximation method will be simulated, varying with the simulation setup (see below).

### 5.4.1 Noise

The estimations are here made from the analytical speed with added relative noise from a Gaussian distribution with a standard deviation of 1%. Figure 5.1 shows the analytical, called *true*, acceleration together with different estimations of it, for a small section of the full simulation, where the number after each spline approximation is the window size in seconds.

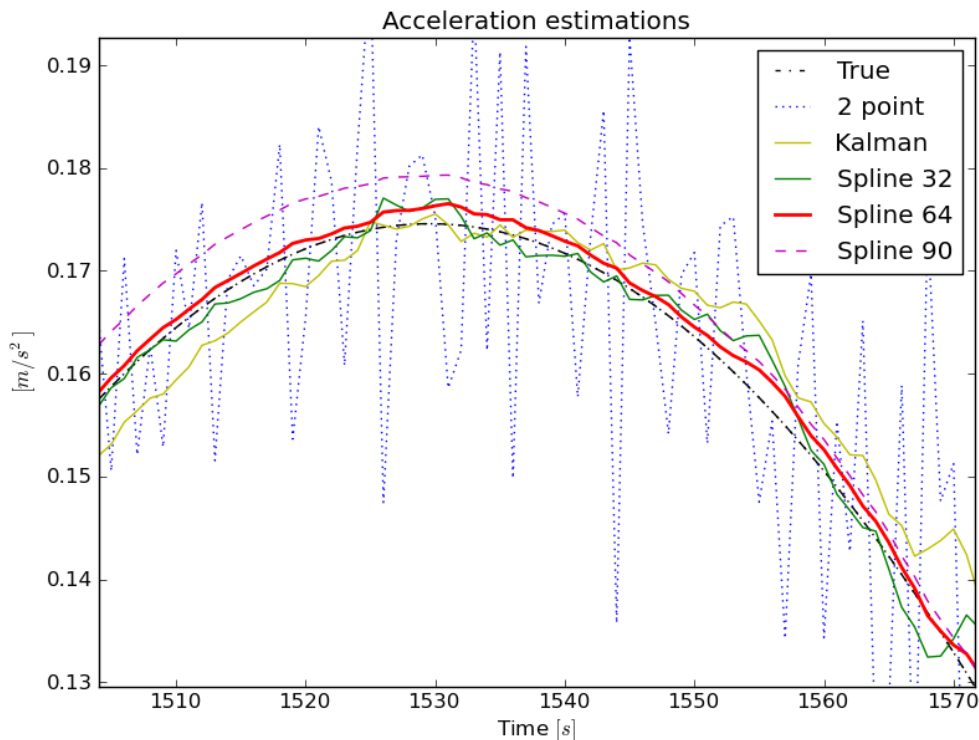


Figure 5.1: The analytical acceleration together with the three estimation methods described, for a small section of the total simulation. The number after each spline is the window size in seconds.

Looking instead at the error each estimation has, as in Figure 5.2, the closeness to the real acceleration can be better indicated. To really evaluate these estimation errors, the error distributions are plotted in Figure 5.3, where the vertical axis is the number of samples with absolute errors

according to the x-axis, which is logarithmic. It is clear that the smoothing spline approximation with a window of 64 seconds performs the best in this simulation.

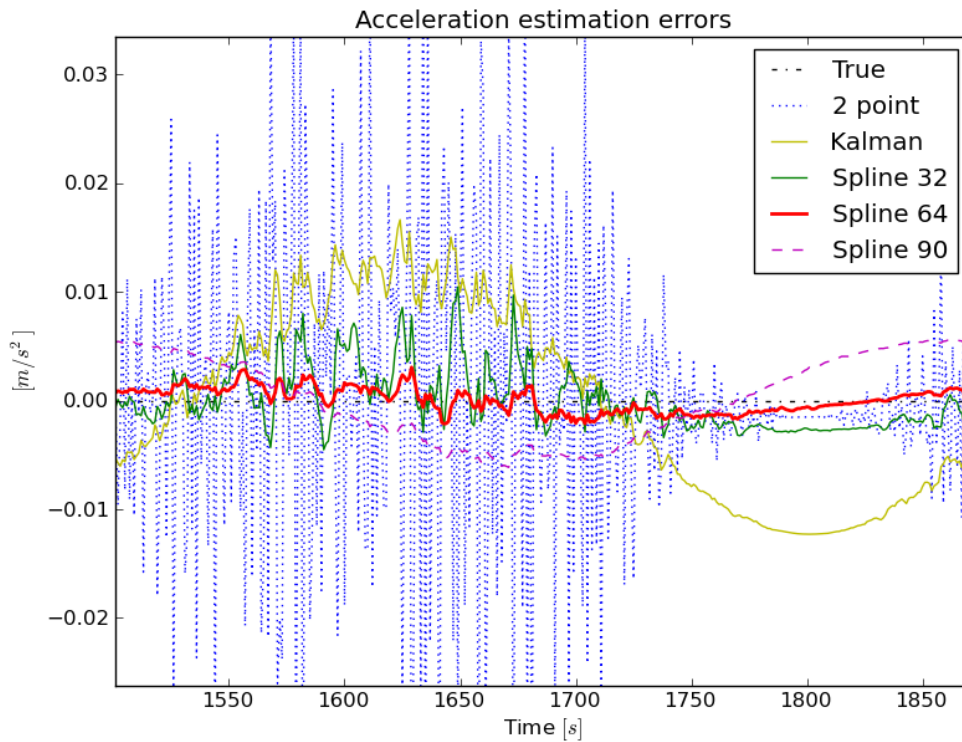


Figure 5.2: The errors for the estimation methods.

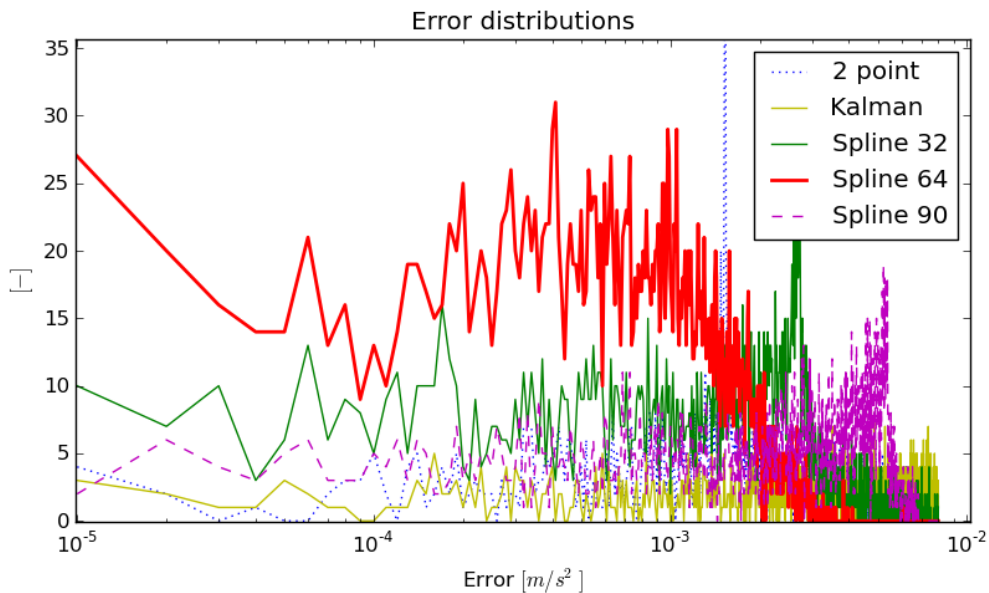


Figure 5.3: The distributions of the estimation errors with a logarithmic scale on the x-axis.

The above simulation was made with the assumption of a sample frequency of the speed of once per second. A higher sample frequency might improve the estimations, but the Gaussian noise added will also increase in frequency, making it harder for especially the two-point differentiation.

As stated in Section 3.1, the minimum sample time of the speed measurement, by the equipment on board many Swedish freight locomotives, is 20 ms. The same simulation as above of the differentiation methods, but with a sample frequency 50 times higher, will produce error distributions for the different estimations as shown in Figure 5.4. Smaller window lengths for the spline approximation method apparently perform better for higher sampling frequencies, and a window size of 18 seconds is doing the best job in this particular case, with an error much smaller than the best estimation in the previous simulation with sample time of 1 s.

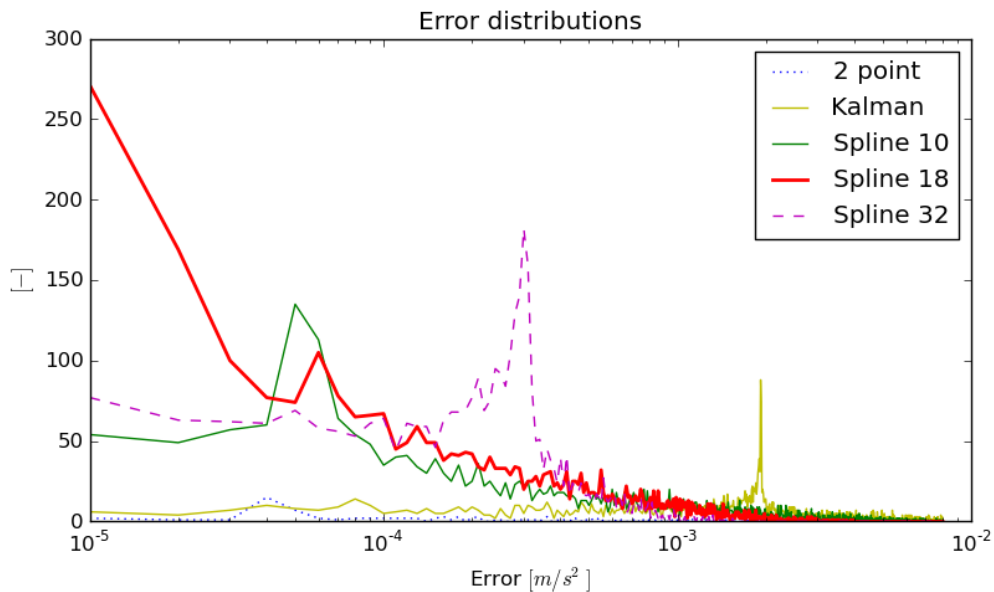


Figure 5.4: The distributions of the errors of the simulated estimation methods where the sample time is decreased to 20 ms, instead of 1 s.

As a final test with noise, noticing the good performance of the spline approximation with 18 seconds window size and with a sample-time of the speed signal of 20 ms, the relative noise is increased with a factor 10, to a standard deviation of 1%. The result, again shown as distributions of the errors of the estimation methods, is shown in Figure 5.5.

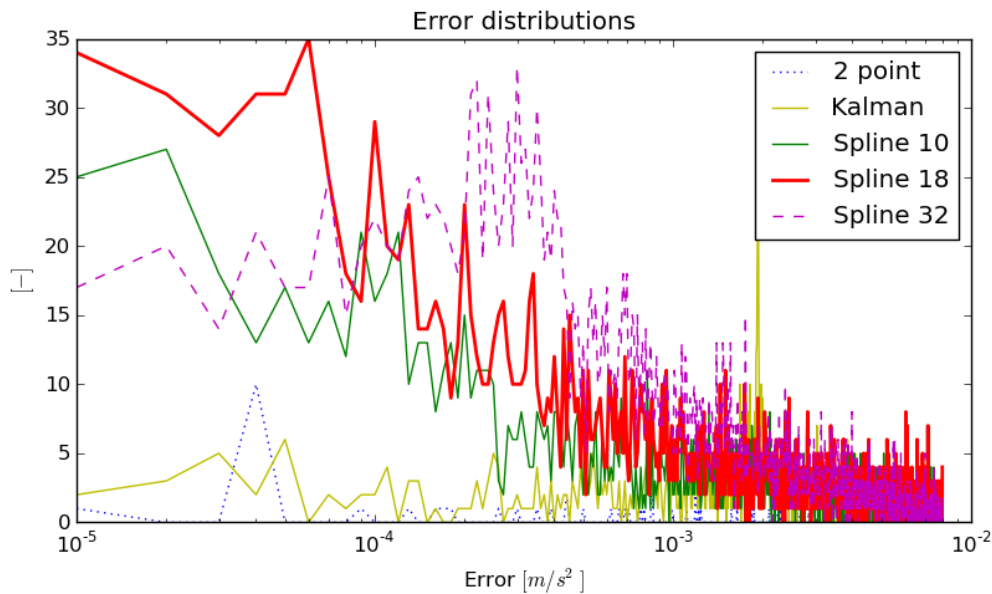


Figure 5.5: Distributions of the estimation errors when the noise is increased to a standard deviation of 1%.

## 5.4.2 Time Delay

All measured signals has some amount of noise of one form or the other. But apart from noise, other type of errors could also be involved. Adding a time delay of 0.1 seconds to the velocity signal with sample time of 1 second, running the three types of estimations described above, error distributions as shown in Figure 5.6 appear. The errors will behave more oscillative than in the case of noise only, but the methods perform similar, ranking in the same order with the 64 s window spline approximation in the first place.

Simulating instead the higher sample frequency of 50 times per second, a time window of 32 seconds is doing well compared to the others, all shown as error distributions in Figure 5.7.

Indicated by this test is that even a short time delay can be problematic for a good estimation result. Important to bear in mind though is that an *absolute* time delay might not be the problem, but rather a *relative* delay, compared to other signals used. All depending on the system.

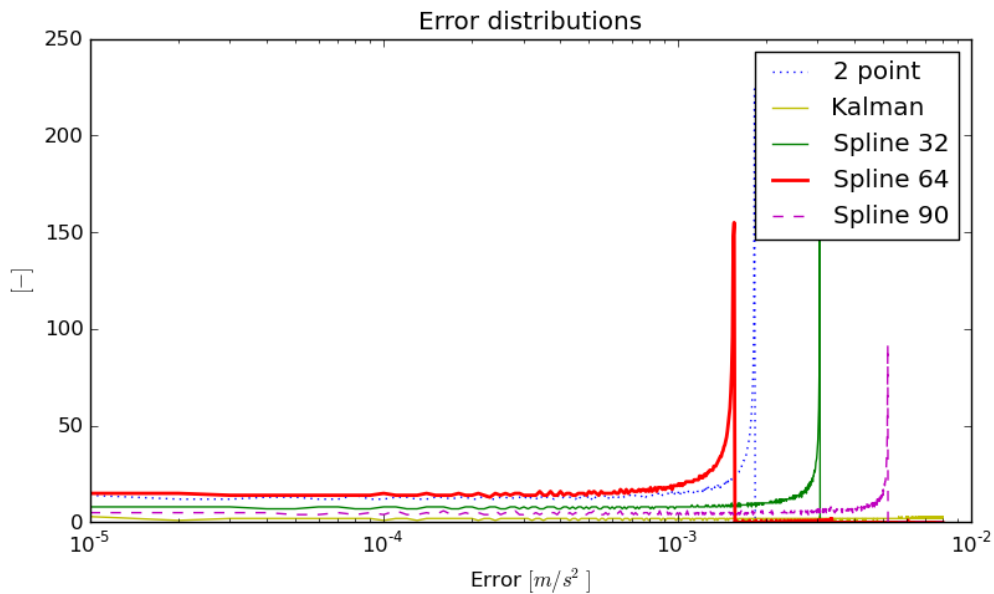


Figure 5.6: Estimation error distributions for the three estimation methods with a time delay on the speed signal of 0.1 s.

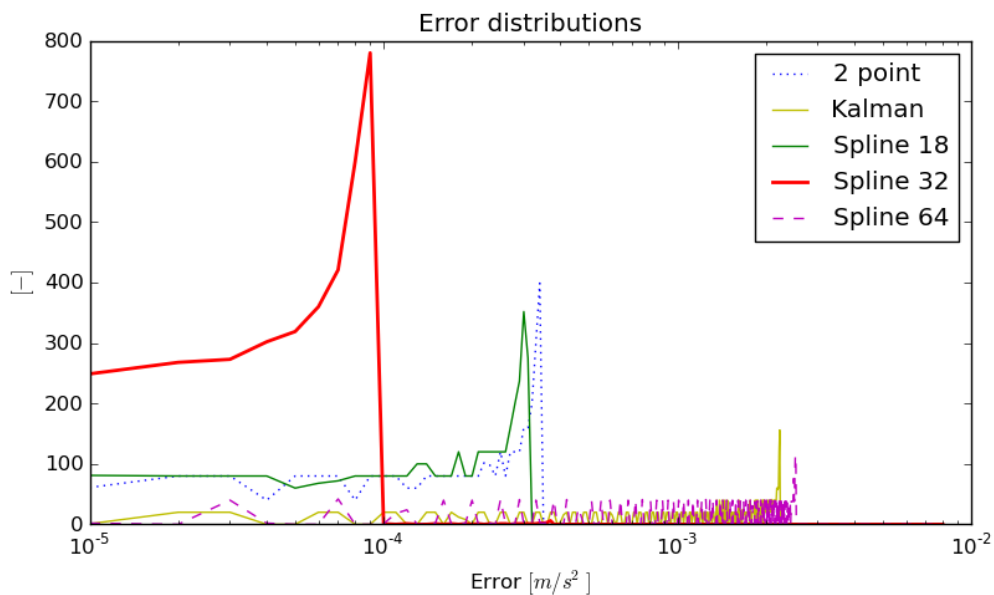


Figure 5.7: Error distributions for the acceleration estimations when the speed is delayed 0.1 s and using a sample frequency of 50 Hz.

To show the errors caused by different time delays, a table (Table 5.1) is compiled showing the maximum error for both the low and the high frequency for a set of delays. For the low frequency of 1 Hz, the 64 second window for the spline approximation is used, and the 32 second one for the high frequency, 50 Hz.

Delay [s]	Maximum error [m/s <sup>2</sup> ]	
	1 Hz, Spline 64	50 Hz, Spline 32
0.1	$1.6 \cdot 10^{-3}$	$8.5 \cdot 10^{-5}$
0.2	$1.8 \cdot 10^{-3}$	$3.31 \cdot 10^{-4}$
0.3	$2.0 \cdot 10^{-3}$	$6.31 \cdot 10^{-4}$
0.4	$2.26 \cdot 10^{-3}$	$9.40 \cdot 10^{-4}$
0.5	$2.52 \cdot 10^{-3}$	$1.24 \cdot 10^{-3}$

Table 5.1: Maximum errors for different time delays in the speed signal, for both 1 Hz sample frequency as well as 50 Hz.

### 5.4.3 Scale Error

As described in Section 3.1, if the speed is measured on a *driven* axle and the train is in *traction*, the creep, or slip, of the wheels is causing a scale error in the speed measurement of, in the worst case, up to 10%. Usually the creep is however much lower than this. Simulating a scale error on the speed of 5%, results in errors as shown in Figure 5.8. As with the other error types, a sample frequency of 50 Hz is also simulated for this scale error of 5%, with results shown in Figure 5.9.

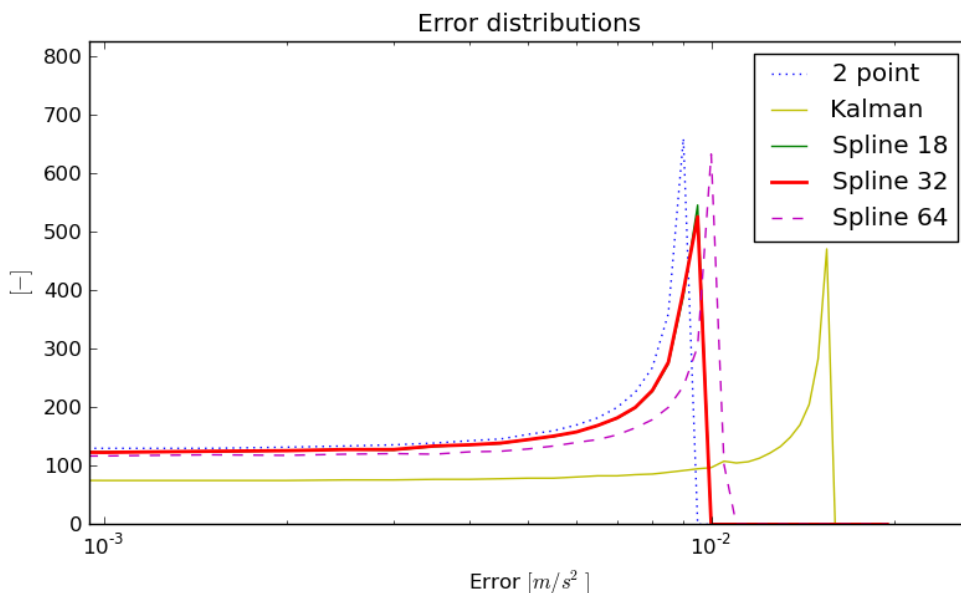


Figure 5.8: A 5% scale error added to the speed results in error distributions for the acceleration estimations as shown here.

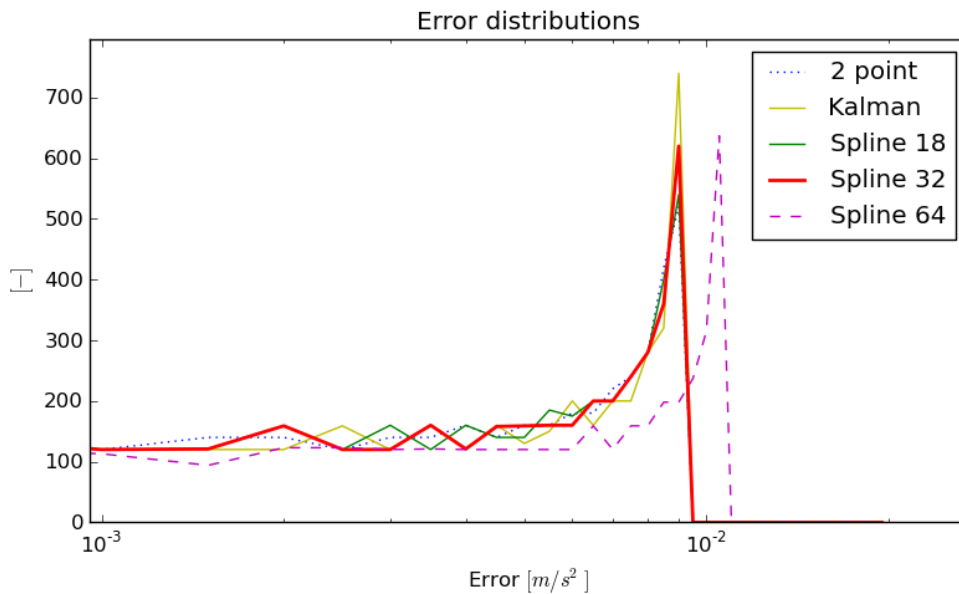


Figure 5.9: Error distributions of acceleration estimations made with 20 ms sample time from speed with 5% scale error.

Obviously, the choice of method does not matter here and the errors are large compared to the other error types simulated. It is clear that an increase in sample frequency does not help the acceleration estimations – only the Kalman filter has a significant difference in its error distribution.

#### 5.4.4 Conclusions

Shown by these simulations is that noise is the least of problems among error types in the speed signal, if the method and design parameters are chosen wisely. A time delay should not be the big problem either, for it is likely that it could be compensated for in the system. In the presence of either noise or a time delay, or both, it is desired to access and use a speed signal with the highest possible frequency.

Shown by the last example, it is highly desired that the speed signal is delivered from a *non-driven* axle on the train. If not, using only the acceleration estimation during coasting is an option. Otherwise the slip must be known should this type of error, with low accuracy on the acceleration estimation as a result, be avoided. Also shown is that a decrease in sample time is not affecting the result in the presence of a scale error.

---

# 6

## Running Resistance with Acceleration Estimation

---

In this chapter, a few simulations of the running resistance parameter estimation are made utilizing the results on acceleration estimation from the previous chapter.

### 6.1 Recorded Data

To evaluate the running resistance parameter estimation and get an indication of how usable it is in reality, a data recording from a running train is used. This section evaluates results from such a recording with a discussion about the possible problems.

#### 6.1.1 The Data

Recorded data of a coasting train was provided by Transrail. The train was brought up to a speed of 20 m/s, traction effort set to zero, the recording of signals started, and the train was let rolling until it almost hit zero speed after about 300 seconds, i. e. 5 minutes.

The train used was 2 IORE locomotives with 68 empty Fanoo ore wagons (see Section 3.2.4 for details on IORE and [29] on details of the Fanoo).

Signals recorded from this coasting experiment are plotted in Figure 6.1, showing the speed,  $v$ , the curve radius,  $r$ , and the gradient,  $G$ . The sample-time during the recording was 1.16 seconds.

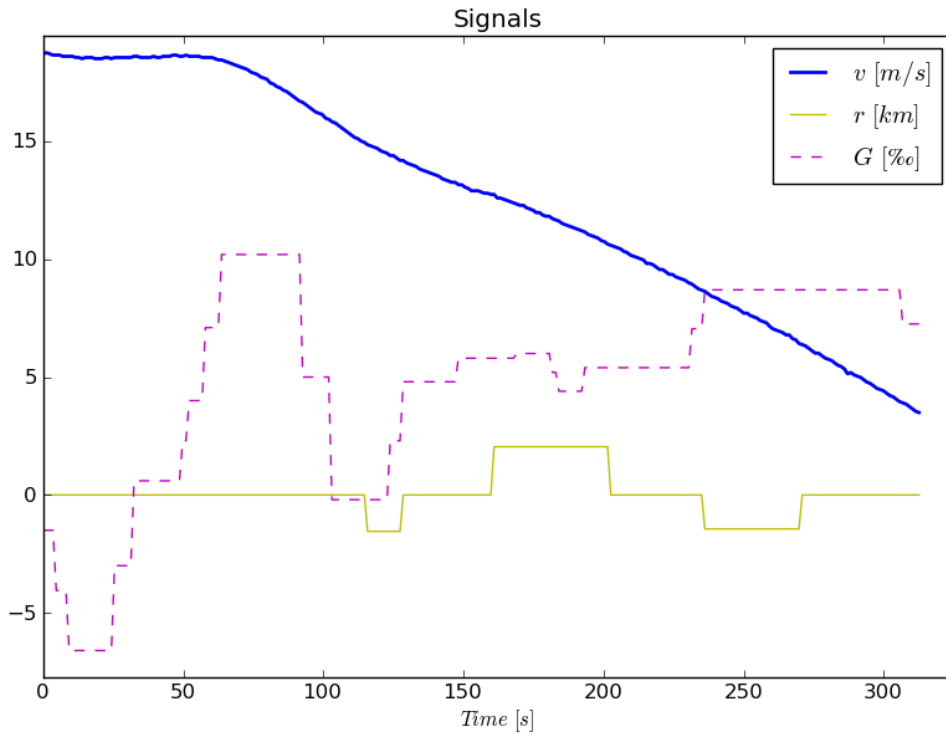


Figure 6.1: Signals from coasting recording.

## 6.1.2 Online Identification of Running Resistance

An EKF setup as in Section 4.4.3, with 4 states for the parameters  $A$ ,  $B$ ,  $C$  and  $D$ , is used. The reference signal, the tractive force,  $F_t$ , is set to zero for the whole simulation, and the acceleration is estimated from the speed with the smoothing spline approximation method described and evaluated in Chapter 5.

### 6.1.2.1 Results

A simulation of the filter and recorded data described above will result in the parameter behavior as shown in Figure 6.2, where the parameters are not normalized. The end values of all parameters are 69,000, 4,400, 1,600 and 7 for  $A$ ,  $B$ ,  $C$  and  $D$  respectively. Variances of the parameters are shown in figure 6.3 indicating lack of observability, something that is also indicated by

the nullspace projection plots in Figure 6.4.

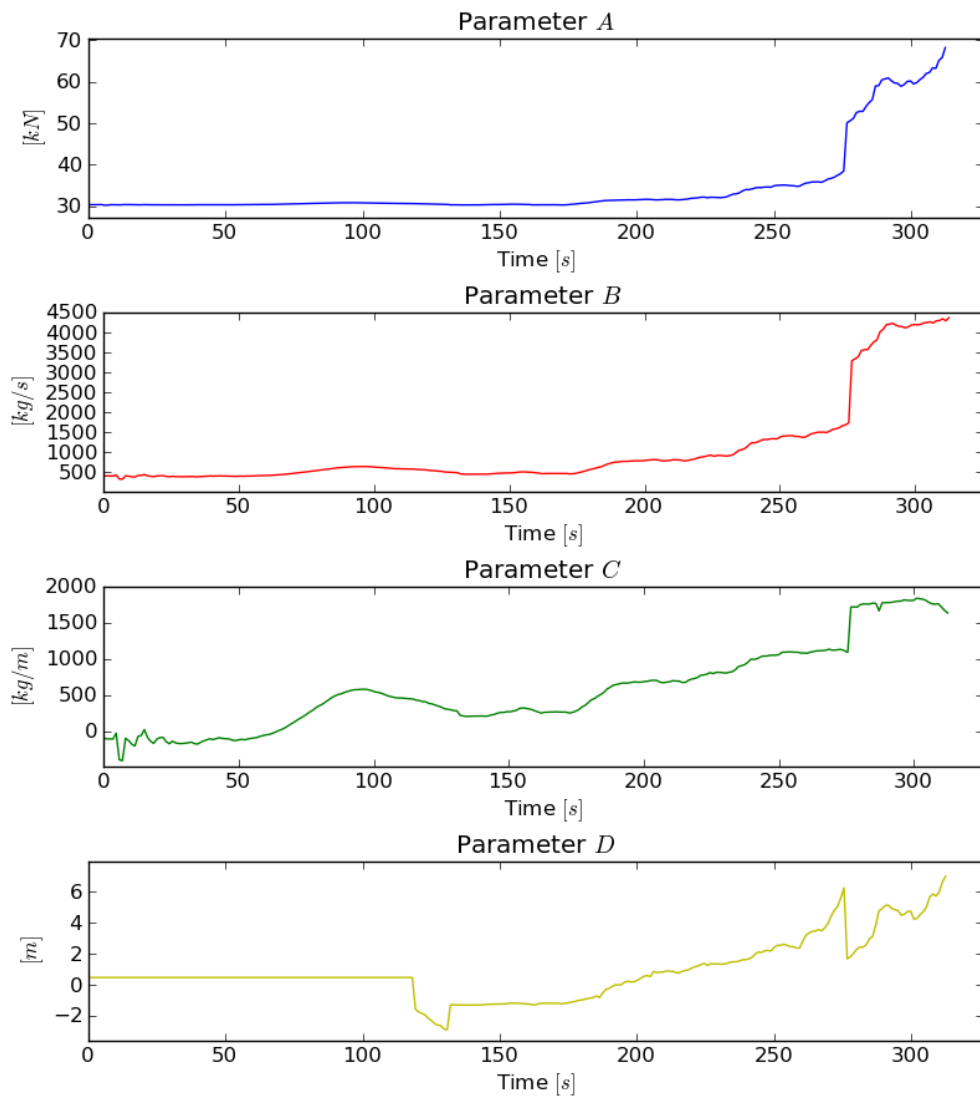


Figure 6.2: Parameter behavior for the EKF with recorded data.

Acceleration estimations, made from the recorded speed, with Kalman filtering and smoothing spline approximation is shown in Figure 6.5, where the spline estimation with a 64 second window is the one used in the filter.

## 6 Running Resistance with Acceleration Estimation

---

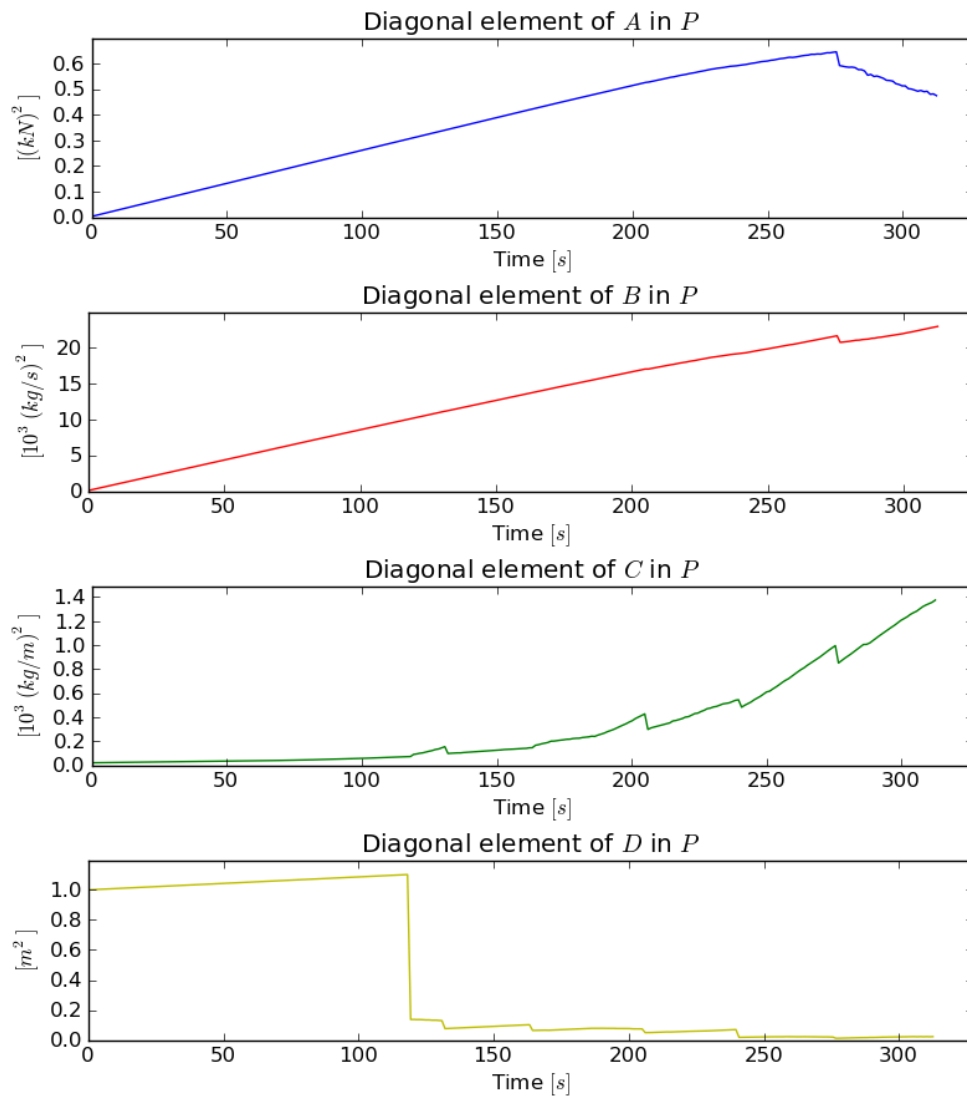


Figure 6.3: Variances of the parameters in the simulation with recorded data.

## 6 Running Resistance with Acceleration Estimation

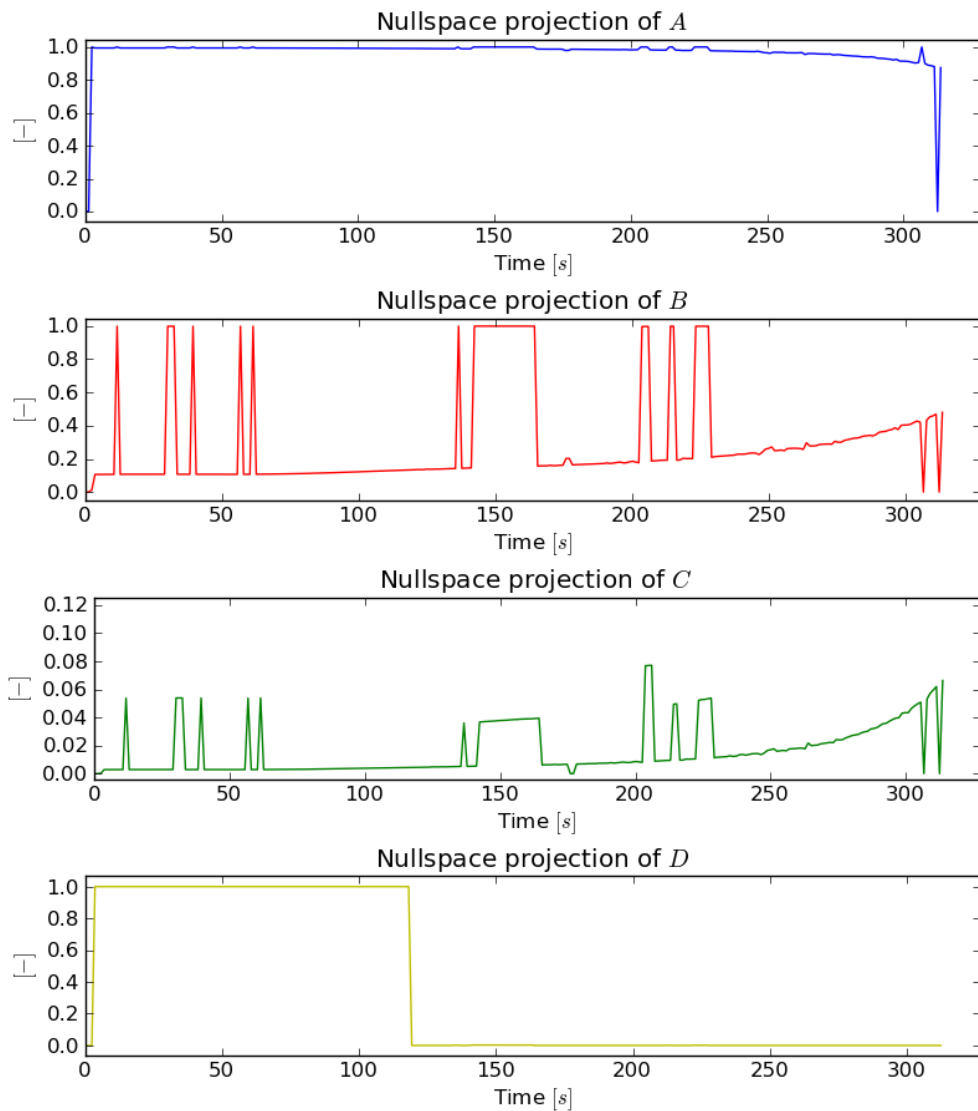


Figure 6.4: Nullspace projection length of each parameter.

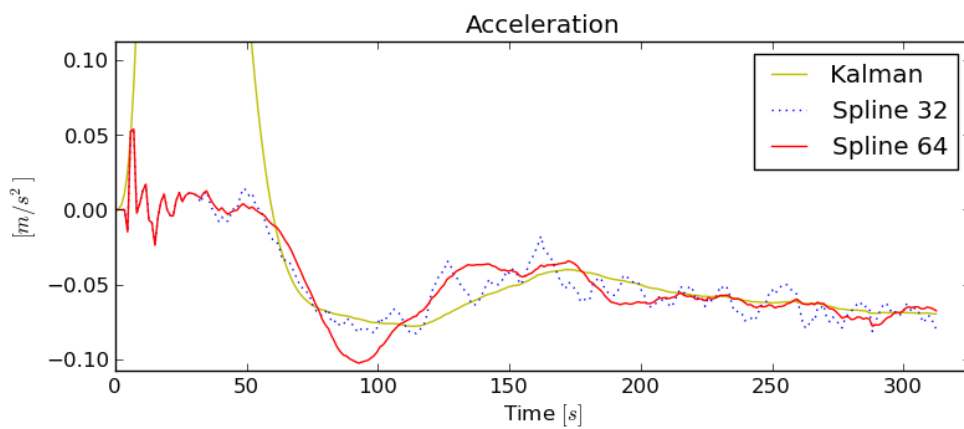


Figure 6.5: Acceleration estimations from the recorded speed signal. The number at each spline is the window length in seconds.

### 6.1.2.2 Discussion

Shown by the variance and nullspace projection plots (Figure 6.3 and 6.4) are that parameter  $A$  is suffering from lack of observability during the whole run, except in the very end of the simulation. In the end the speed drops which increases observability for  $A$ , but decreasing observability of  $C$ . This is all in agreement with the observability analysis made in Section 4.4.3.2.

All parameters except  $A$  show a deviation from the initial value of 1000% or more during the run. Parameter  $A$  off with around 100% at its worst (in the end). Parameter  $C$  and  $D$  experience negative values at some point. If this was true it would mean that the corresponding part of the running resistance is actually pushing the train *forward*. This is of course impossible, and clearly shows that parameter estimation of the running resistance with EKF of this train, with this recording, is not possible with a satisfying result.

There are several possible causes for the unsatisfying result. When leaving the simulated world, many phenomenon are introduced, such as:

- Noise and other signal disturbances
- Model flaws
- Errors in the train configuration constants
- Acceleration estimation difficulties

In a normal case, slip would be present during traction, further obstructing the parameter convergence.

Possible improvements for a better result would include primarily using the maximum possible frequency of the velocity signal, much higher than in this recording. In addition to that, using both GPS velocity and Teloc velocity in sensor fusion could further increase the accuracy. The accuracy in the velocity signal is important for the acceleration estimation. It might also be possible to measure the acceleration explicitly with extra sensors.

Better accuracy of constants related to the train configuration, including weights of locomotives and wagons and their rotary inertia could also contribute to better parameter behavior.

## 6.2 Simulation

A demonstration of the acceleration estimation and its impact on the parameters in the running resistance filter will be presented in this section.

Shown in Section 4.4.3.3, the running resistance estimation is highly sensitive to errors in the acceleration, and the acceleration is estimated from the speed. To evaluate the combination of the EKF parameter estimation for the running resistance and the best performing acceleration estimation compiled in Chapter 5, two simulations will be made. The acceleration will be computed from a *perfect* velocity signal with no errors, and then inputted to the filter along with the other signals without any errors added. The signals will be according to Section 3.2.

### 6.2.1 Sample Time: 1 s

In the first experiment, the speed signal is assumed to be available with a sample time of 1 s, and everything will therefore be run with this frequency. The result is shown in Figure 6.6, where the parameters are plotted. Seen in this figure are parameter deviations of more than 200%, and no indication of convergence to the correct values is seen. Only  $A$  is staying within a reasonable variation. The maximum error in the acceleration is  $0.0014 \text{ m/s}^2$ .

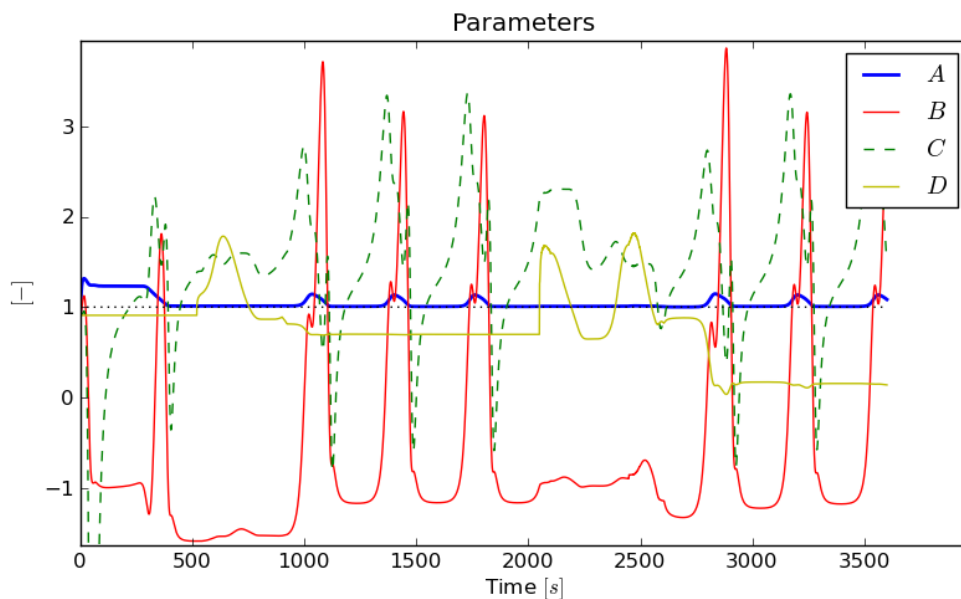


Figure 6.6: Parameter behavior when simulating with acceleration estimation from a perfect speed signal with a sample time of 1 s.

## 6.2.2 Sample Time: 20 ms

In the same manner as in the acceleration evaluation in Chapter 5, the sample time is decreased to 20 ms as this is the maximum frequency of the measured speed signal from the available equipment (see Section 3.1.1). The filter simulation is still run in 1 Hz, but the acceleration is computed 50 times per second. The result can be seen in Figure 6.7, where it is clear that this sole change in the simulation setup had a huge impact on the parameter behavior. After the time where the first curve appears, around 500 seconds into the simulation, all parameters except  $B$  shows a maximum deviation of 2% and  $B$  are regularly peaking 3.5% away from its correct value. The error in the acceleration is now less than  $9 \cdot 10^{-6} \text{ m/s}^2$ .

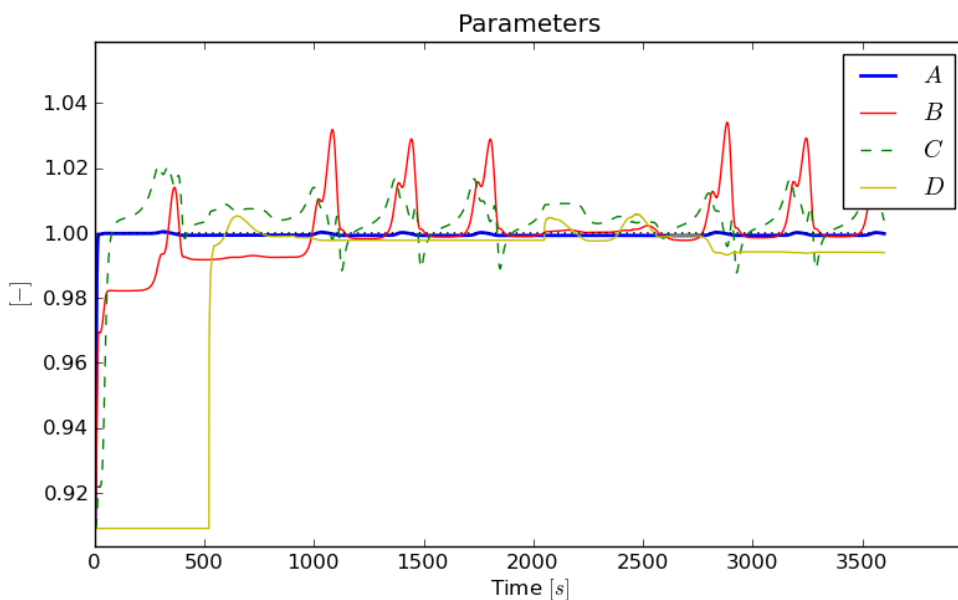


Figure 6.7: The parameter convergence when the acceleration is computed from a correct speed signal every 20 ms.

## 6.3 Conclusions

The overall low system observability demands high accuracy in measured signals along with model correctness. The results of parameter estimation from recorded data indicates that these accuracies are not at all satisfying in the real world. Noise and errors of the measured signals are too high in order to estimate the parameters with the presented setup.

The biggest problem is lack of accuracy in the acceleration signal, because of the system's high sensitivity for it. The second part of this chapter illustrates an important point: If it is assumed that an acceleration estimation made from a speed signal with some errors (as always in reality) will be worse than one made from a perfect speed signal, then the simulations show clearly that the high frequency of the speed signal (50 Hz) is *absolutely necessary* for a satisfying result of running resistance parameter estimation with EKF (and the models and signals as described).



---

# 7

## Adhesion

---

In the same way as for the running resistance, parameter estimation for the available adhesion is investigated in this chapter.

### 7.1 Deducing a System Model

The model for adhesion (2.21) is describing the current maximum available adhesion as a function of the current maximum friction,  $\mu_{max}$  (that varies in time and space), the locomotive's slip control and its ability to stay close to the maximum friction,  $\kappa$ , and the speed,  $v$ :

$$\alpha_{max}(v, \mu_{max}) = \mu_{max} \kappa \left( X + \frac{1}{Y + Z v} \right) \quad [-] \quad (7.1)$$

Combining this with the model for the maximum adhesive force, (2.20), the current limit for the propelling force at the wheel rims of each axle is acquired:

$$F_{t\alpha, max, j}(v, \mu_{max}) = Q_j \mu_{max, j} \kappa \left( X + \frac{1}{Y + Z v} \right) \quad [\text{N}] \quad (7.2)$$

If the slip control system cuts in and limits the tractive effort, it means that the tractive force has hit the limit caused by the current available adhesion, and the tractive force, (2.15), will then be equal to the maximum adhesive force:

$$F_{t\alpha, max} = F_{tj} \quad (7.3)$$

resulting in:

$$Q_j \mu_{max,j} \kappa \left( X + \frac{1}{Y+Zv} \right) = F_{t,j} - K_{J,j} a (1 + \zeta_j) \quad (7.4)$$

which now involves the tractive force,  $F_t$ , that is one of the available signals. Although nothing can be said about the slip,  $\zeta$ , with the data available, thus a simplification of removing this factor is made. The slip is normally a few percent, but if the adhesion is very low it can be up to 10%. Extracting  $F_t$  and looking at the total expression instead of each individual axle, a final system model for the parameter estimation is acquired:

$$F_t(v, a, \mu_{max}) = \sum_{j=1}^{n_d} Q_j \mu_{max,j} \kappa \left( X + \frac{1}{Y+Zv} \right) + \sum_{j=1}^{n_d} K_{J,j} a \quad [\text{N}] \quad (7.5)$$

where  $n_d$  is the number of driven axles.

## 7.2 Initial Parameter Values

It is important to have good initial values for the state variables in the extended Kalman filter ([6]). In this case, the initial values for the parameters  $X$ ,  $Y$  and  $Z$  can be found in the empirical equation describing the adhesion for dry rail computed by Lukaszewicz in [1]:

$$X = \frac{0.161}{\mu_{max} \kappa} \quad [-] \quad (7.6)$$

$$Y = \frac{44 \mu_{max} \kappa}{7.5} \quad [-] \quad (7.7)$$

$$Z = \frac{3.6 \mu_{max} \kappa}{7.5} \quad [-] \quad (7.8)$$

## 7.3 Online Identification

In order to identify the current maximum adhesion online on a running train, extended Kalman filtering will be the approach for investigation (see Section 1.5.1.1 for a description of the EKF). The EKF will continually produce estimations for the parameters chosen, thus adapting the model to the current locomotive.

In this investigation of EKF for the adhesion,  $\mu_{max}$  will be regarded as constant. This is a major simplification, but necessary here due to the lack of information and signals. If the slip were among the available signals,  $\mu_{max}$  could be estimated as described in [9].  $\mu_{max}$  will be set to 0.7 and  $\kappa$  to 0.8.

The simulations will also be made with the assumption that the model is valid for all signal values and that all conditions for it to be valid are met. This is to ease a clear analysis of the filter and its behavior. This will mean that the slip control system will be considered active all the time and that the model will be assumed valid when the train is in breaking mode as well. This assumption will not lead to any errors in these simulations, for the model is here considered absolutely correct.

The parameters in the adhesion model are not expected to vary much in time, but rather on different locomotives. This means that the parameters are expected to lie steady once they reach their correct value, for a certain locomotive. However, it is important to keep in mind that, in reality, disturbances can affect the train configuration differently over time, which could result in varying parameters.

In the evaluation simulations below, the “real” train is assumed to differ in the parameters from the initial values by 10%.

### 7.3.1 A First Approach: EKF with 3 States

Like in the case of the running resistance, having the Kalman filter estimate the acceleration together with the parameters will not be a good idea for the same reason (only the sum of  $X$  and  $a$  can be observed). The acceleration is instead derived from the velocity as described in Chapter 5, and the state vector, input signals and reference signal for the initial Kalman filter approach becomes:

$$x = \begin{pmatrix} X \\ Y \\ Z \end{pmatrix} \quad u = \begin{pmatrix} v \\ a \end{pmatrix} \quad y = F_t \quad (7.9)$$

Further, with this defined, the state update function  $f$ , the  $F$ -matrix, the system function  $h$ , and the  $H$ -matrix, becomes:

$$f(\hat{x}_{k|k}, 0) = \begin{pmatrix} \hat{X}_{k|k} \\ \hat{Y}_{k|k} \\ \hat{Z}_{k|k} \end{pmatrix} \quad (7.10)$$

$$F = \begin{pmatrix} 1 & 0 & 0 \\ 0 & 1 & 0 \\ 0 & 0 & 1 \end{pmatrix} \quad (7.11)$$

$$h(\hat{x}_{k|k-1}, u_k) = \sum_{j=1}^{n_d} Q_j \mu_{max,j} \kappa \left( \hat{X}_{k|k-1} + \frac{1}{\hat{Y}_{k|k-1} + \hat{Z}_{k|k-1} v_k} \right) + \sum_{j=1}^{n_d} K_{J,j} a_k \quad (7.12)$$

$$H = \begin{pmatrix} \sum_{j=1}^{n_d} Q_j \mu_{max,j} \kappa & \frac{-\sum_{j=1}^{n_d} Q_j \mu_{max,j} \kappa}{(\hat{Y}_{k|k-1} + \hat{Z}_{k|k-1} v_k)^2} & \frac{-v_k \sum_{j=1}^{n_d} Q_j \mu_{max,j} \kappa}{(\hat{Y}_{k|k-1} + \hat{Z}_{k|k-1} v_k)^2} \end{pmatrix} \quad (7.13)$$

The filter will be updated according to Section 1.5.1.1 and can be tuned with the design-parameters  $Q$  and  $R$ , which are here chosen as:

$$Q = \begin{pmatrix} 10^{-4} & 0 & 0 \\ 0 & 1 & 0 \\ 0 & 0 & 1 \end{pmatrix} \quad R = 10^{10} \quad (7.14)$$

Using the estimated parameters an estimation for the current maximum adhesion could be calculated with (7.1).

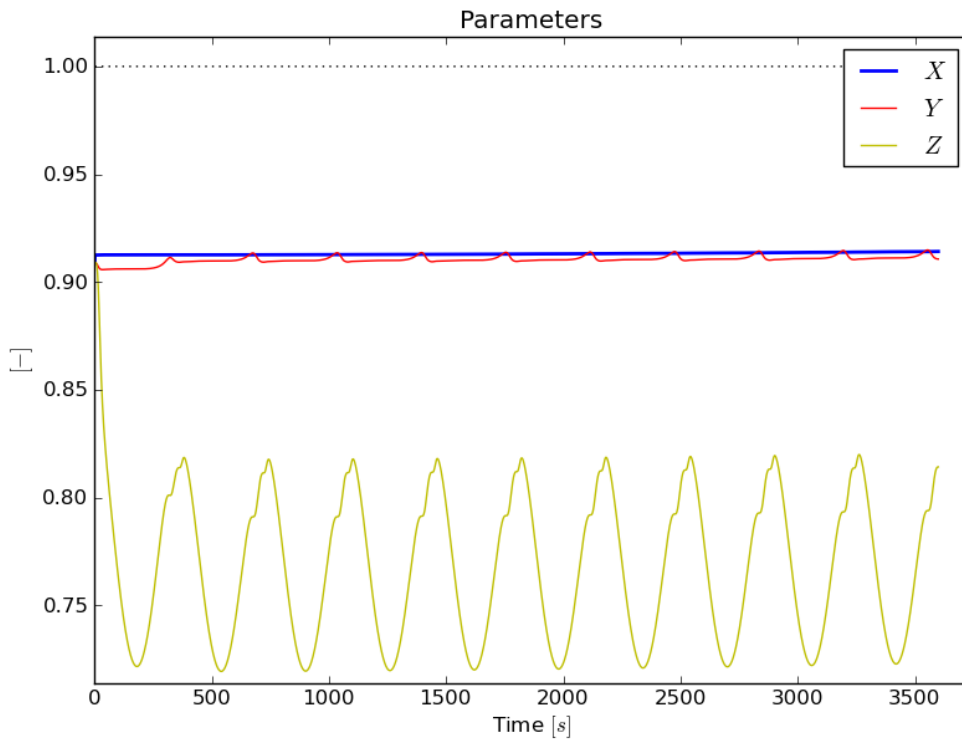


Figure 7.1: Parameter behavior of EKF for the adhesion states  $X$ ,  $Y$  and  $Z$ .

### 7.3.1.1 Results

Simulating the behavior of this filter with the simulation signals described in Section 3.2, the parameters will behave as shown in Figure 7.1 (normalized). Shown by this figure is that none of the parameters converge toward their true value and both  $Y$  and  $Z$  has an oscillating behavior.

### 7.3.1.2 Problems

The simulation indicates poor observability. Plotting the variance of each parameter (the diagonal elements of the  $P$ -matrix in the EKF), shown in Figure 7.2, a diverging behavior over time for all parameters can be seen, especially for  $X$ , indicating lack of observability as described in Section 1.5.3.1.

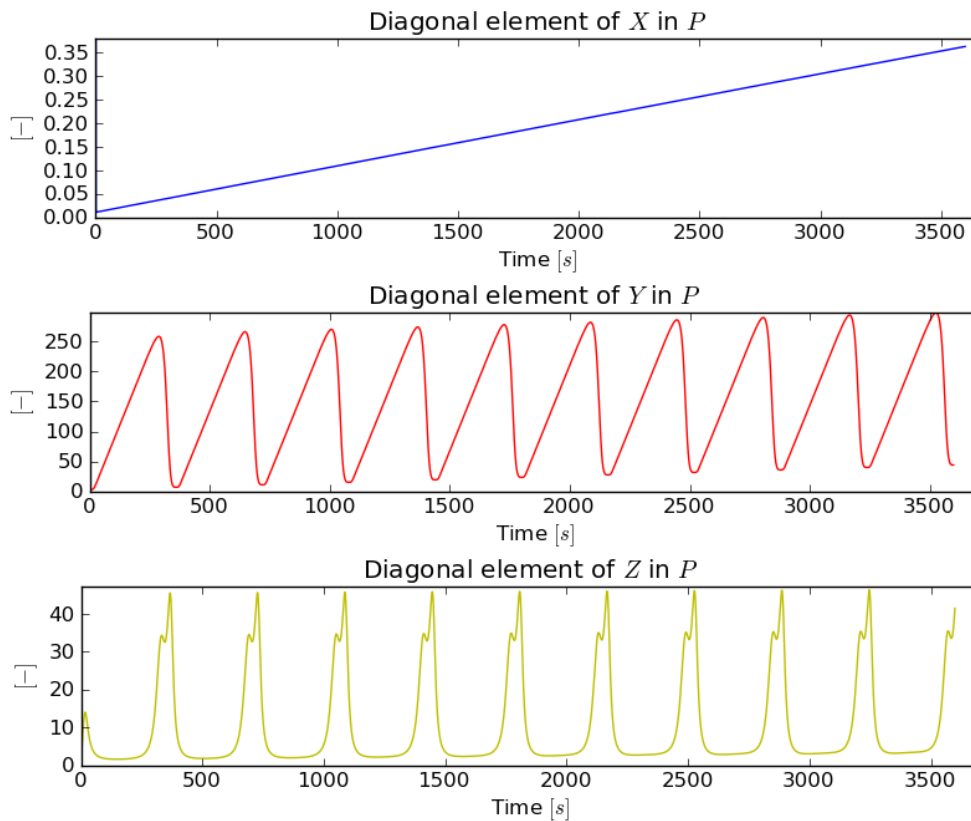


Figure 7.2: Variances of  $X$ ,  $Y$  and  $Z$ .

The parameters  $Y$  and  $Z$  have a coupled behavior, oscillating similar to each other. Mathematically, as seen in the  $H$ -matrix together with the EKF definition, a change in one of these parameters will affect the gain of the other.

### 7.3.1.3 Possible Solution

A way of increasing the possibility to gain observability, along with better convergence of the parameters, is to freeze one of the parameters and thus reducing the number of states to be estimated in the filter. As  $Y$  and  $Z$  has a coupled nature, one of these would be a candidate for removal. The corresponding values for  $Y$  and  $Z$  in the empirical adhesion models for dry and wet rail in [1] are indicating higher dynamics for  $Z$  than for  $Y$ .  $Z$  is also tied to the speed dependence of the model, and keeping this parameter creates a possibility for different speed dependencies of the maximum adhesion for different locomotives.

### 7.3.2 Removing Parameter Y

Removing  $Y$  from the states of the previous filter, the new EKF setup for the state-vector, input signals and reference signal will become:

$$x = \begin{pmatrix} X \\ Z \end{pmatrix} \quad u = \begin{pmatrix} v \\ a \end{pmatrix} \quad y = F_t \quad (7.15)$$

Further, the state update function  $f$  and the  $F$ -matrix becomes:

$$f(\hat{x}_{k|k}, 0) = \begin{pmatrix} \hat{X}_{k|k} \\ \hat{Z}_{k|k} \end{pmatrix} \quad (7.16)$$

$$F = \begin{pmatrix} 1 & 0 \\ 0 & 1 \end{pmatrix} \quad (7.17)$$

Freezing the  $Y$  parameter will result in putting its initial value as a constant,  $\hat{Y}_0$ , in the system function  $h$ :

$$h(\hat{x}_{k|k-1}, u_k) = \sum_{j=1}^{n_d} Q_j \mathbf{u}_{max,j} \kappa \left( \hat{X}_{k|k-1} + \frac{1}{\hat{Y}_0 + \hat{Z}_{k|k-1} v_k} \right) + \sum_{j=1}^{n_d} K_{J,j} a_k \quad (7.18)$$

Finally, the matrix  $H$ , becomes:

$$H = \begin{pmatrix} \sum_{j=1}^{n_d} Q_j \mathbf{u}_{max,j} \kappa & \frac{-v_k \sum_{j=1}^{n_d} Q_j \mathbf{u}_{max,j} \kappa}{\left( \hat{Y}_0 + \hat{Z}_{k|k-1} v_k \right)^2} \end{pmatrix} \quad (7.19)$$

The filter will be updated according to Section 1.5.1.1 and can be tuned with the design-parameters  $Q$  and  $R$ , which are here chosen as:

$$Q = \begin{pmatrix} 10^{-4} & 0 \\ 0 & 1 \end{pmatrix} \quad R = 10^{10} \quad (7.20)$$

Using the estimated parameters an estimation for the current maximum adhesion could be calculated with (7.1).

### 7.3.2.1 Results

Simulating this new filter and plotting the parameters once again, now only  $X$  and  $Z$ , produces the behavior seen in Figure 7.3. A fast convergence of both parameters can be observed, with no oscillating behavior, staying within an error of less than 0.2‰ after 380 seconds.

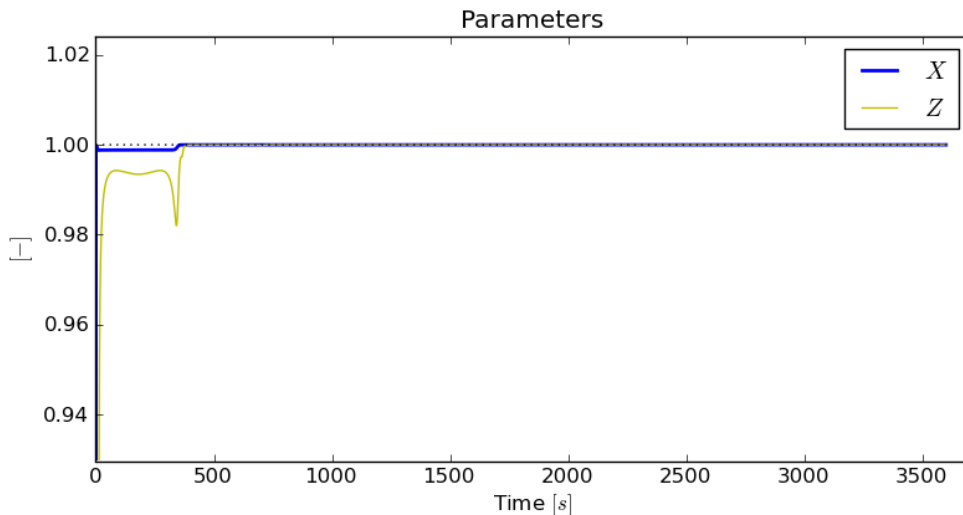


Figure 7.3: Parameters for EKF of the adhesion with  $X$  and  $Z$  as states.

### 7.3.2.2 Observability

The problems with observability has decreased compared to the three state filter, as can be seen in Figure 7.4, showing the variances of the states. However, the problem still suffers from periodic lack of observability. Lack of observability for a state is shown by linearly increasing variance for that state according to Section 1.5.3.1. The variance estimation of the EKF shows that when one parameter increases its observability, the other one suffers from loss of observability and vice versa. An important observation, however, is that the variance of the states does not seem to diverge as for the three state filter shown in Figure 7.4.

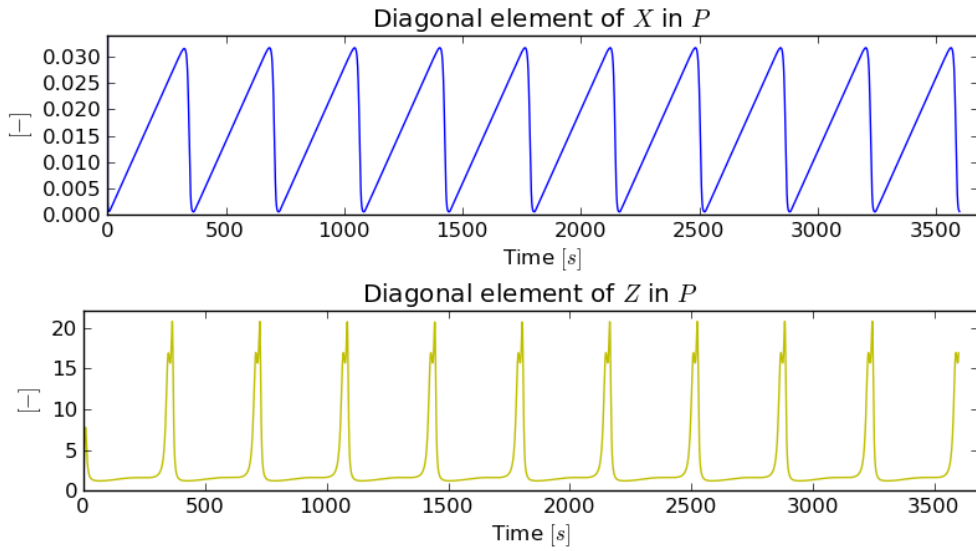


Figure 7.4: Variances for  $X$  and  $Z$ .

### 7.3.2.3 Sensitivity

The system model is differentiated with respect to the input signals according to Section 1.5.4, to gain insight in how errors in the input signals will affect the output signal.

$$H_w = (\nabla_u h(x, u))^T = \left( \begin{array}{c} -\kappa \hat{Z}_{k|k-1} \sum_{j=1}^{n_{\text{nd}}} Q_j \mathbf{u}_{\text{max}, j} \\ (\hat{Y}_0 + \hat{Z}_{k|k-1} \mathbf{v}_k)^2 \end{array} \quad \sum_{j=1}^{n_{\text{nd}}} K_{J, j} \right) \quad (7.21)$$

The two elements of  $H_w$  provides an indication of how much the output signal, in this case the estimation of the tractive force, will be affected by errors in the input signals,  $v$  and  $a$  respectively. The size of these elements are studied for the simulation setup provided, which can be seen in Figure 7.5.

The system is significantly (5 to 10 times) more sensitive to errors in the acceleration input signal. An error of 1 m/s<sup>2</sup> would result in an estimation error of 52 kN, as can be seen in the second plot of Figure 7.5.

Since the acceleration signal is not provided among the available signals, it will be derived from the velocity, thus moving the accuracy demands onto the velocity signal and the method of estimating the acceleration from it.

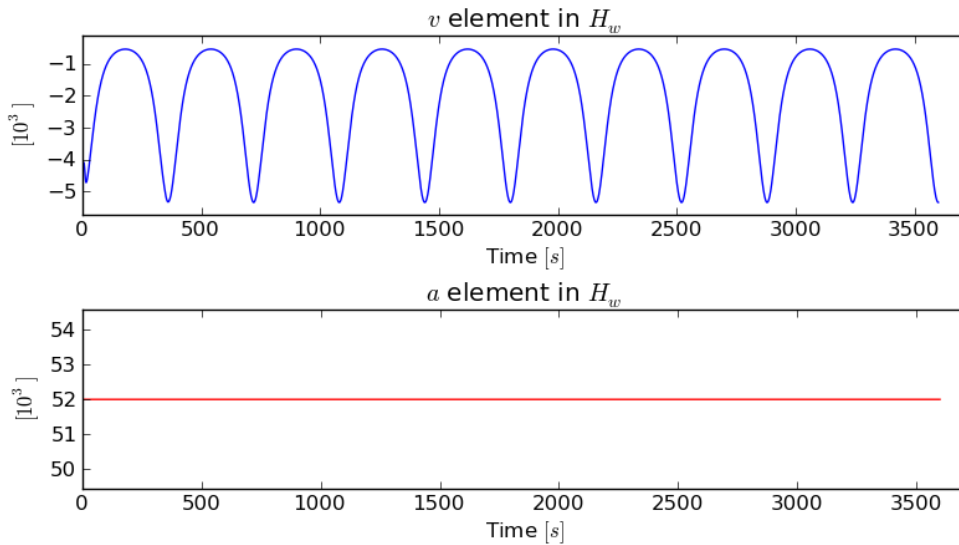


Figure 7.5: The elements of  $H_w$  showing how errors in the input signals affect the output signal, tractive force.

## 7.4 Conclusions

In order to at least achieve local observability of all parameters, one state has to be removed from the original three state model for the simulation setup. The parameter behavior of the two state filter is satisfactory; the parameters converge toward their desired values.

Lack of observability seems to be a problem, studying the behavior of the state variance estimation in Figure 7.4. For the simulated environment, this does not cause any major problems, but will only delay the time it takes for the parameters to reach their desired values. In the real world however, disturbances will affect the system and increase the impact of the observability issues.

---

# 8

## Conclusions & Future Work

---

This chapter will wrap up the thesis in a concluding section followed by possible interesting matters to further investigate, called *future work*.

### 8.1 Conclusions

The most challenging problems that arise with the online prediction and parameter estimation of the running resistance are observability and sensitivity. The number of states observable from the available signals is limited, ending in a model with four estimated parameters. The observability problems arise when these four parameters of the running resistance, only separated by the input signals, are to be estimated using only one reference signal, tractive force. In addition, because of the large masses involved, this tractive force signal consists mostly of the accelerating force rather than the running resistance which is the interesting part for estimation. This makes small variations of the acceleration of the train correspond to large forces, which defines the sensitivity problem.

Just as the running resistance, the parameter model for adhesion with its available input signals suffers from observability problems. The investigation leads to a filter with two estimated parameters, for a satisfying result in simulation.

For both the running resistance and the adhesion, the observability problems will be much more severe in reality than for the simulated case. With added

disturbances, lowering the accuracy of the measured signals, more information is desired in order to observe the real values of the sought parameters.

To further improve the observability, there are a few different paths to investigate. One way is to further reduce the number of states. Another way is to provide additional information by adding more signals, for instance by adding extra sensors. If new, or additional, models were introduced using different calculations or other possibly available signals, that could also be a way of increasing observability for the desired parameters.

In order to solve the sensitivity problem, a very high accuracy in the acceleration signal is needed. The best way to derive the acceleration with the provided signals is by numerically differentiating the velocity signal. The analysis in Chapter 5 indicates that the best way of doing this is with a smoothing spline approximation. A slip free velocity signal (measurement on a non-driven axle, or using GPS) with good accuracy and high frequency (50 Hz) is desired in order to estimate the acceleration with a satisfying result.

Worth to be mentioned is that these two main problems are connected in the sense that poor observability puts a high demand on the quality of the information. Since information is only seen during limited windows in time, it's important that it is valid during that time. With high observability, higher variance of the measurements wouldn't have the same impact on the estimations.

## 8.2 Future Work

### Acceleration

Further study of the possibilities of increasing the accuracy of the acceleration has the potential of greatly improving the estimation of the running resistance. One way of further investigation would be to study the possibility of explicit measurement of the acceleration adding extra sensors.

In the case where the acceleration is estimated from the velocity signal, investigations on how to further improve this could be valuable. Sensor fusion using both GPS and Teloc speed signals, along with perhaps also a

doppler radar, could be used.

## **Gradient**

The GPS signal of the altitude has been evaluated to the extent that it seem to provide data enough to make an estimation of the gradient close to the one provided by BIS. Further use of this information by using sensor fusion, with for instance Kalman Filtering, to improve the accuracy of the gradient signal might very well be possible.

Since BIS is not known to be updated very quickly, nor always provide highly reliable data according to [8], it could definitely be of interest to further investigate the possibility of recording an own, independent, database.

## **Curve Radius**

In a similar manner as for the gradient signal, calculation of the curve radius from the GPS information could be implemented, with possibilities of the same benefits; better accuracy and recording a more flexible database.

## **Slip**

Methods for measuring and estimating the slip is an important field of further investigation. Measurement of the velocity on both a driven and a non-driven axle could give valuable information. Research ([1]) has also shown a relation between the slip and the tractive effort. If train speed was also measured utilizing other methods such as doppler radar technology, the difference in speed of a driven wheel and the train, thus the slip, could be estimated.

## **Adhesion**

The major simplifications made in the adhesion model in this thesis demands further studying of both slip and the maximum friction. The latter could be estimated via the slip, described in [9], where the derivative of the adhesion with respect to the slip is used to determine the maximum friction,  $\mu_{\max}$ .

### **Further Filter Evaluations**

If recorded data with higher data rates were available, it would be interesting to evaluate different filters more thoroughly. Not least a three parameter filter for the running resistance.

It could also be interesting to evaluate if UKF performs better than EKF in the implementations presented. The running resistance model is not assumed to consist of any particularly problematic nonlinearities. The problems lie in areas as observability and sensitivity, wherefore UKF is not expected to provide significant increased performance, however evaluation of this could still be interesting.

---

# 9

## References

---

- [1] P. Lukaszewicz. *Energy Consumption and Running Time for Trains*. Doctoral Thesis, Department of Vehicle Engineering, Royal Institute of Technology, Stockholm, 2001.
- [2] P. Lukaszewicz. *Running Resistance of Passenger and Freight Trains*. Licentiate Thesis, Department of Vehicle Engineering, Royal Institute of Technology, Stockholm, 1995.
- [3] D. Frylmark and S. Johnsson. *Automatic Slip Control for Railway Vehicles*. Master's Thesis, Department of Electrical Engineering at Linköping University, Linköping, 2003.
- [4] G. Hendeby. *Performance and Implementation Aspects of Nonlinear Filtering*. Dissertations, Department of Electrical Engineering, Linköping University, Linköping, 2008.
- [5] S. J. Julier and J. K. Uhlmann. *A New Extension of the Kalman Filter to Nonlinear Systems*. The Robotics Group, Department of Engineering Science, The University of Oxford, 1997.
- [6] D. Simon. *Optimal State Estimation*. John Wiley & Sons, Inc. New Jersey, 2006.
- [7] P. Howlett, P. Pudney and X. Vu. *Estimating Train Parameters with an Unscented Kalman Filter*. Centre for Industrial and Applied Mathematics, University of South Australia, Australia, 2004.

## 9 References

---

- [8] Dr. Piotr Lukaszewicz, Transrail Sweden AB, Stockholm, Sweden.
- [9] F. Gustafsson, L. Ljung and M. Millnert. *Signal Processing*. Studentlitteratur, Lund, 2010.
- [10] W. J. Rugh. *Linear System Theory*. Prentice Hall, 2nd Edition, 1996.
- [11] G.H. Golub, C.F. Van Loan. *Matrix Computations*. Third Edition, The Johns Hopkins University Press, United States, 1996.
- [12] J. Kingstedt and M. Johansson. *Methods for Residual Generation Using Mixed Causality in Model Based Diagnosis*. Master's Thesis, Department of Electrical Engineering, Linköpings Universitet, Linköping, 2008.
- [13] *TELOC®1500 with DATRx, Manual*. HaslerRail AG, Switzerland, 2010.
- [14] E. Höckerdal, *Model Error Compensation in ODE and DAE Estimators with Automotive Engine Applications*. Department of Electrical Engineering, Linköping University, Linköping 2011.
- [15] Erik Hellström. *Look-ahead Control of Heavy Vehicles*. Dissertations, Department of Electrical Engineering, Linköping University, Linköping, 2010.
- [16] P. Lukaszewicz. *Running resistance and energy consumption of ore trains in Sweden*. Paper, Department of Aeronautical and Vehicle Engineering, Royal Institute of Technology, Stockholm, 2008.
- [17] F. Gauffin. *Evaluation of Weak Relations in TracFeed*. Master's Thesis, Department of Computer Science and Electronics, Mälardalens Högskola, 2008.
- [18] O. Polach. *Influence of locomotive tractive effort on the forces between wheel and rail*. Vehicle System Dynamics Supplement 35 (2001), pp. 7-22.
- [19] O. Polach. *Creep forces in simulations of traction vehicles running on adhesion limit*. Bombardier Transportation, CH-8401 Winterthur, Switzerland, 2004.
- [20] H. Chen, T. Ban, M. Ishida and T. Nakahara. *Adhesion between*

- 
- rail/wheel under water lubricated contact*. Railway Technical Research Institute, Tokyo, Japan, 2002.
- [21] M. Spiriyagin, K.S. Lee and H.H. Yoo. *Control system for maximum use of adhesive forces of a railway vehicle in a tractive mode*. School of Mechanical Engineering, Hanyang University, Seoul, Korea, 2007.
- [22] H. Chen, T. Ban, M. Ishida and T. Nakahara. *Experimental investigation of influential factors on adhesion between wheel and rail under wet conditions*. Railway Technical Research Institute, Tokyo, Japan, 2008.
- [23] M. Spiriyagin, K.S. Lee, H.H. Yoo, O. Kashura and O. Kostyukevich. *Modeling of Adhesion for Railway Vehicles*. School of Mechanical Engineering, Hanyang University, Seoul, Korea, 2007.
- [24] A. Steimel. *Electric Traction - Motion Power and Energy Supply*. Oldenbourg Industrieverlag, Munich, 2008.
- [25] V.A. Profillidis. *Railway management and engineering*. Ashgate Publishing Limited, England, 2006.
- [26] R.S. Raghunathan, H.D. Kim and T. Setoguchi. *Aerodynamics of high-speed railway train*. Progress in Aerospace Sciences 38 (2002) 469–514.
- [27] *SciPy Reference Guide*. Release 0.10.0.dev6665, January 21, 2011.
- [28] *TELOC®2500, Leaflet*. HaslerRail AG, Switzerland.  
[http://www.haslerrail.com/fileadmin/redakteur/eng/Leaflet\\_05\\_HaslerRail\\_TELOC2500.pdf](http://www.haslerrail.com/fileadmin/redakteur/eng/Leaflet_05_HaslerRail_TELOC2500.pdf), 13/5/2011.
- [29] Fanoo Data Shart. Kockums Industrier.  
[http://www.kockumsindustrier.se/Products/Freight/Special/TEKNISK\\_A%20DATA%20MALMVAGN%20F050.pdf](http://www.kockumsindustrier.se/Products/Freight/Special/TEKNISK_A%20DATA%20MALMVAGN%20F050.pdf), 21/5/2011. Swedish.
- [30] Philipp Gerber. HaslerRail AG, Bern, Switzerland.
- [31] T. Chalk. *High accuracy speed measurement using GPS*. Scientific Engineering Research P/L, Mt Best, Vic 3960, Australia, 2007.

## 9 References

---



## Description of CATO

---

*(As described in the CATO Leaflet from Trainsrail Sweden AB, 2009, with a modification of the driver's interface to the latest)*

CATO (Computer Aided Train Operation) provides a traffic management system allowing trains to run as efficiently as possible considering the overall traffic situation on a railway line.

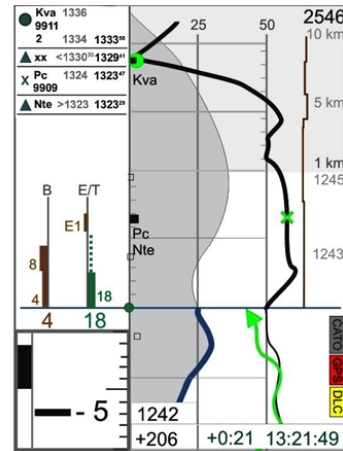
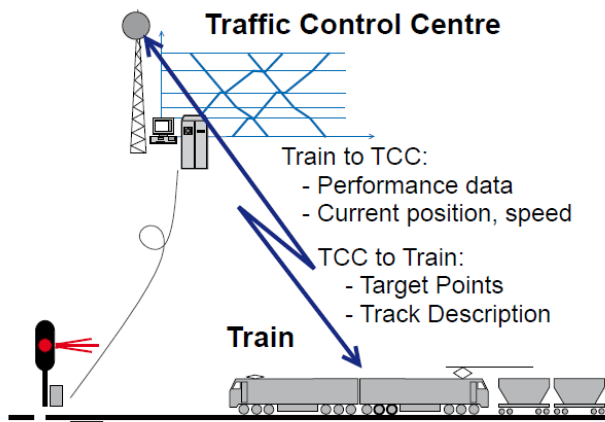
- CATO consists of two modules, CATO-TRAIN and CATO-TCC (Traffic Control Centre).
- Aimed both for train operators and infrastructure administrators.
- CATO-TRAIN can be operated together with CATO-TCC or standalone.
- Follows the European EETROP (Energy Efficient TRain Operation) draft interoperability standard.
- Developed by Trainsrail with funding from the Swedish National Rail Administration and LKAB.

Trials on the LKAB iron ore railway lines have rendered the following

- Reduced energy consumption by 20-25%.
- Increased line capacity by 10%.
- Reduced maintenance cost for brakes by 30%.

If applied to the Swedish railway system, this would yield yearly savings in

the order of 34 MEUR.

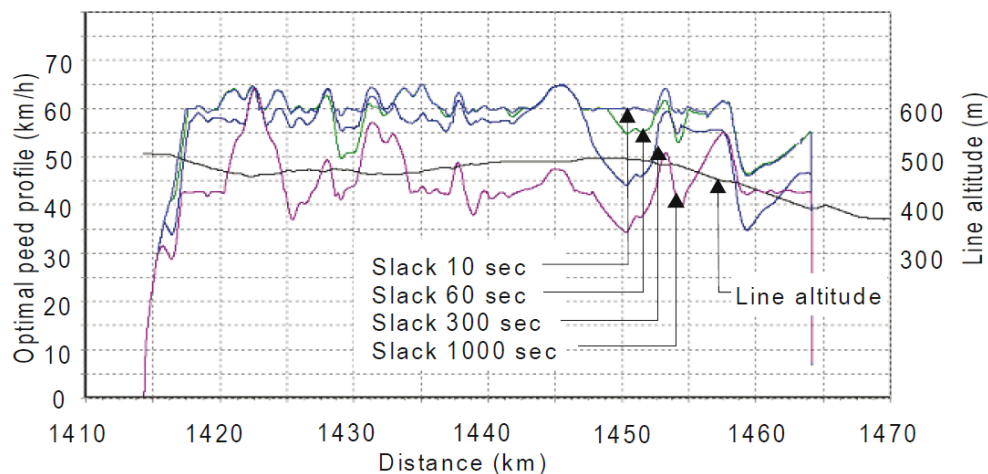


CATO-TCC calculates an optimal real time schedule based on current train data and planned timetable. An individual schedule is then sent to each train via GSM-R radio. CATO-TRAIN calculates the optimal speed profile, and presents it to the driver for manual or autopilot operation

Driver's interface to CATO, displaying among other things the optimal speed profile

### Other benefits

- Increased regularity and punctuality.
- Reduced CO<sub>2</sub> emissions (diesel powered trains).
- Improved utilization of rolling stock and crews.
- Better working environment.



The optimal speed profile depends on the slack times (i.e. time difference between minimum run time and available run time)

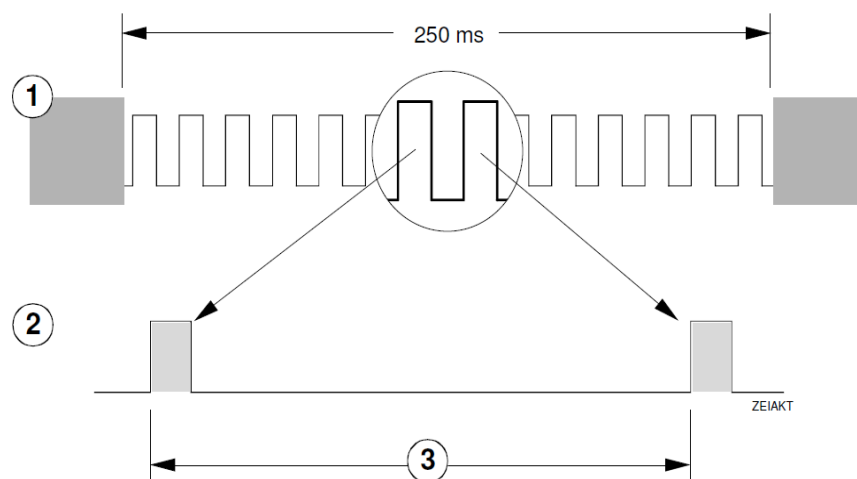
# B

## Teloc Velocity Measurement

### Speed measuring procedure

*(The following is a clipping from [13])*

According to the actual speed, two criteria, “Low Speed” and “High Speed”, form the base for speed calculation. If, with rising speed, the number of pulses rises above 400 pulses per second (pps), the system switches to the “High Speed” criterion; if, vice versa, the number of pulses drops below 320 pps, the system switches to the “Low Speed” mode.



*Measuring cycles high speed – low speed*

1 “High speed” criterion    2 “Low speed” criterion    3 Time between two pulses

In “Low speed“ mode, the speed is computed from the time between two pulses, whereas the first pulse launches a counter being stopped by the second pulse. The actual speed is then differentiated from the counter value. If no further pulse is registered until the counter reaches its maximum value (FFFF), this is defined as vehicle standstill or zero speed.

In “High speed“ criterion, the speed is computed from the number of pulses registered in a 250 ms time slot.

Each frequency generator (sensor, probe) is hardwired to a pulse input of the TELOC®. Each pulse input is configured as analogue input, allowing the interpretation of the measured frequency. The maximum possible frequency is computed from the configured target speed using the formula below:

$$F_{max} = \frac{v_{end} z}{3.6 \pi d}$$

$F_{max}$  Maximum frequency [Hz]

$v_{end}$  Needle deflection [km/h]

$z$  Number of pulses (positive edges) during one wheel revolution

3.6 Conversion factor m/s → km/h

$d$  Wheel diameter [m]

The real recorded (and indicated) speed is proportional to the measured frequency. In case of a wheel diameter correction, the speed is corrected by the “actual wheel diameter / nominal wheel diameter” factor.

The covered distance is incremented every 20 ms with the real speed:

$$Distance\ increment = Real\ speed * 20\ ms$$

The overall covered distance is the sum of all distance increments.

Should it be the case that the speed originates from the frequency inputs then the following formula is valid for the distance calculation.

$$S_n = m_n ds k$$

$S_n$  Distance traveled in the measurement interval  $n$ . [m]

$m_n$  Number of impulses (positive flanks) on the transmitter frequency

---

input, during the measurement interval  $n$ .

$ds$  Distance element per transmitter pulse. [m]

$k$  Correction factor (wheel diameter).

Acceleration with frequency inputs:

$$a = \frac{v_t - v_{t-\Delta t}}{\Delta t} \text{ where } \Delta t = 1s.$$

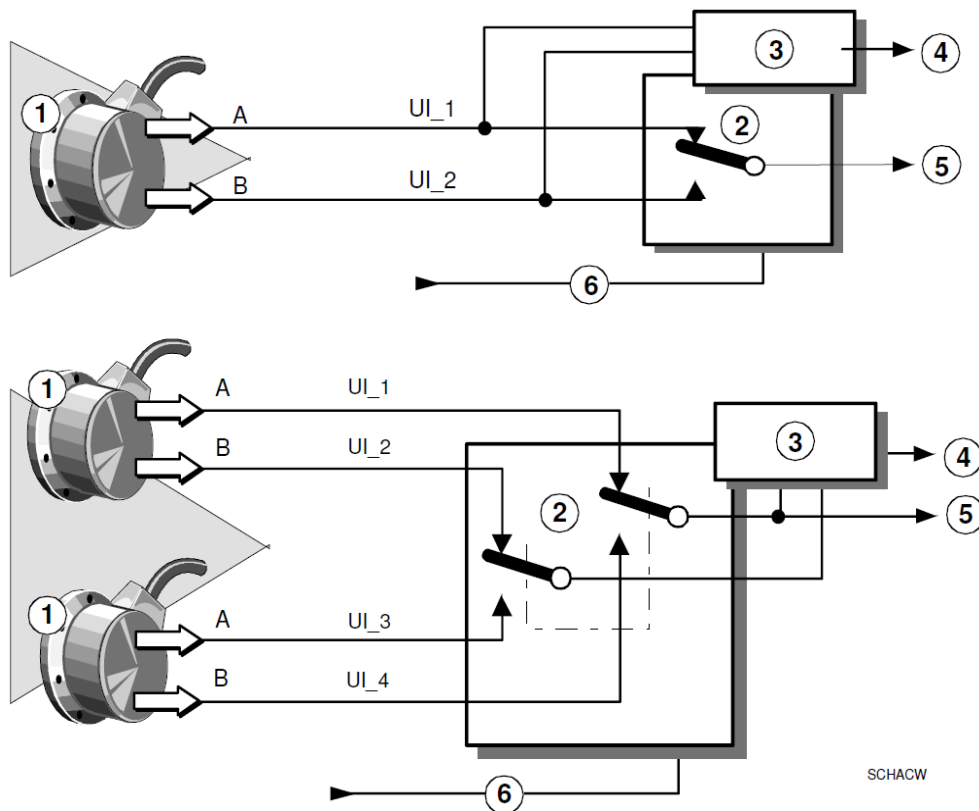
Different configurations are possible:

1. **Pulse generator:** The measured frequency is used to compute speed and distance as well as the operating direction.
2. **Pulse generators mounted on the same or on different axles:** By default, the higher frequency is used to compute speed and distance.
3. **Pulse generators, 2 pulse generator with 2 sensors each, both pulse generator mounted on different axles:** First, the sensors are compared internally in each pulse generator. Then, the higher frequency is compared with the other pulse generator. The sensor producing the highest frequency is used for speed and distance calculation.

Further configurations are feasible on customer demand (e.g. 2 pulse generators on the same axle and the speed is transmitted by a vehicle bus). In these cases, the speed calculation criteria have to be defined mutually by the customer and HaslerRail.

### **Pulse generator monitoring and frequency selection**

Usually, the two sensors used for speed acquisition are delivered with the output signals electrically shifted by  $90^\circ$ . The operating circuit computes the vehicle's direction from this phase shift.



*Pulse generator monitoring principle*

- |   |                                      |   |   |
|---|--------------------------------------|---|---|
| 1 | <i>Pulse generator 1 and 2</i>       | 4 | <i>to roll-back monitoring</i>            |
| 2 | <i>Signal switch</i>                 | 5 | <i>to speed determination</i>             |
| 3 | <i>operating direction detection</i> | 6 | <i>traction- / brake effort criterion</i> |

*(End of the clipping)*

## Velocity calculation

From the description above of the pulse measuring procedure, the equations that Teloc uses to calculate the velocity is deduced:

$$v = \frac{d \pi}{t z}$$

in “Low speed“ criterion and:

$$v = \frac{4 p d \pi}{z}$$

in “High speed“ criterion, where:

$v$  Speed. [m/s]

$d$  Wheel diameter. [m]

$t$  The time between two pulses. [s]

$z$  Number of pulses (positive edges) during one wheel revolution.

$p$  Number of pulses registered in a 250 ms time slot.

These equations are confirmed by [30].